Development of an Electrochemical Aptasensor for Indirect Detection of Target Protein

By

Marwa Y. Shah Alam

A Thesis Submitted to
Saint Mary's University, Halifax, Nova Scotia
in Partial Fulfillment of the Requirements for the
Degree of Bachelor of Science with Honours in Chemistry

April 2015, Halifax, Nova Scotia

Copyright Marwa Y. Shah Alam, 2015

Approved: Dr. Christa Brosseau
Supervisor

Approved: Dr. Jason Clyburne
Examiner

Approved: Dr. Jason Masuda
Examiner

Date: [April 24, 2015]

Table of Contents **Page**

Abstract

Development of an Electrochemical Aptasensor for Indirect Detection of Target Protein

By Marwa Y. Shah Alam

An aptasensor is a biosensor that makes use of aptamers as a recognition element to detect target analytes. Aptamers are sequences of single-stranded DNA (ssDNA) or RNA that can selectively bind to a wide range of target analytes. A spectroelectrochemical based technique called electrochemical surface enhanced Raman spectroscopy (EC-SERS) is an ideal method for aptamer-based target detection based on vibrational spectroscopy. While EC-SERS has been successfully used to develop an aptasensor for detection of heme-protein (cytochrome c), direct detection of non-heme protein such as Human Immunoglobulin E (IgE) remains a challenging task. Therefore, an indirect method of detection is explored with IgE as the target protein for this research. The anti-IgE aptamer has a stem and loop configuration with a double-stranded DNA (dsDNA) stem, which is considered to become an open-loop configuration in the presence of IgE. This change of configuration from dsDNA to ssDNA can be utilized in aptasensor development. The aim of the current research is to develop an EC-SERS based aptasensor to detect non-heme protein by employing Raman reporter molecules that are selective towards dsDNA. For this purpose, five different potential Raman reporter molecules were evaluated, namely methylene blue, proflavine, doxorubicin, ethidium bromide and bisbenzimide H 33258 using SERS, EC-SERS and electrochemical methods to detect DNA hybridization. However, the Raman reporters showed SERS signals for both ssDNA and dsDNA, and hence, hybridization could not be detected. This was likely due to non-specific binding of the reporters to the substrate. A control study suggested the presence of defects in the fabrication of alkanethiol monolayer, which remained a key challenge for this project. Three different methods to reduce defects were explored including mixed monolayer formation by sequential immersion in 11-mercapto-1-undecanol and 6-mercaptohexanol. Such alkanethiol fabrication seemed to be promising to eliminate any defects present in the monolayer and hence, reduce any non-specific binding in future studies.

[April 24, 2015]

Acknowledgements

I would like to thank Dr. Christa Brosseau for giving me this wonderful research opportunity, for being my supervisor and for molding the best out of me. She is one of my ideal figures whose footsteps I would love to follow. I am also grateful towards my second ‘family’ for their guidance and support – both past and present members of Dr. Brosseau Research group: Osai Clarke, Scott Harroun, Mohammed Abul Hasanat, Reem Karaballi, Soraya Merchant, Ashley Robinson and Lili Zhao. I have learnt so much from each one of them that I will treasure forever. Special thanks to Scott Harroun, Lili Zhao and Reem Karaballi for their previous contributions to different aspects of this project. I am also thankful to the Department of Chemistry at SMU for all their support and resources.

No words can describe my gratitude towards my family – ma, baba, appi, chichi, lil’ mommy and my jaan - for all their love, patience and support they have given me. Lastly, I am grateful to my God for all His blessings He has bestowed upon me and without whom, I am nothing.

List of Abbreviations

6-MCH	6-mercaptohexanol
11-MUD	11-mercapto-1-undecanol
12-MDA	12-mercaptododecanoic acid
Ag/AgCl	Silver/ silver chloride reference electrode
AgNP	Silver nanoparticles
AuNP	Gold nanoparticles
Au/Ag	Gold/silver
CV	Cyclic voltammetry or cyclic voltammogram
Cyt c	Cytochrome c
DNA	Deoxyribonucleic acid
DOX	Doxorubicin
DPV	Differential pulse voltammetry
dsDNA	Double-stranded DNA
EC-SERS	Electrochemical surface enhanced Raman spectroscopy
ELISA	Enzyme-linked immunosorbent assay
EtBr	Ethidium bromide
HSAB	Hard and soft (Lewis) acids and bases
IgE	Immunoglobulin E
MB	Methylene blue
P1	Probe 1
PCR	Polymerase chain reaction
PF	Proflavine
RNA	Ribonucleic acid
rpm	Rotations per minute
SAM	Self-assembled monolayer

SELEX	Systematic evolution of ligands by exponential enrichment
SEM	Scanning electron microscope
SERS	Surface enhanced Raman spectroscopy
SERRS	Surface enhanced resonance Raman spectroscopy
SCE	Saturated calomel electrode
SPE	Screen printed electrode
ssDNA	Single-stranded DNA
s.T1	Scrambled target 1
SWV	Square wave voltammetry
T1	Target 1
UV-vis	Ultraviolet-visible

List of Figures

List of Figures continued

List of Figures continued

List of Figures continued

List of Figures continued

List of Figures continued

List of Figures continued

List of Tables

Chapter 1: Literature Review

1.1 Introduction:

There is a growing demand for biosensors that can detect various target analytes at increasingly lower levels and higher speeds.[1] Therefore, the development of new methods that are capable of providing useful diagnostic information is an active area of research. Recently, aptamers as a recognition element for biosensor technology have gained a lot of research attention. Aptamers are sequences of single-stranded DNA or RNA that are highly specific and selective towards a wide range of target molecules including metal ions, small molecules, proteins and complex targets.[2] When aptamers are used as a biological recognition element in a biosensor, it is called an aptasensor. A spectroelectrochemical technique called electrochemical surface enhanced Raman spectroscopy (EC-SERS) is an ideal method for aptamer-based target detection based on vibrational finger printing. This analytical technique is also highly sensitive and non-destructive in nature.[3] While EC-SERS has been employed previously in our group to study various heme proteins, direct detection of non-heme protein such as human immunoglobulin E (IgE) has proved challenging. Recently, our research group has developed an aptasensor for direct detection of heme protein cytochrome c.[4] Cytochrome c contains a heme group that acts as an embedded Raman reporter. Therefore, cyt c can be directly detected using an aptasensor since almost all the SERS peaks arise from the heme group. On the contrary, such direct detection for IgE was not possible as it does not contain a Raman-active heme group. In literature, the development of a SERS-based aptasensor for detection of IgE has not yet been explored. Therefore, an indirect method to detect this non-heme protein human IgE using SERS would be of interest.

The structure of the aptamer for IgE protein has a stem and loop configuration.[5] In this secondary structure, the single-stranded DNA (ssDNA) folds in a way to form base pairs within the strand resulting in a double-stranded DNA (dsDNA) stem. In the presence of IgE, the stem-loop configuration of the anti-IgE aptamer changes to open-loop configuration.[6,7] This feature of the configuration change can be utilized to fabricate a biosensor for an indirect method of detection using EC-SERS based on detection of DNA annealing as illustrated in Figure 1. Therefore, the purpose of this research is to indirectly detect DNA hybridization by using DNA binding agents that are selective towards dsDNA and acts as a Raman reporter. These preliminary studies of hybridization can then be implemented for indirect aptamer-based IgE detection.

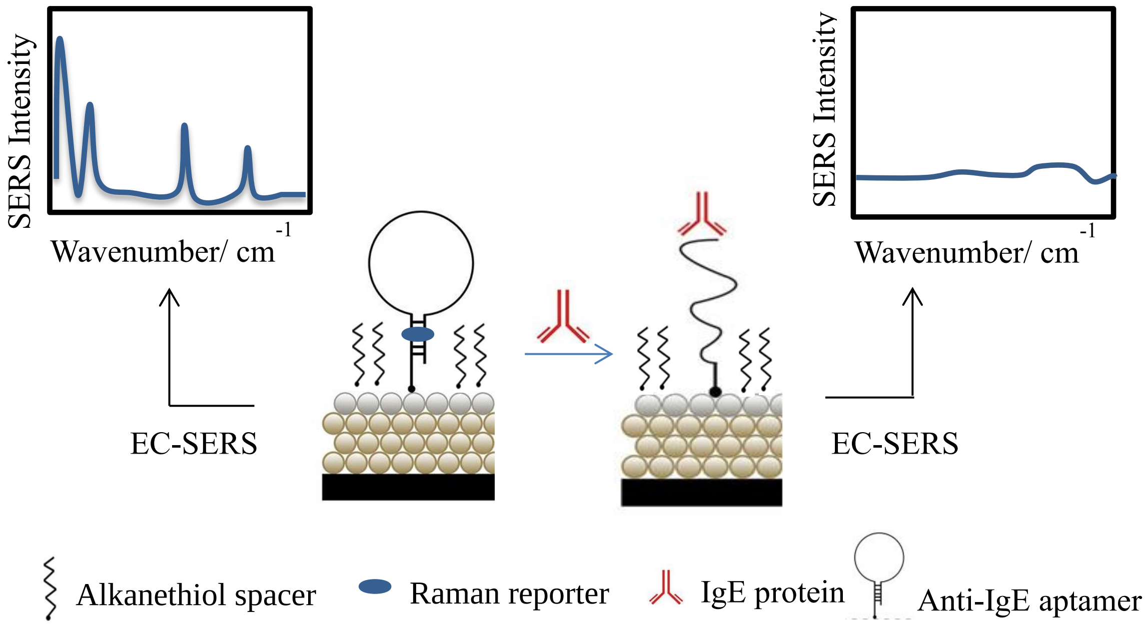

Figure 1: Illustration of fabrication assay plan for indirect aptamer-based IgE detection.

1.2 DNA Aptamers and Aptasensors

A biosensor is made up of two main components: a biological recognition element to detect the target analyte and a signaling component used to obtain detectable signals.[2,8] The biological recognition element can be an enzyme, antibody etc. while the signaling component can be any optical, electrochemical, or thermal technique.[2,8] Recently, aptamers have been developed for use as the biological recognition element in biosensor platforms. Aptamers are a sequence of single-stranded DNA or RNA that can selectively bind to target analytes. Most of the aptamers are obtained by an in vitro selection and amplification process called SELEX – Systematic Evolution of Ligands by EXponential enrichment.[2,9] The conventional SELEX process involves 4 basic steps – incubation, partition, amplification and post-selection.[10] A library of chemically synthesized random single-stranded oligonucleotides (DNA or RNA) is incubated with a target of interest. This library contains about 10^{13} to 10^{15} different sequence of oligonucleotides.[9] The oligonucleotides that bind strongly to the target are separated from the unbound or weakly bound ones. These selected oligonucleotides with binding affinity to the target are amplified by polymerase chain reaction (PCR) technology. The process of selection and amplification is repeated for up to 20 cycles until potential aptamers with optimal binding affinities are obtained.[11] These potential aptamers are then cloned, sequenced and evaluated by various methods for their binding affinities. The conventional SELEX process takes anywhere from a few weeks up to several months to generate aptamers.[11] However, once the oligonucleotide sequence with the optimal binding affinity is known, the chemical synthesis of the aptamer takes just a few hours to complete. Additionally, several different methods such as capillary electrophoresis-SELEX, magnetic bead-based

SELEX etc. have been developed to generate aptamers faster than the conventional SELEX method.[11]

Since the discovery of SELEX by Tuerk and Gold in 1990, a broad spectrum of aptamers have been generated that can bind specifically to various target analytes such as metal ions, small molecules, peptides, proteins, and even whole cells and microorganisms.[2] Aptamers can fold into secondary and tertiary structures, which allows them to bind to their target such as protein with relatively higher specificity and selectivity than antibodies. Aptamers are sometimes described as 'chemical antibodies' as they resemble how antibodies bind to protein.[4] When aptamers are used as a biological recognition element in a biosensor, it is called an aptasensor. The main advantages of using aptamers over antibodies for biosensors are as follows [8]:

1. Aptamer production does not require the use of cell lines or animals, and instead involves highly reproducible nucleic acid synthesis
2. Aptamers have small size, high stability, high binding affinity and ease of chemical modification, as compared to traditional protein-based antibodies

In addition to their application in biosensor development, there are various other uses of aptamers such as in drug delivery, cell imaging and selective chemotherapy, etc.[8]

In recent years, the use of aptamer-based sensors for detection of protein has gained increasing attention over traditional antibody-based sensors. As can be seen by the increasing number of publications in Figure 2, much effort has been dedicated to developing aptamer-based biosensor platforms. One of the growing research sub-topics is the development of an aptasensor for detection of a target protein human immunoglobulin E (IgE) as the majority of current allergy testing assay are based on the antibody receptor.

Additionally, most of the aptamer based detection in literature involve complex strategies, high cost instrumentation and lacks sensitivity.

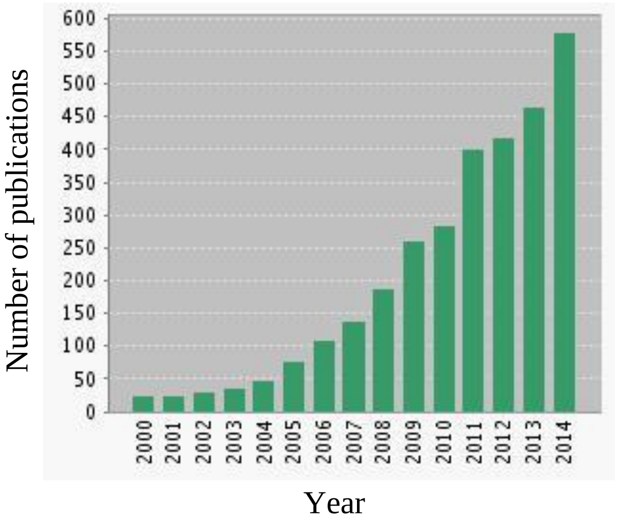

Figure 2: Trend of publications as obtained from the Web of Science database with specific keywords in title “Aptamer” or “Aptasensor”.

The SELEX-based high affinity DNA aptamer for IgE was first isolated by Wiegand et al. and is referred to as the D17.4 aptamer.[5] Since then, this single-stranded anti-IgE aptamer has been used in the development of most IgE aptasensors. This aptamer is 37 nucleotides long. Another anti-IgE aptamer (D17.4ext) was engineered by Liss et al. by extending the DNA sequence of the stem of the aptamer to improve aptamer stability.[12] The predicted secondary structures of both of these anti-IgE aptamers are shown in Figure 3.[12] In both cases, these anti-IgE aptamers have a hairpin loop and a stem region.[5]

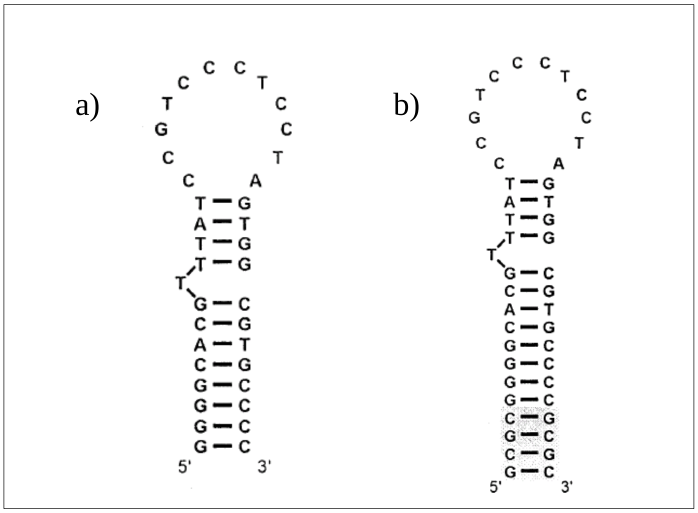

Figure 3: Secondary structure of the published anti-IgE aptamer **(a)** standard D17.4 aptamer and **(b)** the extended D17.4ext aptamer. [11]

According to the study by Liss et al., the D17.4ext with its longer stem achieved by adding 4 G-C base pairs was found to be more stable than the standard one and had improved protein binding characteristics.[12] However, previous studies by Wiegand et al. suggested that the stem region is not important for protein binding but is a factor to stabilize the structure only.[5,13] On the contrary, Katilius et al. studied the standard anti-IgE aptamer sequence and its binding properties in depth, and have reported that a less energetically stable stem can be more beneficial for protein binding.[13] Even though studies using quartz crystal microbalance[12] and atomic force microscopy[14] revealed that the aptamer/IgE binding affinity is higher relative to antibody/IgE binding, the exact binding mechanism of the aptamer/protein complex is largely unknown.[14] However, it is considered that the stem and loop configuration of the anti-IgE aptamer changes to open-loop configuration in the presence of IgE protein. Several electrochemical studies to detect IgE have been performed based on this conformational change whereby the stem of the anti-IgE aptamer changes from double-stranded DNA to single-stranded DNA. For this research, the standard anti-IgE aptamer D17.4 has been used as it is well established and more widely used in literature. The D17.4 aptamer will be referred to as ‘anti-IgE’ aptamer for the remainder of this thesis work.

The anti-IgE aptamer has been used with various techniques to develop IgE aptasensors. These techniques include - quartz crystal microbalance,[12] atomic force microscopy,[14] fluorescence polarization,[16] surface plasmon resonance, [17,18] fluorescence [19,20] as well as electrochemical methods such as differential pulse voltammetry[6,21] and square wave voltammetry.[22] Some of the optical IgE aptasensors will be briefly discussed in this section. Electrochemical IgE aptasensors will be discussed in the corresponding section.

Fluorescence based assays involve labelling the aptamer with a fluorescent molecule for IgE detection. Gokulrangan et al. labelled the anti-IgE aptamer with Texas Red at the 5’ end and used fluorescence polarization to study aptamer/IgE binding in a homogenous system. [16] Due to the difference in molecular weight between free fluorophore-labeled aptamer and the fluorophore-labeled aptamer/IgE complex, an increase in anisotropy (degree of polarized emission) was observed. A detection limit of 350 pM was obtained using this method. However, this method is strongly dependent on the type of fluorophore used as well as the temperature. Nevertheless, based on the fluorescence polarization response, the paper also emphasized that the presence of Mg^{+2} in binding buffers is important in aptamer/IgE complex formation. Jiang et al. studied a label-free homogenous aptamer/IgE binding system by monitoring the luminescence signal change of $[Ru(phen)_2(dppz)]^{2+}$ dye, which is intercalated into the stem of anti-IgE aptamer.[19] Upon aptamer/IgE binding, the luminescence signal decreased with increasing concentration of IgE. A further mechanism study suggested that the decrease in luminescence was due to the decrease in the amount of intercalated dye in the presence of IgE. A detection limit of 100 pM IgE was obtained. The paper performed further control experiments to support the hypothesis that the conformation of the anti-IgE aptamer changes in the presence of IgE protein such that the DNA intercalators are released.

Another spectroscopic method, called surface enhanced Raman spectroscopy (SERS) provides a sensitivity that is usually comparable with fluorescence detection.[23] However, SERS has several advantages over fluorimetry such as molecular fingerprinting of a multitude of analytes, excitation at any available wavelength, reduced photo-bleaching, narrow peak width and higher reproducibility.[23] In addition, there is no need for modification with costly fluorophores.

1.3 DNA Hybridization Biosensors:

Deoxyribonucleic acid (DNA) is the largest known molecule with biological activity that is important for all kinds of life.[24] Double-stranded DNA has a double-helix structure that has two strands running in opposite direction.[25] Each chain is a polymer of subunits called nucleotides. A nucleotide is made up of three fundamental units: a heterocyclic base, a five carbon deoxyribose sugar and a phosphate group. A single-strand of DNA has 2 regions – an identical repeating unit of backbone and differing units of bases. The carbon atom number 3' (three prime) of a sugar molecule is connected through a phosphate group of the 5' (five prime) carbon of the next sugar to form the backbone. This covalent linkage is called 3’–5’ phosphodiester bridge. The carbon atom number 1’ (one prime) of each sugar is covalently linked to one of the four possible bases – adenine (A), guanine (G), cytosine (C) and thymine (T). According to the proposed structure of DNA by Watson and Crick, the double helix structure is based on the complementary base pairing between A and T and C and G as shown in Figure 4.[26]

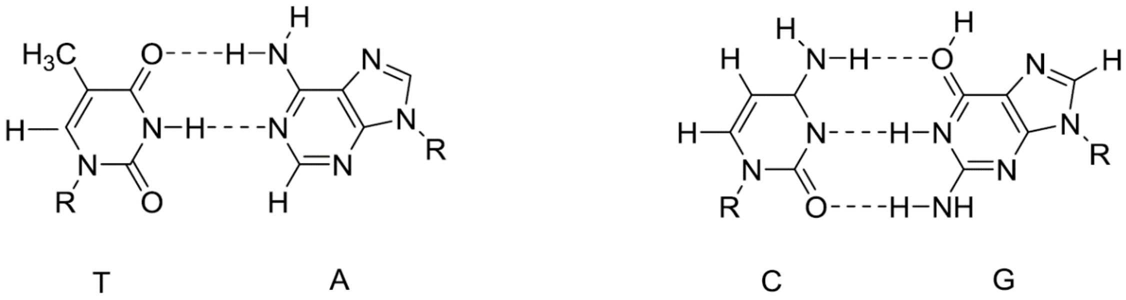

Figure 4: Base-pairing between the four DNA bases: T and A, C and G. [26]

Base pairing between the bases occurs via hydrogen bonds between the carbonyl oxygen and the amino hydrogens in the pairs. The stable dsDNA structures are held together by this hydrogen bonding between base-pairs. Hydrogen bonds can also form between bases within a ssDNA or RNA molecule to form hairpin DNA structures or loops. These are known as the secondary structure of DNA.[25] However, hydrogen bonding in this case depends on the base sequence and the distance of its complementary region on the same strand.[25] Thee major forms of DNA are B-DNA, A-DNA or Z-DNA that differs in helical structures. Most DNA adopts the B-DNA form in living cells. Each of these helical structures differs in their rotational direction and the number of base pairs in each turn. For example, the B form of DNA has right-handed helices and 10 base pairs in each turn. The distance between each turn of the helix is called the pitch. In the helix structure of a DNA, each pitch contains a minor and a major groove where the backbone strands are close together or far apart respectively.

DNA hybridization is the process whereby ssDNA to form a helical dsDNA by complimentary base-pairing. Detection of DNA hybridization between ssDNA (probe) and its complementary DNA (target) is important for developing DNA biosensor technology. Hybridization can be used for analysis and detection of specific DNA sequences, which plays an important role in clinical diagnosis, forensics, environmental analyses, and food safety monitoring.[28] DNA biosensors can also be used to detect mutations in DNA that are the cause of a wide range of genetic diseases.[29] A typical DNA biosensor is prepared by immobilizing a specifically designed ssDNA probe with a known sequence on the sensor surface. The immobilization strategies differ based on the type of surface and modification of the probe. For example, the simplest and most common strategy is covalent attachment where the probe is functionalized with a thiol or disulfide bond.[25] A self-assembled monolayer (SAM) is formed on the surface (i.e. gold electrode) when the oligo modified thiols are reduced at the gold surface to form gold-sulphur bonds:

$$\text{DNA} - \text{SH} + \text{Au} \rightarrow \text{DNA} - \text{S} - \text{Au} + e^- + H^+$$

Other immobilization methods may include physical adsorption and affinity binding via avidin-biotin binding, for example.[25] After immobilization of the probe, the sensor platform is then allowed to interact with the target DNA to form dsDNA. This hybridization event is converted into an analytical signal by the transducer. Such a detection method for hybridization should be able to distinguish between ssDNA and dsDNA. This can be achieved by various detection strategies such as using redox-modified oligonucleotides, or through changes in the physiochemical properties of the sensing layer (i.e. changes in the capacitance).[25,30]] Recently, there has been an increased interest in label-free methods that do not make use of covalently attached label groups for detection. For example, Halas et al. developed a SERS based hybridization detection method by substituting adenine in a surface-immobilized probe with 2-aminopurine.[31] Hybridization is then identified based on the adenine in the target DNA, which gives rise to an adenine SERS peak at 736 cm^{-1}. Similarly, Brosseau et al. developed a label-free direct detection strategy for DNA hybridization using SERS.[26] In this work, the surface immobilized probe contained no adenine nucleotides. However, adenine nucleotides were present in the complementary target. Upon successful DNA hybridization between the probe and the target, SERS peaks of adenine at 1328 and 730 cm^{-1} appeared. Another interesting EC-SERS based approach is that by Bartlett et al.[29] In this case, a binding agent is used that is selective for dsDNA only and acts as a Raman reporter. In this work, the authors explored five different binding agents and concluded that methylene blue (MB) was best for the hybridization assay.

1.4 DNA binding agents (Raman reporters)

There are two broad classes of non-covalent DNA binding agents –intercalators and groove-binders.[32] Non-covalent interactions include hydrogen bonding, electrostatic and van der Waals interactions. Intercalators bind by inserting a planar aromatic chromophore between adjacent DNA base pairs of dsDNA, whereas groove binders fit into the DNA minor groove causing slight changes in the DNA structure. [32] There are a few major modes for reversible binding of such molecules with dsDNA. These are: (i) electrostatic attractions with the anionic sugar phosphate backbone of DNA, (ii) hydrogen bonding to DNA through major groove, (iii) hydrogen bonding and electrostatic interactions with the DNA minor groove, (iv) intercalation between base pairs via the DNA major groove, (v) intercalation between base pairs via the DNA minor groove, and (vi) threading intercalation mode.[32] The three types of interactions are represented in Figure 5. Small organic molecules such as methylene blue (MB) and proflavine (PF) bind to dsDNA via the classic intercalative mode.[32, 33] On the other hand, DNA binding agents with bulky groups tend to intercalate into dsDNA via a threading mode. For example, ethidium bromide (EtBr) and doxorubicin (DOX) intercalate into dsDNA by placing the substituent group into the DNA major or minor groove.[32] Bisbenzimide H 33258 (Hoechst 33258) is another organic dye that binds to dsDNA via the minor groove only.[29]

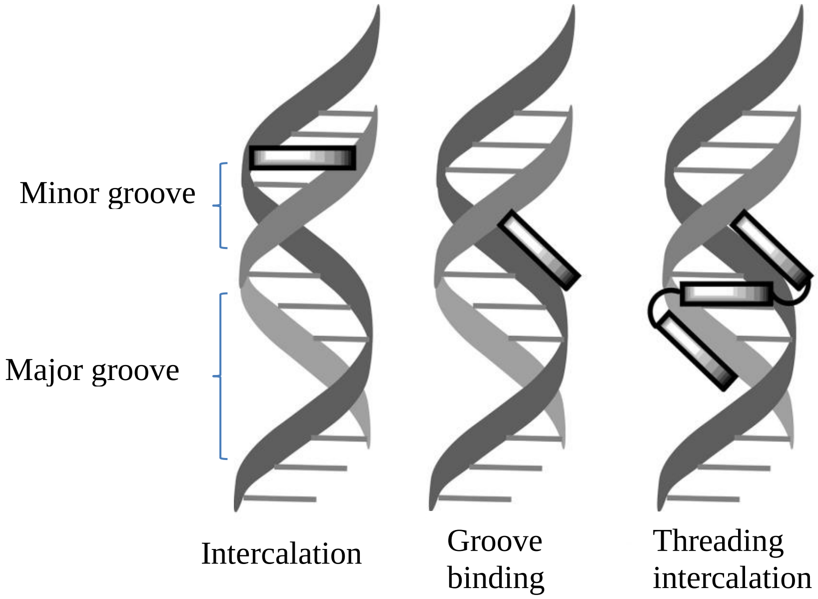

Figure 5: Schematic representation of classical intercalation, groove binding and threading intercalation mode of DNA.[32] Reproduced with permission from Rescifina, A.; Zagni, C.; Varrica, M.G.; Pistarà, V. *Eur. J. Med. Chem.* **2014**, *74*, 95-115. Copyright © 2014 Elsevier Masson SAS.

Methylene Blue (MB) is an organic cationic dye that belongs to phenothiazine family. Traditionally, MB has been widely used as a redox indicator that has a formal potential in the range of -0.10 to -0.40 V (versus SCE) in pH 4 - 11.[32, 34] This potential range is close to the redox potentials of many biomolecules and so it had been used as an electron transfer mediator.[34] In literature, there is inconsistency with regards to the exact binding mode of MB to dsDNA. Bartlett et al. considers that MB has multiple modes of binding, which includes electrostatic interactions with the DNA phosphate backbone, intercalation, minor-groove interaction and binding to guanine bases.[29] He further reported that the binding mode of MB with DNA also appears to be related to the ionic strength of the DNA solution.[29] On the other hand, Rescifina et al. reports in a recent review paper that MB binds to dsDNA via a classic intercalation mode only.[32] In literature, the redox properties of MB has been widely utilized in the development of electrochemical based aptasensors used to detect DNA hybridization. For example, using differential pulse voltammetry (DPV) Kerman et al. observed a higher current when MB was bound to ssDNA as opposed to dsDNA.[35] In contrast, using a SERS based method Bartlett et al. found that MB provided a stronger SERS signal when bound to dsDNA as compared to ssDNA.[29] One possible reason for the differing affinities of MB towards ssDNA and dsDNA among different research groups may be due to the difference in the sequences of probe and target strands used. Bartlett et al. used a probe and a target with A-T (adenine- thymine) rich base pairs, whereas Kerman et al. used a G-C (guanine-cytosine) rich DNA sequence. A review paper by Neto et al., reports that the interactions of DNA binding agents to dsDNA is a sequence-dependent process since the reactive sites present on dsDNA varies accordingly.[36]

Similar to MB, Rescifina et al. reported that proflavine (PF) is also known to intercalate into dsDNA via the classic intercalation mode alone.[32] PF is a heterocyclic organic dye which belongs to the aminoacridine family.[37] PF is reported as a binding agent far less commonly than MB in aptamer-based research to detect DNA hybridization. According to Girousi et al., PF binds to dsDNA in a complicated manner.[33] The paper further reports that the acridine dyes bind to ds-DNA via two different types of interaction. One of the interactions involves a strong binding process where saturation occurs when one dye molecule is bound per 4-5 nucleotides. This stronger binding process was later referred as an intercalation mode binding. A weak binding mechanism occurs at high ratios of dye to DNA, and its limit is reached when one dye molecule is bound per nucleotide. However, the exact process of weak interaction is not mentioned. According to Bereznyak et al. the weaker binding process is via an external binding mode.[37] Grützke et al. employed PF to detect DNA hybridization using electrochemical impedance spectroscopy (EIS) and SERS.[38] In this work, it was found that the PF was specific to dsDNA and bound to it via intercalation. This was concluded based on the disappearance of the SERS peak at 390 cm^{-1} upon intercalation with dsDNA. The SERS peak at 390 cm^{-1} was due to the free $-NH_2$ groups in PF.

Ethidium bromide (EtBr) has been widely known to intercalate into dsDNA quite efficiently.[39, 40] Recently, Miljanic et al. studied the interactions of EtBr with DNA using near infrared SERS.[39] Most of the vibrational modes of EtBr arise from phenanthridinium, which is the intercalating moiety. The comparison among SERS spectra of various concentrations of EtBr indicated that at low concentration (5×10^{-6} M) these EtBr molecules exist as monomers, hence providing relatively stronger and better defined spectra than that at higher concentration. EtBr usually forms dimer at higher concentration because EtBr can self-associate in aqueous solutions due to the planar aromatic structure. The absorption maximum of the EtBr monomers was found to be 480 nm, which shifted to 518 nm after forming a complex with ds-DNA. Minasyan et al. studied EtBr binding with ds-DNA using DPV. [40] The voltammetric studies revealed that at low ionic strength the EtBr molecules bind to DNA via intercalation and electrostatic interactions. At high ionic strength, the binding becomes semi-intercalative and electrostatic interactions. However, according to Rescifina et al., EtBr binds to dsDNA via threading intercalation where the substituent group attached to the intercalating moiety is placed into the major or minor groove of DNA.[32]

Hydroxyldaunorubicin or Doxorubicin (DOX) belongs to the anthracycline family and is one of the most effective anticancer drugs currently in use.[41] In literature, the mechanism of DOX binding to DNA has not yet been fully understood. It is recognized that the tetracyclic region of the DOX can intercalate into the DNA base pairs, and therefore, DOX has been classified as a classical intercalating agent. However, DOX also has a bulky substituent attached to it, which can be placed in the groove of the DNA and therefore it is also considered to be a threading intercalator.[32.41]

Bisbenzimide H 33258, commonly referred as Hoechst 33258 is well known to be a DNA groove binder in the literature. These dyes are widely used as tools for staining DNA and analyzing side population cells.[42] Hoechst 33258 is known to reversibly bind to A-T rich sequences of the minor groove of dsDNA and hence, is very selective towards dsDNA. According to literature it preferentially binds to dsDNA when 4-5 adjacent AT base pairs are present.[42] According to Fox et al. the affinity of Hoechst

33258 varies widely between different arrangements of AT base pairs with highest affinity for AATT and lowest affinity for TATA.[43] Recently, Bartlett et al. used Hoechst 33258 as a DNA hybridization indicator and found it to be completely selective towards dsDNA.[29]

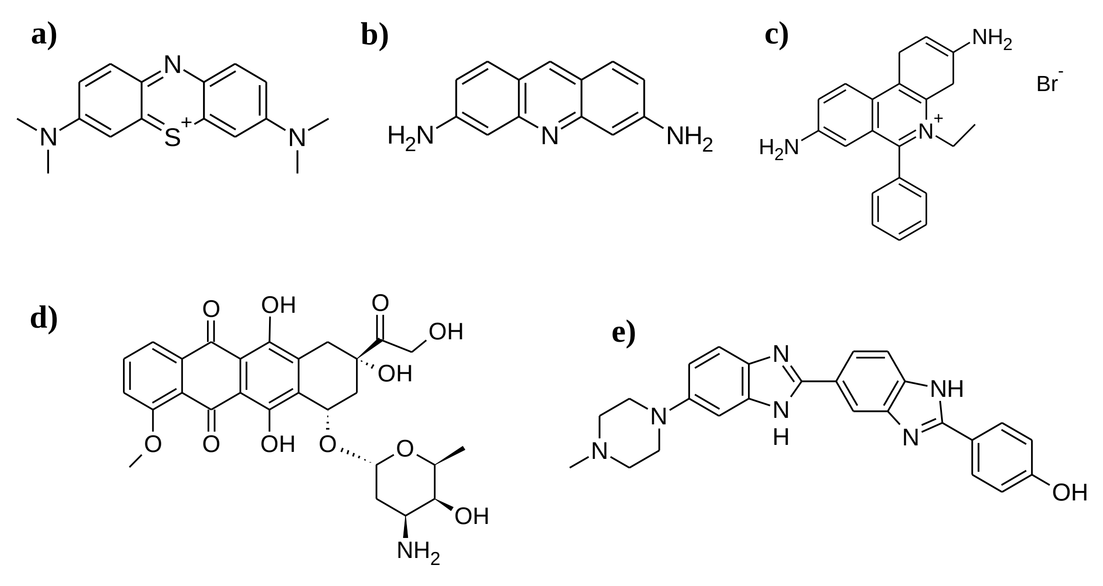

Figure 6: (a) Methylene blue (MB); **(b)** Proflavine (PF); **(c)** Ethidium Bromide (EtBr); **(d)** Doxorubicin (DOX) and **(e)** Bisbenzimide H 33258 (Hoechst 33258).

Based on this literature search, it can be concluded that the interactions of DNA binding agents to dsDNA is dependent on several factors such as the structure of binding agents, various experimental conditions (i.e. pH, ionic strength) and the sequence of the DNA used. Therefore, performing experiments to optimize the binding affinity can be a challenging task. Nevertheless, the flexibility and availability of different binding agents makes the indirect method to detect DNA hybridization simple in comparison to synthetically modifying the DNA probes. Additionally, most of the research articles mentioned previously studied the DNA-dye interactions in aqueous solution only. These interactions may possibly be quite different when the ssDNA or dsDNA are immobilized on a solid substrate. In addition, most indirect methods of detection for hybridization have been limited to MB only. Therefore, exploring different binding agents as a potential DNA hybridization indicator would be beneficial.

1.5 Surface enhanced Raman spectroscopy (SERS)

Raman spectroscopy is a common vibrational technique based on the inelastic scattering (Raman scattering) of monochromatic light, usually from a laser in the visible, near-infrared or near-ultraviolet range of the electromagnetic spectrum.[3,44,45] Light can interact with matter in three ways – the photons that make up the light may be absorbed, emitted or scattered by atoms and molecules.[44] Figure 7 illustrates the energy-level diagram when light is scattered by a molecule. At room temperature, most of the molecules are in ground vibrational state with a much lower population in the first excited vibrational state.[46] The ground vibrational state interacts with a photon, which causes the molecule to be excited to an intermediate level called a virtual state. A virtual state is a transient state and does not correspond to a real energy level of a molecule. In brief, the scattering process can be elastic or inelastic as shown in Figure 7. Elastic scattering, called Rayleigh scattering, is the most probable scattering, where the scattered photon has the same energy as the incident photon. In contrast, inelastic scattering is where the scattered photon has a different energy than the incident photon. Inelastic scattering is a Stokes process when the photon has lost energy to the molecule, and an anti-Stokes process when the photon has gained energy from the molecule. Raman spectra consist of bands that correspond to the vibrational transitions specific to the molecular structure.[44] These spectra provide chemical ‘fingerprints,’ which can be used to identify the analyte molecule. However, since only one in every 10^6 – 10^8 photons are Raman scattered, it is inherently a very weak process.[3,44,45] The weak Raman signal can be greatly enhanced by up to 10^4 – 10^{11} orders of magnitude by having molecular adsorption of the analyte onto a nanostructured noble metal surface (e.g. Au, Ag and Cu).[45] This powerful spectroscopic technique is then called surface enhanced Raman spectroscopy (SERS).

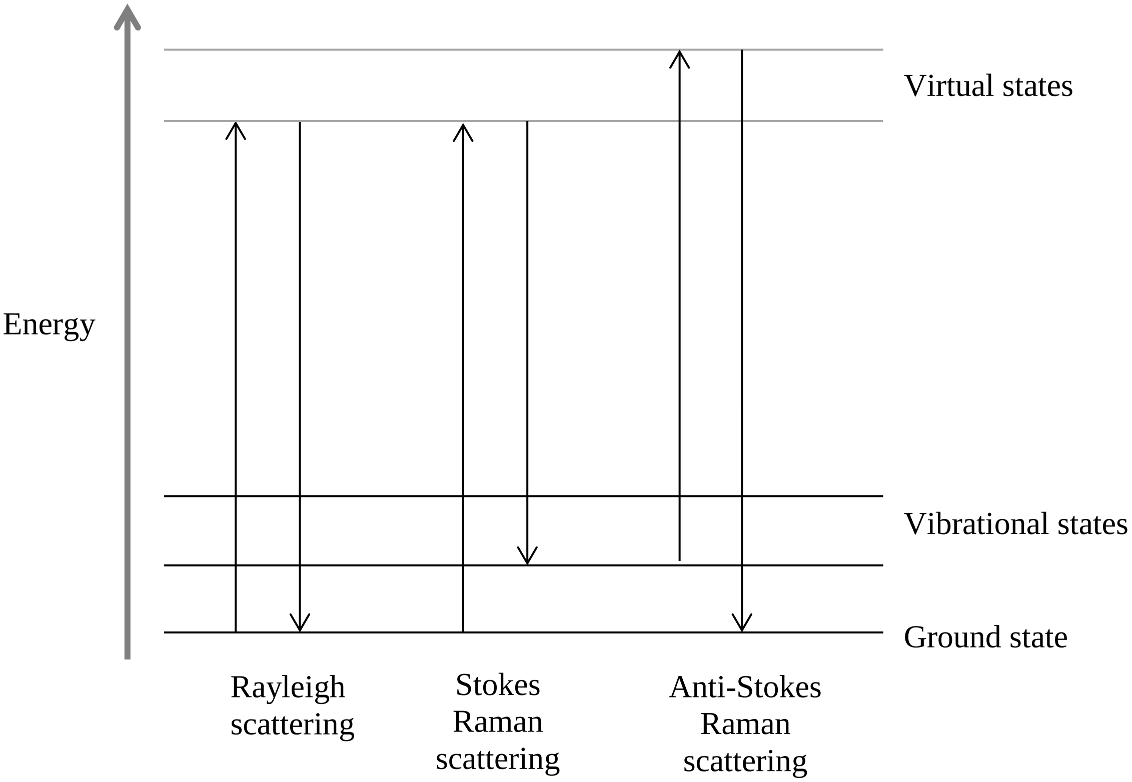

Figure 7: Three different scattering processes – Rayleigh scattering (elastic), Stokes and Anti-Stokes scattering (inelastic).[44]

SERS was initially observed in 1974 by Fleischman et al.[45] The exact mechanism for the enhancement effect is still a matter of controversy in literature.[3] However, there are two likely mechanisms for such dramatic enhancement; an electromagnetic effect and a chemical effect.[3] The electromagnetic effect is due to the presence of a localized surface plasmon resonance (LSPR) on noble metal nanostructures, whereas the chemical enhancement effect relies on the charge transfer interaction between the adsorbed molecule and the metal surface. Some of the main features of the SERS technique include high sensitivity, non-destructive nature, and fluorescence-quenching properties of the metal surface. In order to have reproducible SERS spectra, it is important that a uniform nanostructured SERS substrate is used and that analyte molecules are brought as close as possible (ideally within a few nanometers) to the substrate. This distance dependence is a unique feature of the electromagnetic enhancement.[46] Studies have shown that the optimal detectable distance of an analyte from a SERS active substrate is within ~ 100 Å (10 nm).[46]

Most of the SERS-based aptasensors developed this far make use of this distance-dependence signal for detection, as well as the conformational changes of certain aptamers upon target binding. Cho et al. developed a SERS based aptasensor for the detection of thrombin with a detection limit of 100 pM.[47] In this work, a methylene blue (MB) labelled thrombin aptamer was used, which is adsorbed onto a gold nanoparticle substrate. In the presence of thrombin, the aptamer changed conformation and was displaced from the surface. This displacement reduced the SERS intensity of MB peaks and hence, with increasing concentration of thrombin the signal intensity decreased accordingly. Similarly, Chen et al. developed a SERS based aptasensor for cocaine detection where the aptamer was labelled with terminal tetramethylrhodamine (TMR).[48] However, in this case, the TMR labelled region of the aptamer came in close proximity to the SERS-active surface upon binding to cocaine, hence increasing its SERS intensity. A detection limit of 1μM was achieved. Both of these methods involved covalent labelling of the aptamer, which can have some drawbacks. For example, the labelling position has to be done carefully in order to avoid any interference with the aptamer folding in the presence of target analyte.[25]. Such modification of aptamers may affect their target affinity as well as stability. Another example of a SERS-based aptasensor for thrombin is that by Hu et al., which utilized the change in electrostatic interaction between the aptamer and crystal violet (CV) molecules.[23, 49] In the absence of thrombin, the electrostatic effect of the hairpin aptamer (immobilized on a SERS substrate) created a barrier between the CV molecules and the surface. This gave rise to weak SERS spectra of the CV molecules. However, the aptamer conformation changed upon binding with thrombin, which weakened this electrostatic barrier and hence, allowed more CV molecules to reach the SERS active surface. This resulted in a strong SERS signal with a detection limit of 20 pM. However, most of the development of SERS based aptasensors have been focused towards the detection of thrombin, cocaine, adenosine and Hg^{2+}.[23] The development of a SERS-based aptasensor for detection of IgE has not yet been explored. This is possibly because non-heme protein gives weak Raman/SERS spectra unlike heme/conjugated protein.[50] Hence, indirect strategies to detect IgE may be useful.

SERS can be coupled with electrochemistry, which is then called EC-SERS.[51] EC-SERS can provide meaningful information on adsorption behavior, orientation and redox behavior. This technique has been used to detect DNA hybridization [29] as well as for diagnostic purposes. For example, Brosseau et al. has recently employed EC-SERS to detect melamine and uric acid.[51] Additionally, this group has recently developed an EC-SERS based aptasensor for direct detection of cytochrome c protein.[4] In this work, anticyt c aptamer was immobilized on a silver nanoparticle substrate. On adding cyt c protein, it bound to the aptamer and gave rise to cyt c peaks when a negative potential was applied to the electrode. A spacer was added to avoid any non-specific binding of the protein. Unlike cyt c protein, such direct detection of non-heme protein IgE was not possible as it gave rise to a weak Raman/SERS spectrum.[4] Therefore, an indirect method needs to be explored to develop IgE aptasensor using EC-SERS. A literature search reveals that this spectroelectrochemical technique has not been used for aptasensor development by other research groups. However, electrochemical techniques have been widely used for aptasensor in various research papers. One such method will be discussed in the next section.

1.6 Differential pulse voltammetry (DPV):

Differential pulse voltammetry (DPV) is an electrochemical technique where the potential is applied as a ramped square wave.[52] In this technique, small pulses of constant amplitude are superimposed upon a staircase wave and the current is sampled twice in each pulse period. As shown in Figure 8a, the current is sampled prior to the pulse at point 1 and again before the end of the pulse at point 2. The difference in current per pulse is recorded as a function of the linearly increasing voltage. This results in a differential curve where the height of the peak is directly proportional to the analyte concentration as depicted by Figure 8b. The potential amplitude of the pulse (ΔE pulse) is typically of the order of 50 mV and the potential step (ΔE step) is 10 mV or less.[53] The timescale of the pulse is usually in the range of 5 to 100 ms and the duration of the whole step is typically 0.5 – 5 s. [53] This voltammetric method has an increased sensitivity compared to other voltammetric methods. The greater sensitivity in DPV is due to an enhancement of the Faradic current relative to the capacitive current. Faradic current is associated with the transfer of electrons resulting from the oxidation or reduction of electroactive species of interest.[54] Capacitive background current arises as oppositely charged ions from the supporting electrolyte forming a layer near the electrode (double layer charging).[54] This leads to a capacitive arrangement in the cell, which charges and discharges as the electrode potential is varied. Generally, the capacitive currents relax within 1 or 2 milliseconds, which is faster than the Faradic current.[53] Therefore, DPV provides a lower limit of detection and the signal-to-noise ratio is larger as compared to traditional cyclic voltammetry. These advantages of DPV make it a common electroanalytical technique in biosensor development.

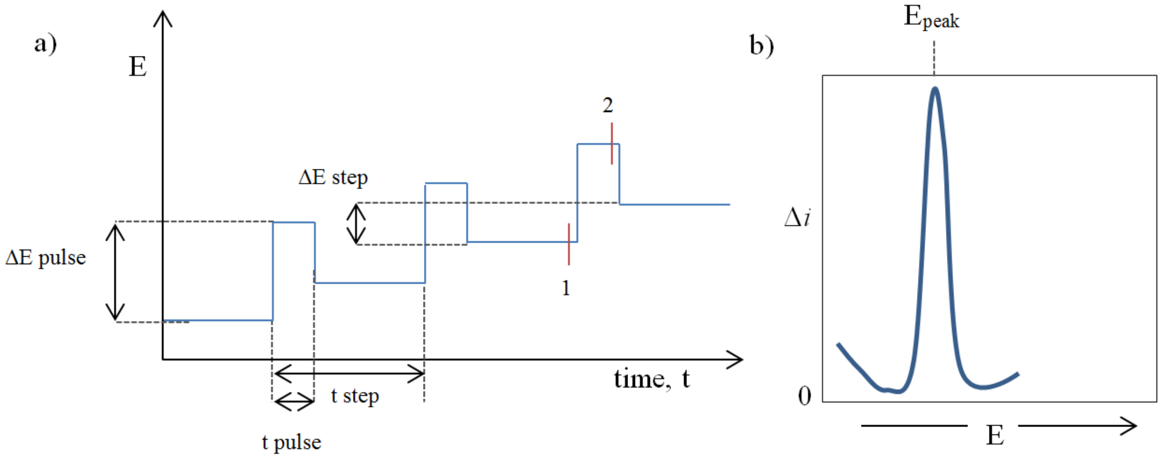

Figure 8: (a) Potential waveform for differential pulse voltammetry (DPV);[53] **(b)** Typical voltammogram for differential pulse voltammetry.[52]

Another common voltammetric technique is square wave voltammetry (SWV). The potential waveform of SWV is similar to DPV. In this case, the difference in current between the forward and reverse pulse is plotted as a function of potential. Lee et al. and S. Khezrian et al. utilized voltammetric techniques for developing an IgE aptasensor. Lee et al. used methylene blue (MB) as a redox indicator with square wave voltammetry to develop a sandwich type assay.[22] The anti-IgE aptamer was first immobilized on the gold nanoparticle modified electrode. This electrode was immersed in a solution where competition to bind with the aptamer took place between IgE and a specially designed detection probe. This designed detection probe is guanine rich and has a complementary sequence to the anti-IgE aptamer. When the IgE concentration is high, fewer guanine-rich detection probes would be bound to the aptamer and vice versa. MB was then introduced, which specifically binds to the guanine rich detection probe, and SWV was performed. Therefore, in the presence of IgE, the electrochemical signal due to MB was low since fewer guanine-rich detection probes bound to the anti-IgE aptamers. The MB peak increased when no IgE was present since more guanine-rich detection probe binds to anti-IgE aptamers. The limit of detection of IgE was determined to be 0.16 pM. Similarly, S. Khezrian et al. immobilized anti-IgE aptamer on a modified carbon electrode.[6] Methylene blue (MB) was then intercalated into the aptamer, which acts as an electrochemical indicator for DPV. On formation of the aptamer/IgE complex, the intercalated MB is released and hence, a decrease in peak current of MB is observed. The estimated detection limit of the IgE in this case was 37 nM. This method is quite simple and straightforward compared to those that involve a covalently labelled aptamer, or a complicated fabrication assay.

1.7 Target protein: Human Immunoglobulin E (IgE)

Human Immunoglobulin E (IgE) is a protein antibody that is released in response to Type I hypersensitivity reactions.[55,56] Type I hypersensitivity occurs very rapidly after exposure to common allergens such as certain foods, pollens, drugs, insect venoms, dust mites, mold spores, and animal hair/dander.[55] The typical symptoms of type I hypersensitivity reactions include allergic rhinitis, asthma, dermatitis, urticarial, gastrointestinal reactions and life-threatening systemic anaphylaxis.[55,56] The total IgE level in human serum is used as a biomarker for such hypersensitivity reactions. In healthy people, the IgE concentration in human serum is extremely low, in the range of about 0.3-0.12 µg ml^{-1}.[56] In allergic patients, the IgE concentration increases to over 10 times the normal level, and is found to be greater than 1.08 µg ml^{-1} at an early stage of an allergic reaction.[22,56] Skin tests, including intradermal and scratch tests are usually performed for initial allergy testing.[55,57] These tests are cheap, sensitive, easy to perform and provide immediate results.[55] However, skin tests cannot be performed on sites in which patient has developed active dermatitis. Skin tests are unresponsive when the patient is taking allergy medications.[55] Also, skin tests can sometimes induce large local reactions or, rarely, severe systematic allergic reactions.[55]

Currently, the majority of allergy testing is based on the antibody receptor.[58] Anti-IgE antibodies are used in clinical IgE tests, which include the radioimmunosorbent test (RIST) and radioallergosorbent test (RAST).[55] RIST is used to quantify the total serum IgE, whereas RAST is used measure allergen-specific IgE levels. These methods are relatively less sensitive, more expensive and time-consuming than skin tests. The commercially available allergy testing kits for quantification of IgE in human serum is based on a traditional sandwich based enzyme-linked immunosorbent assay (ELISA).[58,59] The minimum detectable concentration using such an assay was estimated to be 12 ng ml^{-1}.[58] Kreuzer et al. developed an ELISA based competitive immunoassay for detecting IgE in blood samples using anti-IgE antibodies.[57] This method incorporated disposable screen-printed carbon electrodes and amperometry to detect IgE concentrations as low as 0.09 ng ml^{-1}. Besides the ELISA method, several other researchers have focused on using an anti-IgE antibody based bioassay for IgE detection. Su et al. used a surface plasmon resonance sensor to detect human IgE by immobilizing the anti-IgE antibodies on a gold electrode.[59] This sensor could detect IgE in a linear range from 12 - 720 ng ml^{-1}. However, all of these methods make use of antibodies as probes for protein detection, but the use of antibodies has several limitations. For example, antibodies are sensitive to temperature and humidity, and are prone to irreversible denaturation.[2] As well, the production of antibodies often involves animals, and there can be significant batch-to-batch variation.[2] Therefore, development of new non-antibody based methods to detect IgE protein is still desirable.

Chapter 2: Materials and Methods:

2.1 Reagents:

Thiolated DNA aptamers (Probe 1, Target 1, scrambled Target 1) were purchased from Integrated DNA Technology (IDT) (Table 1). Auric chloride (99.999%, $HAuCl_4$), silver nitrate (99.9995%, $AgNO_3$), sodium borohydride (99%, $NaBH_4$), sodium fluoride (99.99%, NaF), proflavine (95%, PF), 11-mercapto-1-undecanol (11-MUD) and 6-mercapto-1-hexanol (99%) were all purchased from Sigma Aldrich (St. Louis, MO). Purified human Immunoglobulin E (IgE) of ≥99% purity from serum (Myeloma, kappa & lambda) was purchased from Scripps Laboratories (San Diego, CA, USA). Methylene Blue (60-100%, MB) was purchased from Anachemia Canada and sodium citrate (≥99%, $Na_3C_6H_5O_7$) was purchased from ACP chemicals (Montreal). Citric acid (99+%) was purchased from Alfa Aesar (Wardhill, MA). Doxorubicin hydrochloride (98.0 – 102.0%) and bisbenzimide H 33258 (≥98.0%) were purchased from Sigma Aldrich. Ethidium bromide was generously provided by Dr. Timothy Frasier. All solutions were prepared using Millipore water (>18.2 MΩ.cm). K_2HPO_4 (≥98.0%) was purchased from Anachemia Canada (Montreal, QC, Canada). KH_2PO_4 (≥99.0%) and trisodium citrate (≥99.0%) was purchased from ACP Chemicals (Montreal, QC, Canada). The glassware was cleaned in an acid bath prior to experiments. Some glassware (involving AuNP preparation) was cleaned in bath of aqua regia solution (HCl/HNO_3, 3:1). Screen-printed carbon electrodes (SPEs) were purchased from Pine Research Instrumentation (Durham, North Carolina USA). Special care should be taken in handling and disposal of DNA intercalating molecules MB, PF, EtBr, DOX and bisbenzimide H 33258 (Hoechst 33258), which are potential carcinogens. Refer to material safety data sheet (MSDS) for details on handling and disposal.

Table 1. The sequence for Probe 1, Target 1, scrambled Target 1 and anti-IgE aptamers.

Aptamer	**Sequence**
Probe 1	5'- /5ThioMC6-D/TCC TGG GCT GGC GGG TCG CTT CC -3'
Target 1	5'-GGA AGC GAC CCG CCA GCC CAG GA -3'
Scrambled Target 1	5'-ACC GAG CCA CGC AGC CAG GGC AC-3'
Anti-IgE	5'-HO-$(CH_2)_6$-S-S-$(CH_2)_6$- GGG GCA CGT TTA TCC GTC CCT CCT AGT GGC GTG CCC C-3'

5'- /5ThioMC6-D – 5' Thiol Modifier C6 S-S

2.2 Instrumentation:

2.2.1 Raman Spectroscopy:

All spectral data for experiments were collected using a DXR Smart Raman spectrometer with a 180 degree sampling accessory manufactured by Thermo Fisher Scientific Inc. (Madison, WI, USA). The laser wavelength can be changed between visible 532 nm (diode-pumped, solid state) and near-infrared 780 nm (frequency-stabilized single mode diode laser). The high-resolution grating has a range of 1800-50 cm^{-1}, with a spectral resolution of 3.0 cm^{-1}. The 532 and 780 nm lasers have power ranges of 1-10 and 10-150 mW, respectively. In these studies, Au/Ag modified screen printed electrodes were used as substrates for Surface-Enhanced Raman Spectroscopy (SERS). For this project, only the 532 nm laser with power at 3 mW was used with an acquisition time of 30 s to avoid any possibility of photo-bleaching. All the spectra collected were analyzed using Origin 9.0 software.

2.2.2 Potentiostat/ Galvanostat:

Electrochemical (EC) measurements for experiments were performed using a WaveNow USB Potentiostat / Galvanostat produced by Pine Research Instrumentation (Durham, NC, USA). The instrument connects to a standard computer (PC). The software for setting electrochemical parameters is Aftermath Data Organizer (version 1.2.4361), also produced by Pine Research Instrumentation. The SPEs electrodes were used with the potentiostat. These SPEs have a circular carbon working electrode (2 mm diameter); Ag/AgCl reference electrode, and a carbon counter electrode. Electrochemical methods such as EC-SERS were performed using this USB potentiostat. This potentiostat was used to conduct both EC-SERS and DPV experiments.

2.2.3 Electrochemical SERS setup

Electrochemical SERS (EC-SERS) set up was made by combining the Raman spectrometer with the potentiostat. The Raman laser is focused on the modified working electrode of a SPE in the electrochemical small-volume cell. Raman spectra can then be collected at the desired applied potential. The potential was applied from 0.0 V to – 1.0 V at 0.1 V increments (cathodic direction). The potential was then returned from -1.0 V to 0.0 V (anodic direction). At each potential, a spectrum was collected for a time interval of 30 s. The supporting electrolyte used for EC-SERS was a deaerated 0.1M NaF solution. A diagram of the electrochemical SERS setup is shown in Figure 9.

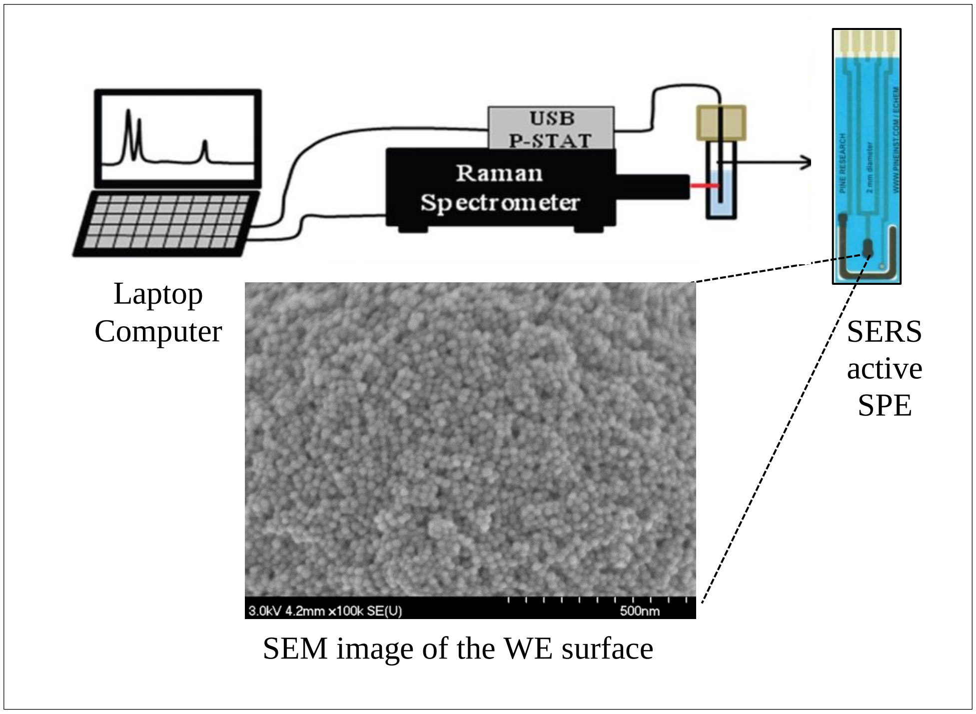

Figure 9: Schematic setup of the electrochemical surface enhanced Raman spectroscopy setup. The inset shows an SEM image of the Au/Ag deposited onto the working electrode of a disposable screen printed electrode.[53, 62]

2.2.4 Differential pulse voltammetry (DPV) and cyclic voltammetry (CV)

The DPV voltammogram was collected within the potential range from 0.0 V to -1 V. The potential amplitude (ΔE pulse) was 25 mV with a step potential (ΔE step) of 5 mV. The supporting electrolyte was phosphate buffer at pH 7.4. The overlay of voltammograms was plotted using Aftermath Data Organizer (version 1.2.4361).

Cyclic voltammetry was conducted to assess the quality of the SPEs and to characterize the redox potential of the Raman reporters within the potential window of 0.0V to -1 V. The supporting electrolyte was 20 μM Raman reporter prepared in phosphate buffer at pH 7.4.

2.2.5 Signal processing

Raman spectral data were processed using Origin 9 software, produced by OriginLab Corporation (Northamton, MA, USA). Data from the Raman spectrometers were saved as a .CSV (comma-separated values) file type, and imported into Origin. All spectra were normalized for both laser power and acquisition time for ease of data comparison. All spectra were smoothed using adjacent averaging method with 9 points of window. CV and DPV data were also plotted using Origin 9 software. The data were copied from the electrochemical software (Aftermath) into Origin 9. To resolve different overlapping SERS peaks in a spectrum (composite spectrum), the Multi-Component Search tool of the Thermo Scientific OMNIC specta software was used. For this purpose, first a library of SERS spectra for Probe 1, Target 1, 11-MUD and different Raman reporters at OCP cathodic, -1.0 V and OCP anodic were created. Based on this spectral library, OMNIC Specta software delivers a mathematical combination of reference spectra that best describes the overlapping composite spectrum, and provides a composite value. The composite value is a scaling factor indicating the amount of each found reference represented in the composite spectrum. For example, a composite value of 55% means the component contributes 55% of the total. However, this does not necessarily mean the sample mixture contains 55% of that component.

2.3 Biosensor Preparation:

Gold/silver nanoparticles were prepared according to a literature method.[60] This method is described below.

2.3.1 Preparation of Gold Nanoparticles (AuNP):

Briefly, 100.0 mL of aqueous $HAuCl_4$ (0.25 mM) solution in a 250 mL three-necked flat bottom flask is brought to boil under reflux and magnetic stirring. Then, 1 mL of 5% sodium citrate solution is added. The reaction solution is allowed to boil for about 20 min until the solution is wine red in color. The colloidal gold nanoparticles are then cooled to room temperature. The maximum absorption peak of the colloidal gold nanoparticle suspension is ~520 nm.

2.3.2 Preparation of Silver Nanoparticles (AgNP):

Briefly, 1 mL of $AgNO_3$ solution (0.1 M), 3.4 mL of aqueous sodium citrate (0.17 M) and 0.6 mL of citric acid (0.17 M) is added into a 250 mL three-necked flat bottom round flask with 95 mL water. Then, 0.2 mL of freshly prepared sodium borohydride solution (0.1 mM) is added into the above mixture at 25 ˚C under magnetic stirring. The mixture is allowed to stand for 1 minute at 25˚C and then brought to boil within 20 min under reflux and magnetic stirring. After boiling for 1 h, the colloidal silver nanoparticle suspension is cooled to room temperature in air. The maximum absorption peak of the colloidal silver nanoparticle suspension is ~392 nm.

2.3.3 Preparation of Au/Ag SERS-active substrate:

The AuNP colloidal suspension obtained from above procedure is centrifuged at 8000 rpm for 20 minutes. The supernatant is then be removed and discarded, and the pellet in each Eppendorf tube is collected together and centrifuged again at 8000 rpm for 20 min to obtain the gold concentrate. The AgNP colloidal suspension is centrifuged in the same manner as above to obtain silver concentrate (silver atom concentration of 0.4

M). Au/Ag substrates were prepared by drop-coating in 1.8 µl aliquots of 3 layers of gold concentrate followed by 1 layer of silver concentrate onto the carbon working electrode of SPEs. The electrodes were allowed to dry for at least 20 minutes after drop-coating each layer.

2.3.4 Fabrication of the Au/Ag modified substrate:

Fabrication of the Au/Ag modified substrates were performed according to the literature.[26] On the Au/Ag modified substrate, 1.8 µl of probe 1 (2 mM) was drop-coated followed by overnight air drying. The probe modified electrode was incubated in 1 mM of 11-MUD solution for 2 h, followed by gentle rinsing with ethanol (Probe 1+ 11-MUD). Once air dried, 1.8 µl of Target 1 (4 mM) was drop-coated on this substrate and left overnight to allow hybridization to occur, after which it was rinsed well and air dried (Probe 1+ 11-MUD + Target 1). Probe 1+ 11-MUD (ssDNA) immobilized Au/Ag substrate and Probe 1+ 11-MUD + Target 1(dsDNA) Au/Ag substrate were then incubated in 20 µM of Raman reporter solution for 10 minutes while stirring followed by well rinsing with Millipore water. The solutions for all Raman reporters were prepared in phosphate buffer solution at pH 7.4.

For spacer studies by coadsorption method, 1 mM of different volume of 6-MCH and 11-MUD were used to prepare 0%, 20%, 40%, 80% and 100% mole percent of 6-MCH solution. A total volume of 5 mL was used. For all spacer studies, target 1 was replaced with scrambled target 1.

Chapter 3: Results and Discussion

3.1 Characterization of Raman reporters

The Raman reporters selected for this study were mainly characterized by SERS, EC-SERS and CV. Normal Raman spectra were collected for MB and PF powder in order to determine the optimal excitation wavelength. The normal Raman data is helpful for the interpretation of SERS data. In addition, a comparison between the normal Raman bands and SERS bands can reveal the type of mechanism of molecular adsorption on the metal surface. The SERS spectrum of physisorbed molecule is almost the same as that of free molecule and therefore, correlates well with the normal Raman.[61] A large difference between the two spectra indicates that chemisorption has taken place as the molecule is bonded to metal surface.[61] Normal Raman spectra were not collected for DOX, EtBr and BBIH due to the limited amount of sample available. Nevertheless, SERS spectra for all the Raman reporters were collected to find out if these were sufficiently SERS active at 532 nm without considerable background fluorescence. These SERS spectra will serve as the reference for interpreting the EC-SERS results.

Based on previous research in our lab, Au/Ag modified electrodes were chosen as the SERS substrates since these have nanoscale surfaces which are uniform in size, shape and distribution.[60] This is one of the important aspects of performing any SERS/EC-SERS experiment as otherwise reproducible signals cannot be obtained. The SERS effect becomes stronger if the frequency of the excitation laser is in resonance with the main absorption band of the molecule. This is called surface-enhanced resonance Raman scattering, SERRS. In order to predict if the enhanced SERS signal observed were due to resonance enhancement of the Raman reporters, the maximum absorbance values for the Raman reporters were referenced from literature in the corresponding section.

EC-SERS spectra were also collected to observe any potential-induced changes in peak intensity. The change in SERS signal on varying potential arises due to changes in surface coverage or the orientation of the adsorbed reporters.[62] It can also be due to redox activity of the adsorbed species, change in bonding interaction with the surface or manifestation of charge-transfer (CT) mechanism on applying potential. A change in bonding strength may affect the geometric and electronic structure of the adsorbed molecule, which in turn results in change in spectral feature.[62] In case of CT mechanism, applying potential may affect the electronic states of metal and molecule, which may cause a charge transfer from metal to molecule or molecule to metal depending on the excitation wavelength. The Raman surface selection rule states that most intense bands in Raman spectra are associated with a vibrational mode that has a component of the polarizability tensor in a direction perpendicular to the surface.[29] Vibrational modes that have a polarizability tensor parallel to the surface give rise to weaker bands in SERS spectra.[29] Specifically, for a molecule adsorbed flat on the surface, its out-of-plane bending modes will be more enhanced when compared with its in-plane bending modes, and vice-versa when it is adsorbed perpendicular to the surface. CV data were collected in order to probe the redox behaviour of the reporters within the specified potential window of 0.0 V to -1.0V vs. Ag/AgCl. A qualitative assessment of the waveshape and peak potential separation of the voltammograms would reveal if the redox process is reversible, irreversible, or quasi-reversible.[53, 63] The waveshape for a reversible redox couple appears sharper than that for an irreversible redox couple. The peak potential separation for a reversible couple can be found by the following equation 1:

$$\Delta E_p = E_{p,a} - E_{p,c} = 0.059/n \text{ V} \quad [1]$$

where ΔE_p is the peak-to-peak separation (unit voltage, V), $E_{p,a}$ and $E_{p,c}$ are anodic and cathodic peak potentials respectively, and n is the number of electrons transferred. The ΔE_p value for a one-electron transfer at 25°*C* should ideally be about 59 mV. A value greater than 59 mV suggests that the electron transfer is either irreversible or quasi-reversible. The potential peaks and the nature of the redox processes would be important for any future investigations using differential pulse voltammetry.

3.1.1 Methylene Blue (MB)

The normal Raman for the MB powder was collected using both visible 532 nm and the near-infrared (NIR) 780 nm excitation in order to determine which was optimal for signal collection. The overlay of the normal Raman spectra for MB collected at both wavelengths is shown in Figure 10. It was found that 532 nm wavelength excitation was more suitable as the spectrum obtained was less noisy, and displayed more distinct and intense peaks compared to the spectrum at 785 nm. Signal is better at 532 nm because the radiation is higher in energy. Once the Raman spectra were collected, band assignments were completed using literature sources. The peak assignments of MB are provided in Table A-1. It can be seen that most of the strong Raman bands are from the phenothiazine aromatic moiety of the reporter.

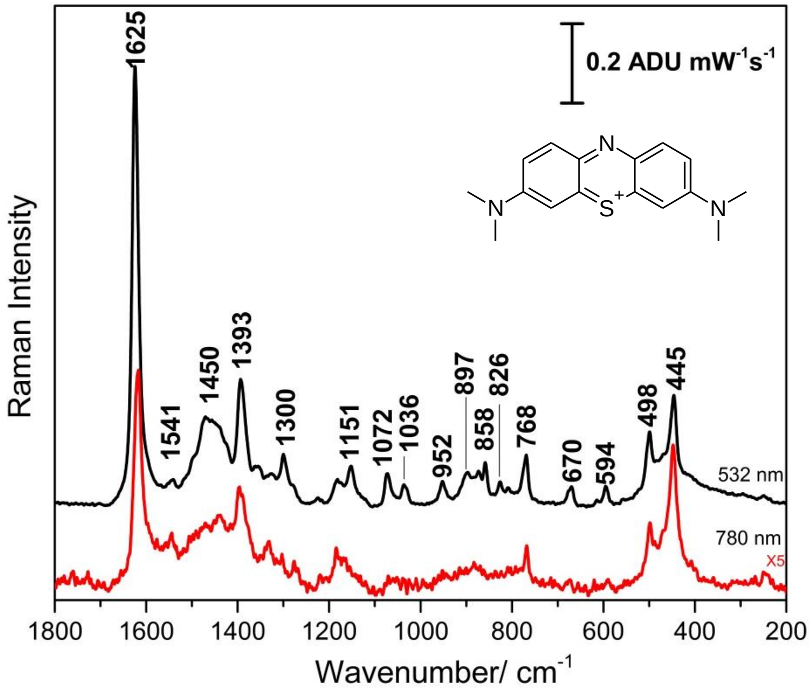

Figure 10: Comparison of Normal Raman spectra of methylene blue powder at 532 nm and 780 nm laser excitation. For 532 nm laser excitation: power 10 mW, collection time

40 s. For 780 nm laser excitation: power 20 mW, collection time 40 s; 780 nm spectrum is multiplied by 5 for ease of visual comparison.

The CV collected for MB using a Au/Ag electrode shows a cathodic peak on the forward scan at about -0.48 V due to reduction of MB (Figure 11a). However, no obvious anodic peak is observed during the reverse scan. This redox behaviour suggests that the reduced products formed during the forward scan did not completely oxidize in the reverse scan. Since the redox reaction involves two-electron transfer, it was expected that the CV will give rise to two peaks in cathodic and anodic direction. The irreversible redox behaviour can be due to limitation in mass transport whereby the reduced species form a film on the surface. This finding is consistent with the literature, which suggests that two cathodic peaks occur at -0.270 V and -0.365 V vs SCE, and that the electrochemical reduction is partially controlled by mass-transport limitations.[64] According to literature, the redox equation of MB is as follows[29]:

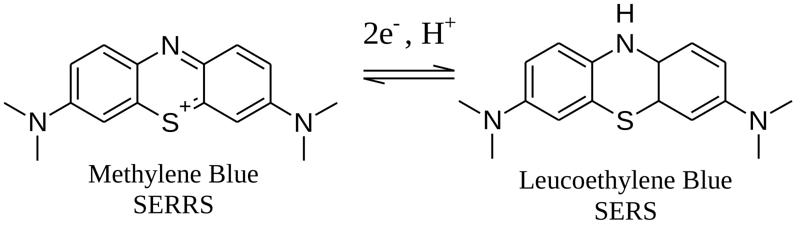

Scheme 1

The EC-SERS of MB in Figure 11b shows that the intensity of strong peaks of MB reduces gradually on applying negative potential until the peaks nearly disappear at -0.6 V. Interestingly, these peaks reappear with weaker intensity on reversing the applied potential in the positive direction (Figure A-1). At -0.6 V, some peaks disappear completely at 1073, 859, 501 and 447 cm^{-1}, which are due to the asymmetric stretch of (C-S-C), (C-H) bending and (C-N-C) skeletal deformation respectively. Other MB peaks can be observed with significantly reduced intensity at this potential. Such changes in bands on approaching -0.6 V suggest that the reduced product LMB is present on the surface. This reversible disappearance of the peaks on changing potential is also consistent with literature, where the disappearance of SERS peaks is attributed to the switching between resonant and non-resonant forms of MB and LMB.[29] It can also be seen by comparing the scale bar that the EC-SERS of MB at open circuit potential (OCP) potential is significantly enhanced compared to the normal Raman in Figure 10. Additionally, there are not any significant shifts in the Raman and SERS peaks. However, a new peak at 250 cm^{-1} appeared at OCP, which is indicative of either (Ag-S) or (Ag-N) stretching in the thiazine ring of the molecule. It is more likely that the S atom would preferentially bind to Ag according to the HSAB theory, which states that hard acids react preferentially with hard bases whereas soft acid with soft bases. Ag is a soft acid and S atom is a soft base. The interaction between a soft acid and soft base is mostly covalent in nature, whereas hard acid and hard base interaction is mostly ionic in nature.[65] Additionally, MB has a positive charge on the S atom of the phenothiazine ring at pH 7.4.[64] Therefore, the S atom is likely to interact with the surface via electrostatic interactions.

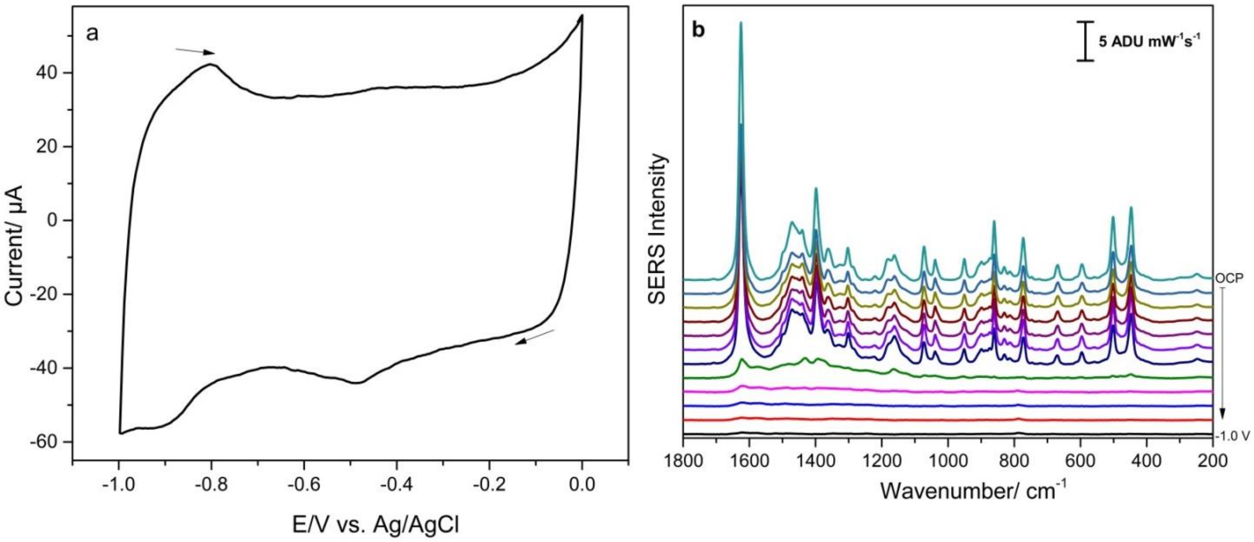

Figure 11: (a) Cyclic voltammogram of bare Au/Ag modified electrode in supporting electrolyte containing 20 μM MB in phosphate buffer (pH 7.4). Arrows indicate the scan direction; **(b)** EC-SERS signal of MB (1 mM) drop-coated on a Au/Ag modified SERS substrate, collected using 532 nm laser excitation at 3 mW for 30 s, at the cathodic direction in 0.1M NaF supporting electrolyte.

3.1.2 Proflavine (PF)

The normal Raman of PF powder collected at 532 nm excitation shows several intense and distinct peaks of PF as shown in Figure 12a. According to literature, the maximum absorption wavelength of PF is 438 nm.[66] Even though 532 nm wavelength excitation is quite close to the emission wavelength of PF (511 nm), no significant fluorescence background was observed. The peak assignments of PF are provided in Table A-2. The CV of PF does not show any obvious redox activity but a slight increase in current can be seen at about -0.4 V in the forward scan in Figure 12b. This is also consistent with the EC-SERS of PF in Figure 13 where no significant change is observed in peak intensity at around -0.4 V. Therefore, it is likely that no redox activity for PF is expected to occur in the potential window between 0.0 V to -1.0 V on this electrode surface. This is consistent with the literature where CV using a carbon paste working electrode gave rise to two poorly separated peaks at 0.94 V and 0.19 V vs Ag/AgCl.[33] These peaks correspond to the oxidation of the amino groups of PF and redox behaviour of the oxidation products respectively.[33] The EC-SERS in Figure 13 shows that minor changes in SERS intensity at 1463, 1391, 592 and 345 cm^{-1} which are due to (N-H) vibration and skeletal vibrations of the (C-N-C) in the acridine ring. Minor changes in relative intensity indicate changing orientation of the molecule on surface as applied potential is changed.

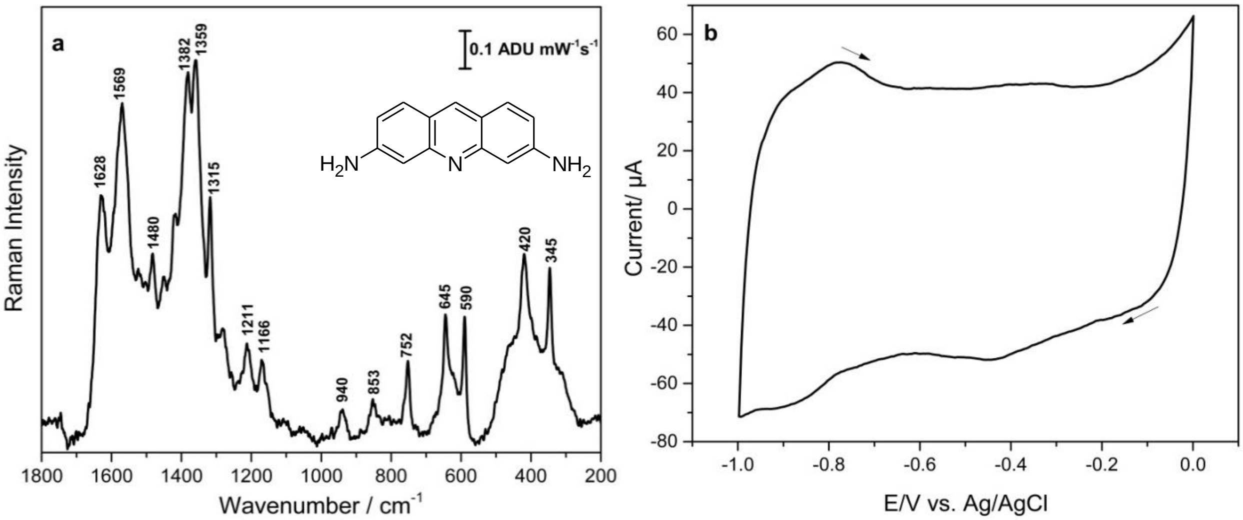

Figure 12: **(a)** Raman signal of proflavine powder collected using 532 nm laser excitation at 10 mW for 40 s; **(b)** Cyclic voltammogram of the Au/Ag modified electrode in a supporting electrolyte containing 20 μM PF in phosphate buffer (pH 7.4). Arrows indicate the scan direction.

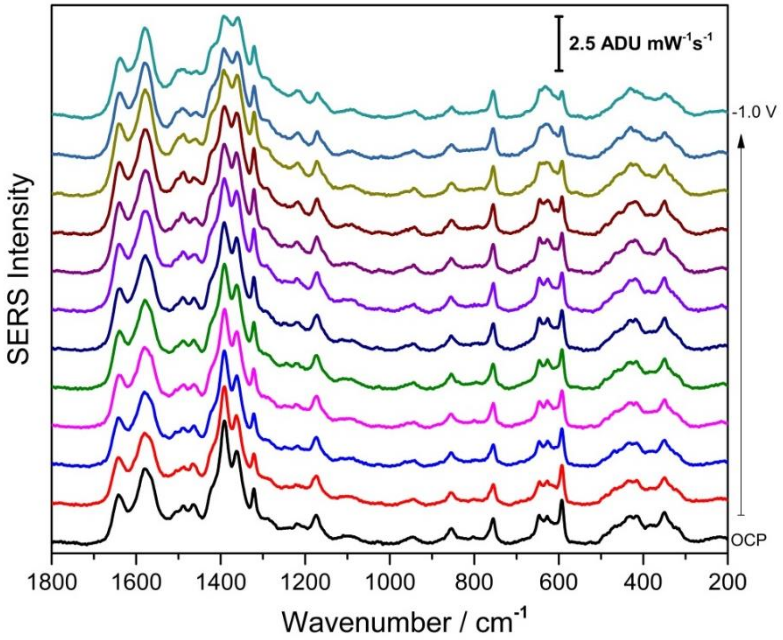

Figure 13: EC-SERS signal of PF (1 mM) drop-coated on a Au/Ag modified SERS substrate, collected using 532 nm laser excitation at 3 mW for 30 s, at the cathodic direction in 0.1M NaF supporting electrolyte.

3.1.3 Doxorubicin (DOX)

The SERS spectrum of DOX shows intense peaks, as would be expected for a molecular structure containing conjugated aromatic rings. According to literature, the maximum absorption wavelength of DOX is 495 nm.[67] The most intense peaks are at 451, 1267, 1405, and 1574 cm^{-1} as shown in Figure 14a. The peak assignments of DOX are provided in Table A-3. The CV shows that there is no significant redox activity of the DOX molecule between 0.0 V to -1.0 V. According to literature, the electrochemical reduction of quinone moiety of the tetracyclic ring in DOX occurs at a lower pH 3.5 as shown in Scheme 2.[68] In this work, the CV was collected at pH 7.4, at which the reduced form of DOX becomes unstable. This is a possible reason for observing no significant redox activity for the DOX molecule at pH 7.4.

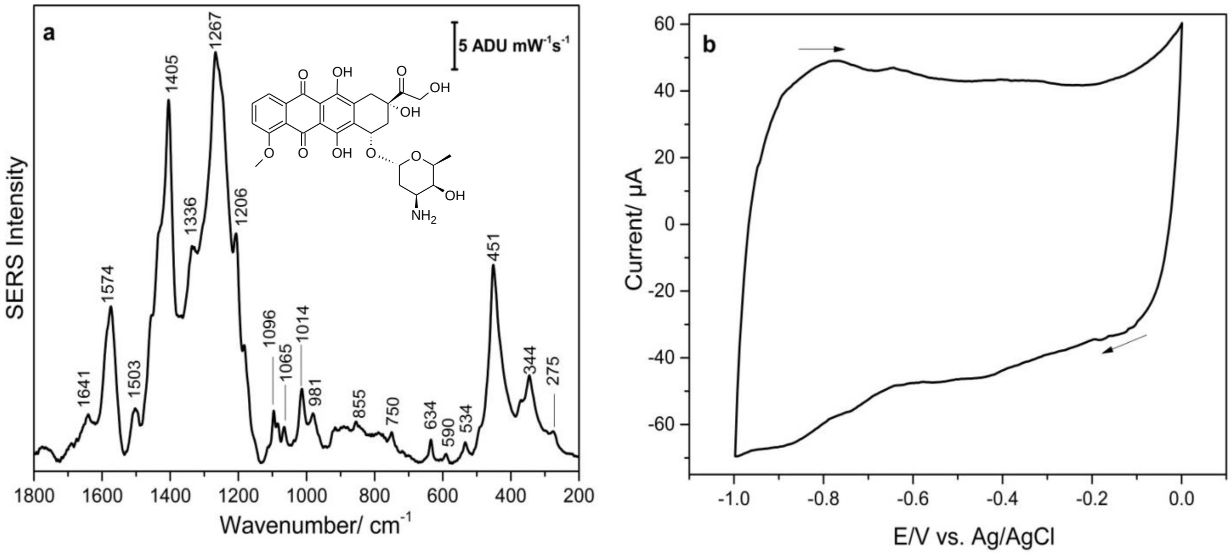

Figure 14: (a) SERS signal of doxorubicin (1 mM) drop-coated on a Au/Ag modified SERS substrate, collected using 532 nm laser excitation at 3 mW for 30 s; **(b)** Cyclic voltammogram of bare Au/Ag modified electrode with a supporting electrolyte containing 20 μM PF in phosphate buffer (pH 7.4). Arrows indicate the scan direction.

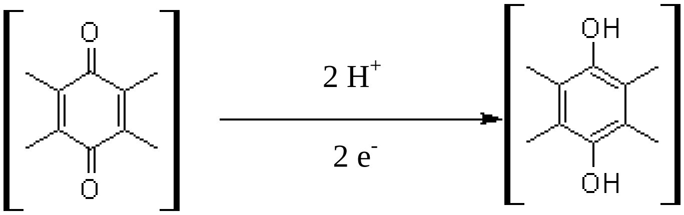

Scheme 2

In aqueous solution at pH 7.4, DOX has a unit positive charge due to the protonation of the amino group in the sugar moiety. This is shown in Figure 15.

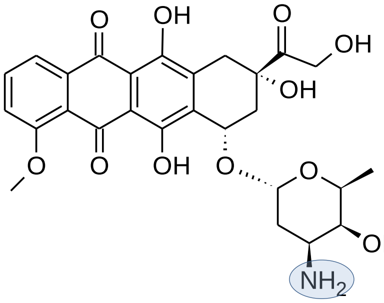

Figure 15: Structure of DOX in its neutral form. At physiological pH ~ 7.4, the amino group of the sugar moiety (shaded circle) is protonated to give a unit positive charge to the DOX molecule.[69]

This amino group can interact with the negatively charged citrate on the AgNP modified surface via electrostatic interactions. On applying potential in the cathodic direction, the citrate ions desorb from the surface due to the increasingly less positive surface charge. This results in a change in orientation of the DOX molecule and hence, the intensity of the DOX peak changes on applying potential as seen in Figure 16a. From the comparison of DOX peaks at different potentials in Figure 16b, it can be seen that on returning the potential to 0.0 V in the anodic direction, only 451, 1267 and 1405 cm^{-1} remain as distinct bands. These peaks are due to the sugar moiety of the DOX molecule. Based on the surface selection rules, this is suggestive that the tetracyclic region of the DOX molecule is parallel to the surface while the sugar moiety remains either in a perpendicular or tilted orientation. The interaction between the N atom of the sugar moiety and Ag on the substrate can also be confirmed by the 270 cm^{-1} peak due to (Ag-N) stretching as the two most intense peaks at 1405 and 1206 cm^{-1} are due to –NH_2.[70] However, another strong peak at 451 cm^{-1} is due to the bending vibration of the C=O group.

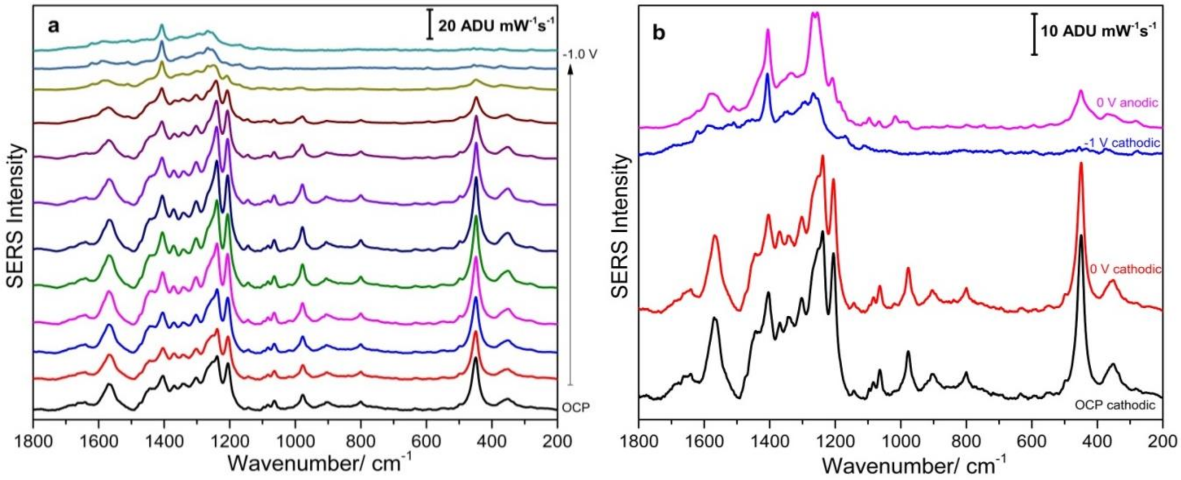

Figure 16: (a) EC-SERS signal of doxorubicin (1 mM) drop-coated on Au/Ag modified SERS substrate, collected using 532 nm laser excitation at 3 mW for 30 s, at the cathodic direction in 0.1M NaF supporting electrolyte; **(b)** Overlay of EC-SERS spectra of DOX at different potentials.

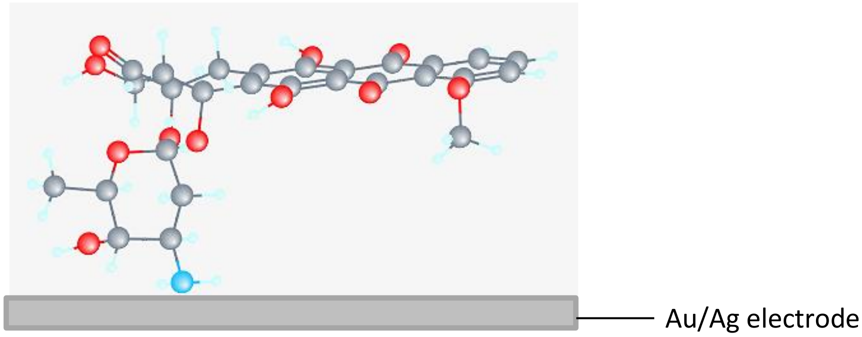

Figure 17: Cartoon representation of the proposed orientation of DOX molecule on a bare Au/Ag modified electrode.[71]

3.1.4 Ethidium Bromide (EtBr)

According to literature, the maximum absorption and emission of EtBr occurs at 486 nm and 606 nm respectively.[72] Although the wavelength of the excitation laser 532 nm is close to both the absorption and emission maxima, a strong SERS signal of EtBr was generated without any background fluorescence. The SERS active EtBr gave rise to intense peaks at 1610, 1567 and 1369 cm^{-1}, which is due to the stretching of the (C-C/C-N) in the phenanthridinum ring. A complete peak assignment of EtBr is provided in Table A-4. From the CV, it appears that a small cathodic peak at -0.35 V is present. This could be due to an electrochemical reduction of EtBr. There is no anodic peak present on reversing potential, which suggests that the redox process is irreversible in nature. This irreversible redox behaviour is also consistent with the literature.[73] However, the formal reduction potential reported in literature is at -0.616 V (*vs.* Ag/AgCl) with an additional undefined reduction peak at about -0.280 V. This suggests that the redox reaction of EtBr involves a two electron transfer. A proposed mechanism of electrochemical reduction of EtBr is given by Scheme 3.[73]

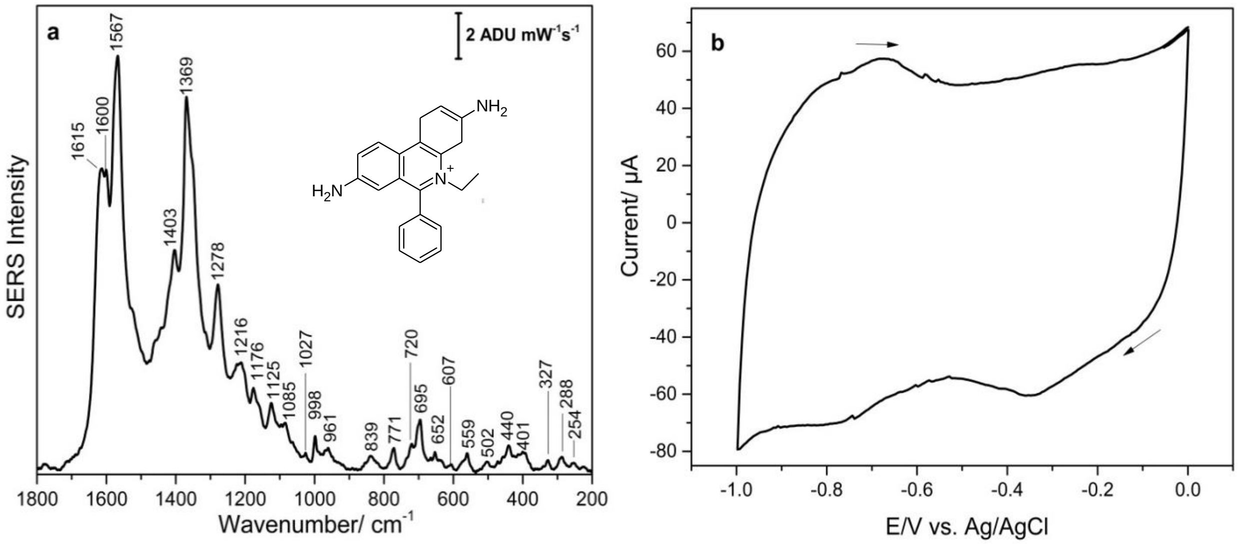

Figure 18: (a) SERS signal of ethidium bromide (1 mM) drop-coated on a Au/Ag modified SERS substrate, collected using 532 nm laser excitation at 3 mW for 30 s; **(b)** Cyclic voltammogram of bare Au/Ag modified electrode with a supporting electrolyte of 20 μM EtBr in phosphate buffer (pH 7.4). Arrows indicate the scan direction.

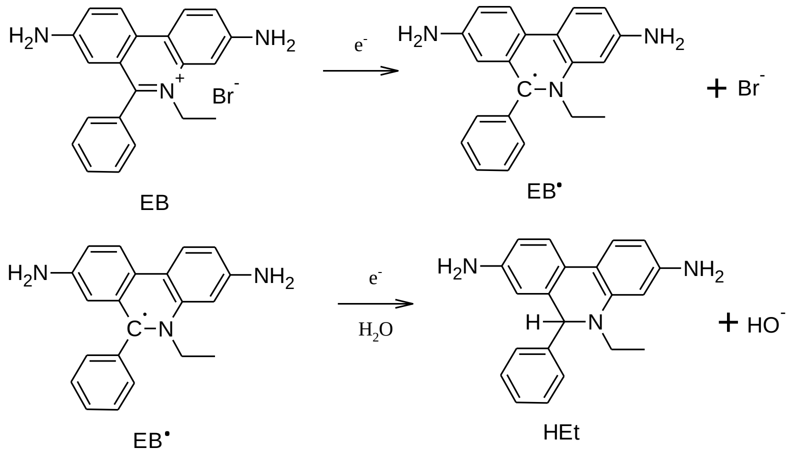

According to scheme 3, EtBr receives an electron to form a carbon-centered free radical EB$^\bullet$, which undergoes further reduction to form hydroethidine.[73] Figure 19a shows that there is no change in the EC-SERS signal on reaching a potential of about -

0.35 V in terms of both SERS intensity and appearance/disappearance of peaks. This suggests that even if an electrochemical reduction took place, the reduced product is too unstable. Therefore, it cannot be observed using this spectroelectrochemical technique. However, an overlay of EtBr EC-SERS spectra at different potentials in Figure 19b shows some slight changes in the signal. Some of the weak SERS peaks at low wavenumbers disappear or are significantly reduced in intensity on reaching -1.0 V. These peaks are due to bending and out-of-plane torsion of the phenanthridinium ring. The peaks remain with reduced intensity on returning the potential to 0.0 V at positive direction. This may be due to the change in orientation of the EtBr molecule adsorbed on the Au/Ag substrate on changing the potential. As stated previously, according to the SERS surface selection rules - weakening of out-of-plane bending vibrations indicate that EtBr molecules are adsorbed with a perpendicular or tilted orientation with respect to the electrode surface. From the structure of EtBr, it can be seen that EtBr has a positive charge on the N atom of endocyclic iminium group at neutral pH. This means it can interact electrostatically with the surface of the Au/Ag electrode similar to DOX. However, the bulky ethyl group attached to this N atom can interfere with the adsorption of EtBr.

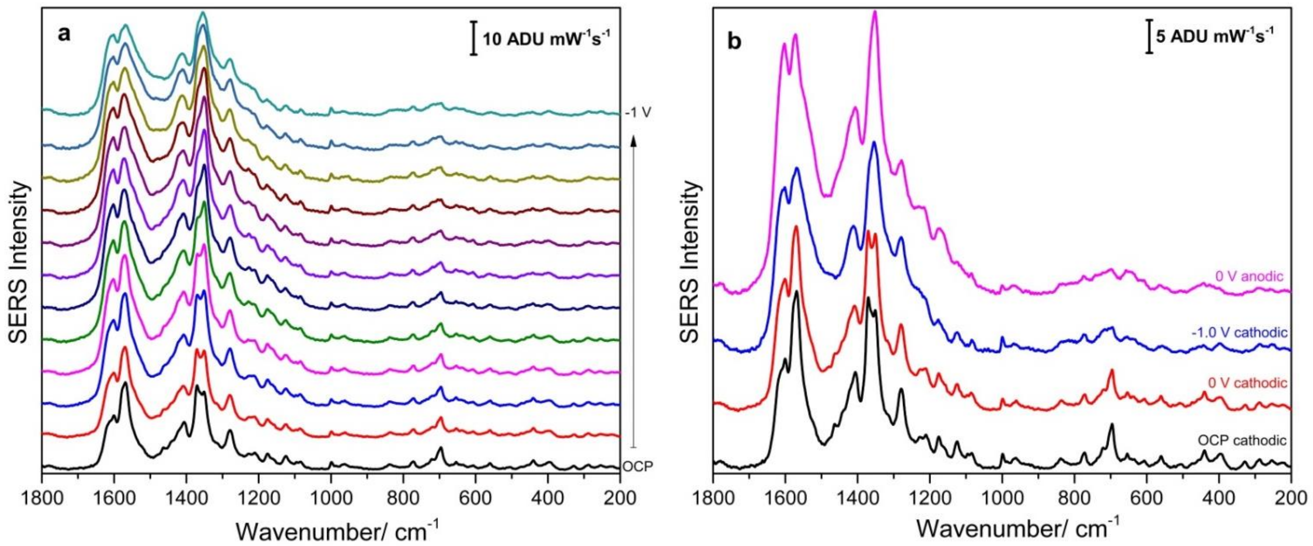

Figure 19: (a) EC-SERS signal of ethidium bromide (1 mM) drop-coated on a Au/Ag modified SERS substrate, collected using 532 nm laser excitation at 3 mW for 30 s, at the cathodic direction in 0.1M NaF supporting electrolyte; **(b)** Overlay of EC-SERS spectra of EtBr at different potentials.

3.1.5 Bisbenzimide H 33258 (Hoechst 33258)

Bisbenzimide H 33258 or Hoechst 33258 is SERS active at 532 nm as can be seen from the SERS spectra in Figure 20a with intense bands at 1552, 1443, 1265, 978 and 240 cm^{-1}. The absorbance and emission maximum for Hoechst 33258 is reported to be at 338 and 505 nm respectively.[74] No fluorescence background was observed even though the emission maximum is close to the 532 laser excitation wavelength. The peak assignment for Hoechst 33258 is provided in Table A-5. Most of these intense peaks are assigned to the two benzimidazole groups of the molecule; phenolic groups and piperazine rings usually give rise to weak SERS signal. Since the peaks due to in-plane vibrational modes are more intense than the out-of-plane vibrations, it is likely that the molecule is oriented perpendicular to the surface. The region between 200 to 250 cm^{-1} indicates the presence of any Ag-N/Ag-O/Ag-S stretching vibration. For the Hoechst 33258

molecule, the band at 240 cm^{-1} can be assigned as either a (Ag-N) or (Ag-O) stretching vibration.

The EC-SERS spectra of Hoechst 33258 were also collected to observe changes in the SERS signal on application of a voltage. According to our knowledge, this study is the first report of EC-SERS of Hoechst 33258 in literature. As can be seen in Figure 22a, the EC-SERS displayed mostly weak SERS signal and a strong 240 cm^{-1} peak at OCP as well as when the potential was applied up to -0.2 V. This may suggest that initially Hoechst 33258 binds to the surface though the –OH of the phenol group. On reaching -0.3 V, this strong peak disappeared, a better SERS signal for Hoechst 33258 was obtained, and at -1.0 V, a weak peak at around 277 cm^{-1} indicates (Ag-N) stretching.

However, the peak at 240 cm^{-1} could also be due to citrate (Ag-O), which disappears as citrate molecules are displaced from the surface followed by adsorption of Hoechst 33258. The peaks of Hoechst 33258 remain largely consistent on returning the potential to 0.0 V in the anodic direction as shown in Figure 22b. According to literature, at neutral pH Hoechst 33258 has a cationic charge on the nitrogen atom of the piperazine group.[75] This N atom can have electrostatic interaction with the Au/Ag surface.

The CV obtained for Hoechst 33258 shows a possible reduction at -0.41 V and -0.83 V, and an anodic peak at about -0.69 V. This suggests that a 2 electron transfer redox reaction takes place. Since an anodic peak appears, ΔE_p can be calculated using equation 1. The ΔE_p is found to be 140 mV, which is greater than 29.5 mV and hence, this redox process is irreversible in nature. The irreversible redox nature of Hoechst 33258 is consistent with the literature, whereby only an anodic peak at 0.55 V vs Ag/AgCl was observed using glassy carbon electrode.[76]

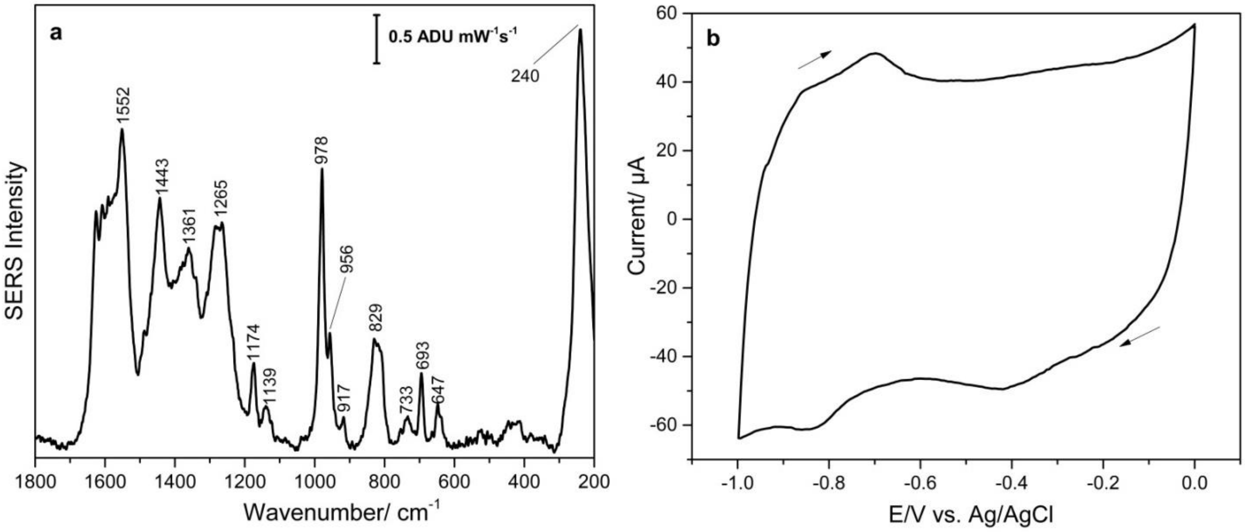

Figure 20: (a) SERS signal of Hoechst 33258 (1 mM) drop-coated on Au/Ag modified SERS substrate, collected using 532 nm laser excitation at 3 mW for 30 s; **(b)** Cyclic voltammogram of bare Au/Ag modified electrode with a supporting electrolyte of 20 µM Hoechst 33258 in phosphate buffer (pH 7.4). Arrows indicate the scan direction.

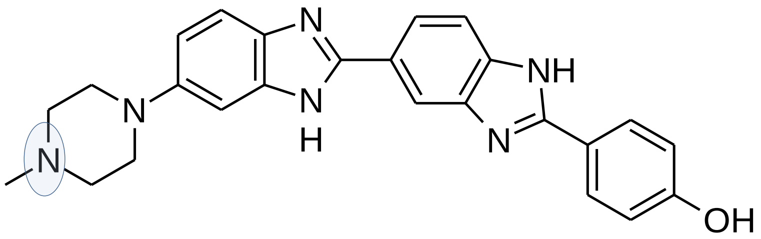

Figure 21: Structure of Hoechst 33258 at neutral pH. At physiological pH ~ 7.4, the nitrogen atom of piperazine group (shaded circle) gets protonated (as NH^+) to give a unit positive charge to the Hoechst 33258 molecule.

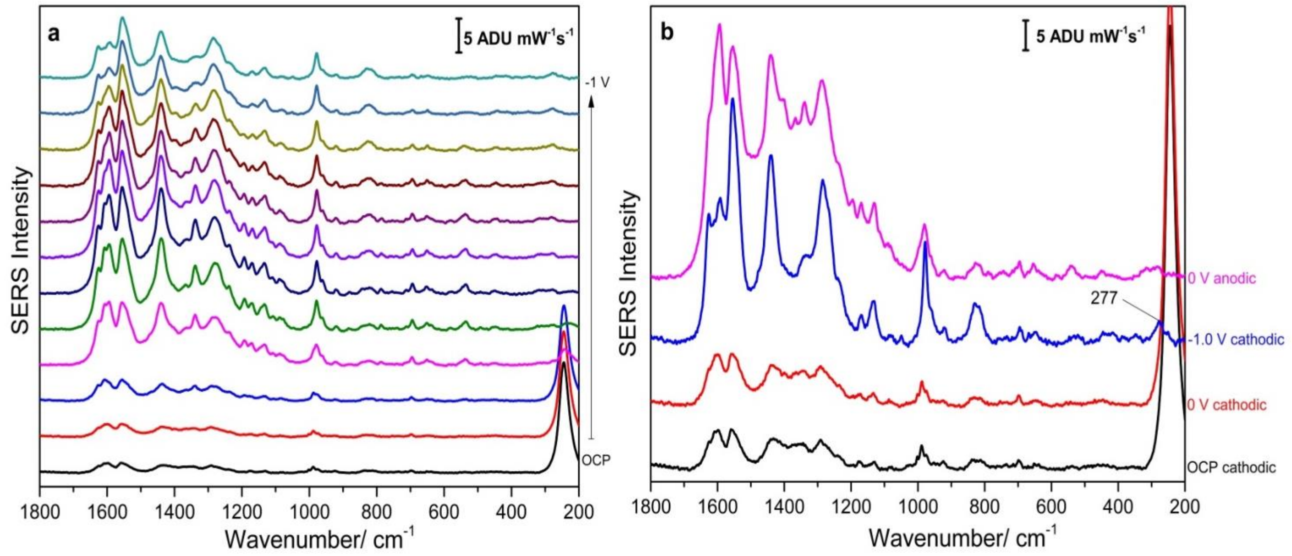

Figure 22: (a) EC-SERS signal of Hoechst 33258 (1 mM) drop-coated on Au/Ag modified SERS substrate, collected using 532 nm laser excitation at 3 mW for 30 s, at the cathodic direction in 0.1M NaF supporting electrolyte; **(b)** Overlay of EC-SERS spectra of Hoechst 33258 at different potentials.

3.1.6 Characterization Summary

In this study, five different Raman reporters namely MB, PF, DOX, EtBr and Hoechst 33258 were successfully characterized using SERS, EC-SERS and CV. All the Raman reporters provided intense and distinct SERS peaks at 532 nm excitation wavelength. According to our knowledge, this is the first report of EC-SERS on PF, DOX, EtBr and Hoechst 33258. The characterization study also revealed that there is no significant redox activity within 0.0 V to -1.0 V for most of the Raman reporters as observed by CV. The change in any peak intensity in EC-SERS spectra are attributed to the change in orientation of the Raman reporters adsorbed on the Au/Ag surface. The results suggest that differential pulse voltammetry (DPV) may not be quite useful in indirect detection of DNA hybridization. However, EC-SERS may be useful as any changes in molecular orientation upon interaction with ssDNA or dsDNA can be observed in the EC-SERS spectra. These EC-SERS spectra can be compared to those obtained for Raman reporters during characterization, which may indicate if non-specific adsorption of the Raman reporters takes place.

3.2 DNA Hybridization Detection by indirect method – EC-SERS and DPV

3.2.1 Methylene Blue

Methylene blue was chosen as a Raman reporter because of two main reasons. Firstly, it is one of the most commonly used redox indicators in the literature. Secondly, it has been used in a number of electrochemical aptamer based studies as a DNA intercalator for indirect voltammetric detection of IgE protein. Additionally, it is cost-effective and readily available. The initial studies of MB were done with just probe 1 (ssDNA) and probe 1 + target 1 (dsDNA) modified electrodes in the absence of any spacer as shown in Figure A-2. It was found that a strong SERS signal for the MB was observed for both cases. Therefore, an alkanethiol spacer was introduced via backfilling in an effort to reduce non-specific adsorption of the MB onto the electrode surface. The role of the spacer molecule is to displace any DNA aptamers that are not covalently bound to the electrode surface. It also promotes an upright orientation of the aptamers so that an efficient hybridization can occur with the target. In addition, thiol-backfilling is used to prevent any non-specific binding of the Raman reporter to the electrode surface by blocking surface access. In thiol-backfilling, a thiol is added to the surface after the self-assembly of the aptamer. Previously, ethanolic alkanethiol solutions of 1.0 mM 11-mercapto-1-undecanol (11-MUD), 12-mercaptododecanoic acid (12-MDA) and 6-mercapto-1-hexanol (6-MCH) with an incubation time of 2 h were all found to be ideal for thiol-backfilling.[4, 26] However, 12-MDA has a carboxylic group as a head group, which may interfere and cause non-specific binding with the IgE protein in future studies. Previous studies have shown that 6-MCH as a spacer is not stable for long periods of time. Therefore, 11-MUD was chosen as the alkanethiol spacer for these studies. In addition, previous studies have shown that the direct detection of a heme-protein was possible using 11-MUD as a spacer.[4]

The interaction between MB and a ssDNA modified electrode backfilled with 11-MUD spacer is strong at OCP. As shown in Figure 23a, the intensity of MB peaks is reduced greatly as a negative potential is applied. At -0.6 V, almost all of the peaks for MB disappear. The same trend was observed in the case of a dsDNA modified electrode backfilled with 11-MUD spacer. In fact, similar behaviour was observed during the characterization of MB on the Au/Ag modified electrode. As explained earlier, this can possibly be due to the reduction of MB to leucomethylene blue as the potential is changed. Another possible reason in this case can be that MB molecules interact with both the ssDNA and dsDNA. MB is a cationic dye that can interact with the negatively charged phosphate backbone of the ssDNA via electrostatic interactions. Nevertheless, the presence of the adenine peak at 730 cm^{-1} in Figure 23b indicates that hybridization between probe 1 and target 1 has indeed taken place. The 730 cm^{-1} peak is more prominent as the potential is changed in the cathodic direction.

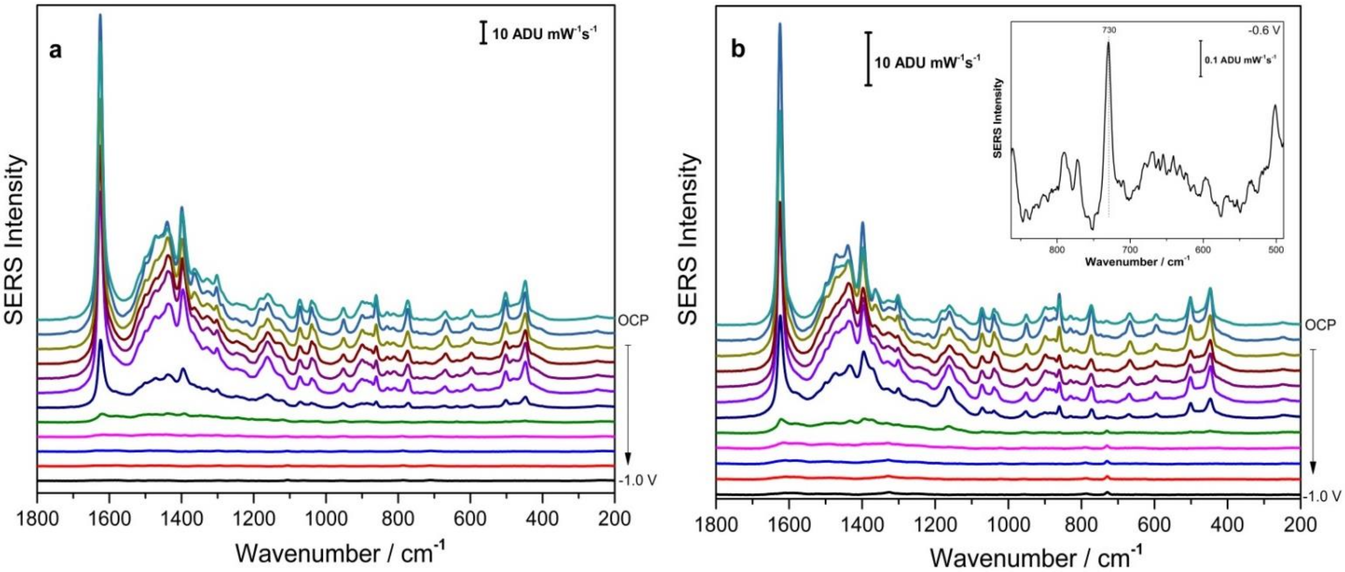

Figure 23: (a) EC-SERS signal of P1+ 11-MUD + MB (ssDNA) modified Au/Ag modified substrate, collected using 532 nm laser excitation at 3 mW for 30 s, at the cathodic direction in 0.1M NaF supporting electrolyte; **(b)** EC-SERS signal of P1+ 11-MUD + T1+ MB (dsDNA) modified Au/Ag modified substrate, collected using 532 nm laser excitation at 3 mW for 30 s, at the cathodic direction in 0.1M NaF supporting electrolyte. Inset shows enlarged adenine peak at -0.6 V.

In literature, there is no exact mechanism of MB binding specifically to either ssDNA or dsDNA as discussed previously. However, from the comparison of MB SERS signal between ssDNA and dsDNA in Figure 24a, it can be seen that the intensity of MB is relatively greater with ssDNA as opposed to dsDNA. This may suggest that MB preferentially binds to ssDNA. The ssDNA and dsDNA cannot be distinguished based on the SERS of the Raman reporter. For comparison, SERS signal at only OCP cathodic is shown where most of the peaks are observed. Additionally, dsDNA denaturation does not take place at OCP as according to Bartlett et al., electrochemical denaturation of dsDNA occurs when a potential of about -0.7 V is applied in the negative direction.[77] However, the SERS intensity of MB was similar for ssDNA and dsDNA on reversing the potential to OCP anodic (Figure A – 3b). From the raw data of DPV studies in Figure 24b, it is evident that MB molecules are present within the double layer of both the ssDNA and dsDNA modified electrodes as no apparent changes in DPV peak height is observed in either case.

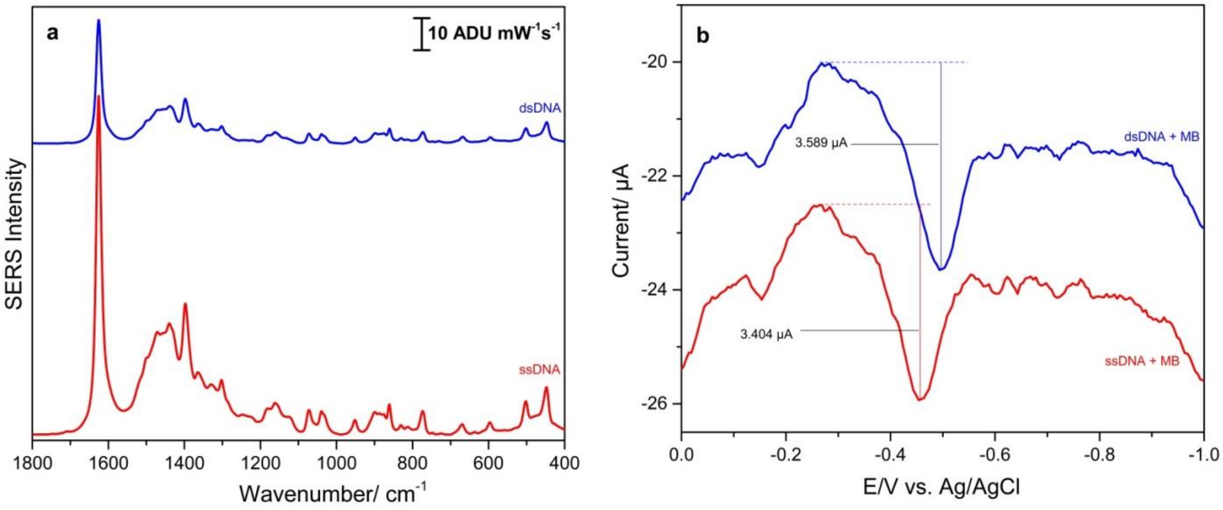

Figure 24: (a) Comparison of EC-SERS signal of MB from ssDNA vs dsDNA modified Au/Ag substrate collected using 532 nm laser excitation at 3 mW for 30 s, at OCP cathodic in 0.1M NaF supporting electrolyte; **(b)** Comparison of DPV raw data of MB from ssDNA vs dsDNA modified Au/Ag substrate collected with an amplitude of 25 mV at 5 mV increments in phosphate buffer (pH 7.4).

3.2.2 Proflavine

Proflavine is also known to function as a classic intercalator although the exact mechanism of its interaction is complex as discussed in the literature review. Unlike MB, the SERS signal of PF is considerably weaker with both ssDNA and dsDNA as shown in Figure 25. Also, the SERS signal gets stronger in the cathodic direction in both cases. A faint peak at 734 cm^{-1} is indicative of DNA hybridization in Figure 25b.

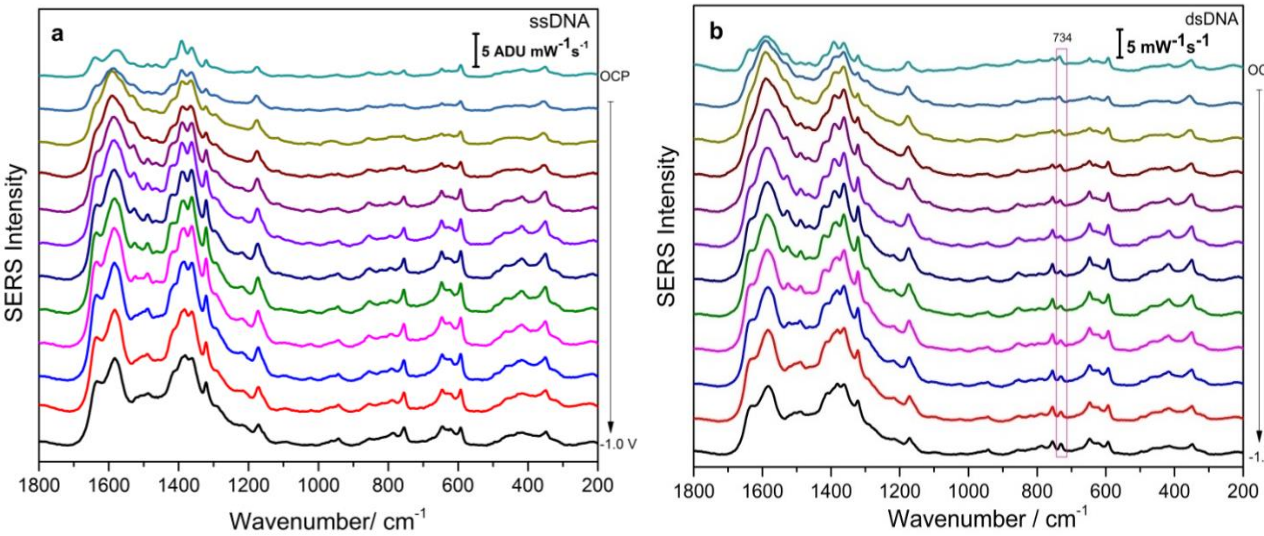

Figure 25: (a) EC-SERS signal of P1+ 11-MUD + PF (ssDNA) modified Au/Ag substrate collected using 532 nm laser excitation at 3 mW for 30 s, at the cathodic direction in 0.1M NaF supporting electrolyte; **(b)** EC-SERS signal of P1+ 11-MUD + T1+ PF (dsDNA) modified Au/Ag substrate collected using 532 nm laser excitation at 3 mW for 30 s, at the cathodic direction in 0.1M NaF supporting electrolyte.

A comparison between ssDNA and dsDNA in Figure 26a reveals that the SERS signal is relatively similar for both ssDNA and dsDNA, and cannot be used to distinguish between them. The DPV data for dsDNA shows a small redox peak at around -0.24 V in Figure 26b. Since DPV is a very sensitive technique, noise in the data is difficult to remove completely. The parameters for DPV were chosen after much trial and error in order to obtain the best possible DPV. Nevertheless, ssDNA and dsDNA could not be distinguished using DPV either. Future DPV work should use a Faraday cage in order to remove electrical noise interference.

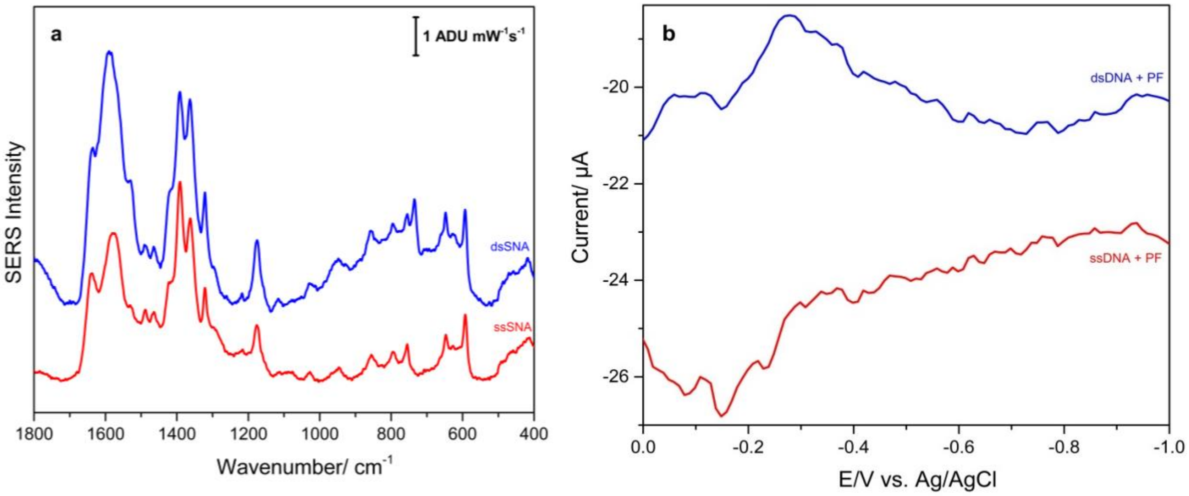

Figure 26: (a) Comparison of EC-SERS signal of PF from ssDNA vs dsDNA modified Au/Ag substrate collected using 532 nm laser excitation at 3 mW for 30 s, at OCP cathodic in 0.1M NaF supporting electrolyte; **(b)** Comparison of DPV raw data of PF from ssDNA vs dsDNA modified Au/Ag substrate collected with amplitude of 25 mV at 10 mV increments in phosphate buffer (pH 7.4).

3.2.3 Doxorubicin

According to literature, DOX is reported to be a threading intercalator whereby the sugar moiety resides in the grooves of the dsDNA.[32] The DOX SERS for ssDNA at OCP cathodic did not give rise to any new peaks but the SERS intensity is significantly reduced when compared to that of DOX on the Au/Ag electrode. Significant decrease in SERS intensity is also observed for dsDNA in addition to appearance of the adenine peak at 730 cm^{-1}. The EC-SERS for ssDNA + DOX in Figure 27a shows similar trend as observed for DOX on a bare electrode. This could possibly indicate non-specific interaction of DOX with the electrode, despite the backfilled monolayer. An opposite trend was observed for EC-SERS of dsDNA + DOX where applying a negative potential increased the intensity of the peaks in Figure 27b.

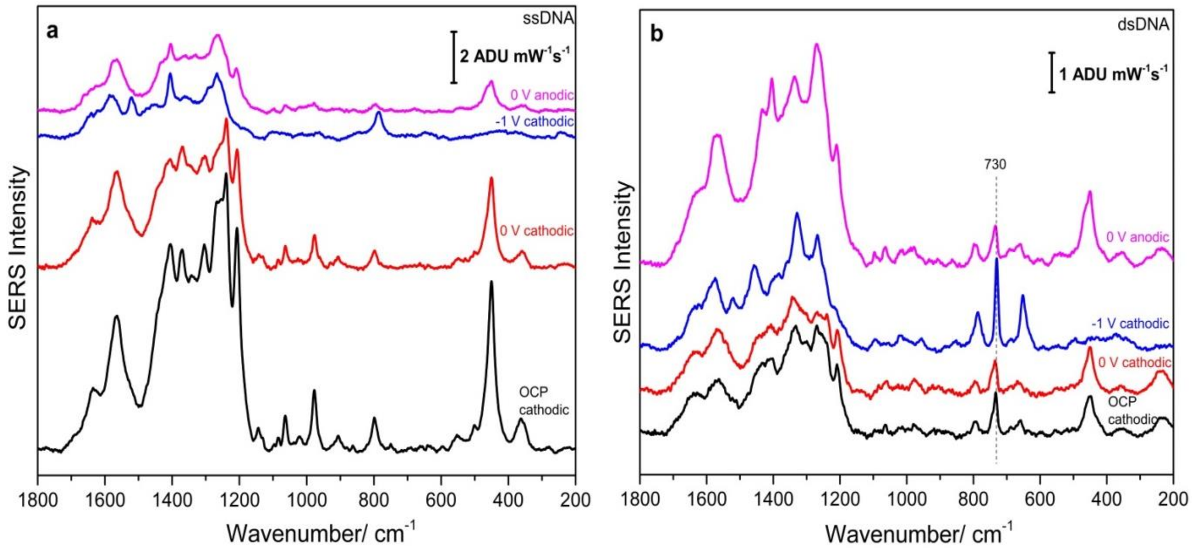

Figure 27: (a) Comparison of EC-SERS signal of P1+ 11-MUD + DOX (ssDNA) modified Au/Ag substrate, collected using 532 nm laser excitation at 3 mW for 30 s in 0.1M NaF supporting electrolyte, at different potentials; **(b)** Comparison of EC-SERS

signal of P1+ 11-MUD + T1+ DOX modified Au/Ag substrate collected using 532 nm laser excitation at 3 mW for 30 s, at different potentials.

A comparison between ssDNA + DOX and dsDNA + DOX at OCP cathodic in Figure 28a shows that DOX SERS signal for ssDNA is relatively stronger than dsDNA. This could perhaps indicate that DOX binds preferentially to ssDNA as compared to dsDNA. However, on applying a negative potential and then reversing it, intense DOX peaks now appear for dsDNA. Since there are multiple overlaps of peaks, a complete assignment of peaks at different potentials is a difficult task. Hence, a composite percentage of reference spectra for ssDNA + DOX and dsDNA+ DOX at different potential are shown in Figure 29. The results indicates that on applying a negative potential, the percentage of SERS signal due to DOX decreases and upon reversing the potential, DOX peaks become dominant. At any potential, the DOX signal is higher for ssDNA compared to dsDNA. Like most of the previous Raman reporters, it is likely that the interaction of DOX with ssDNA is electrostatic in nature. The hybridization of DNA could not be detected indirectly via EC-SERS. DPV was also collected to monitor differences in current between ssDNA and dsDNA. Figure 30 shows an undefined peak at -0.25 V for dsDNA, while no change in current for ssDNA.

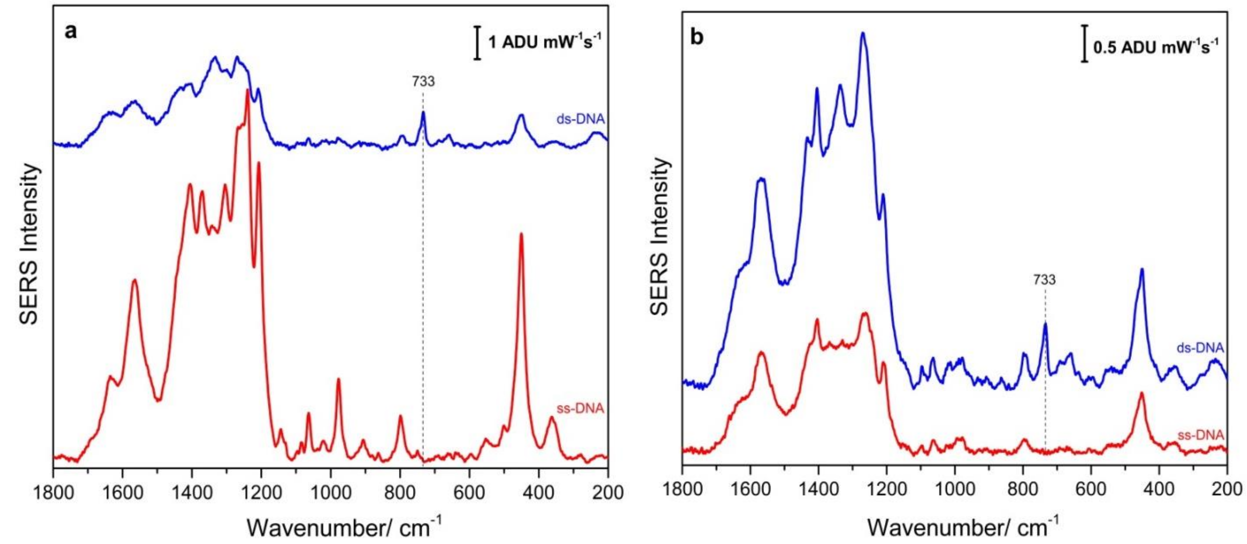

Figure 28: (a) Comparison of EC-SERS signal of DOX from ssDNA vs dsDNA modified Au/Ag substrate collected using 532 nm laser excitation at 3 mW for 30 s, at OCP cathodic in 0.1M NaF supporting electrolyte; **(b)** Comparison of EC-SERS signal of DOX from ssDNA vs dsDNA modified Au/Ag substrate collected excitation 532 nm laser excitation at 3 mW for 30 s, at OCP anodic in 0.1M NaF supporting electrolyte.

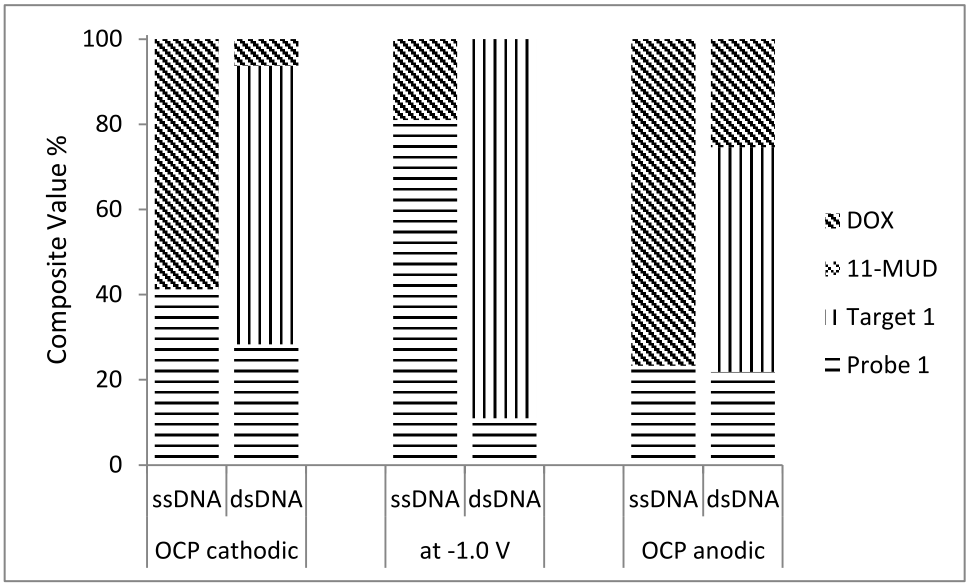

Figure 29: The percentage composite value of each set of reference spectra of P1, T1, 11-MUD and DOX at different potentials for ssDNA + DOX and dsDNA + DOX obtained using OMNIC Specta software.

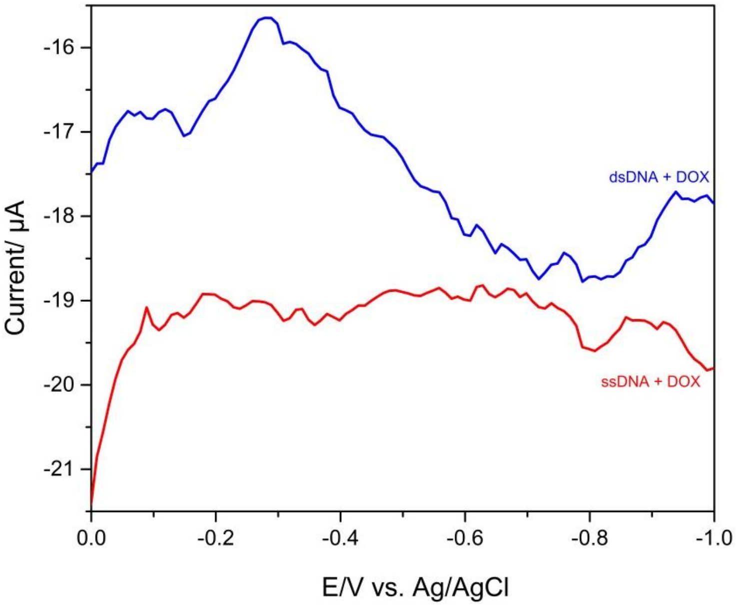

Figure 30: Comparison of DPV raw data of DOX from ssDNA vs dsDNA modified Au/Ag substrate collected with amplitude of 25 mV at 10 mV increments in phosphate buffer (pH 7.4).

3.2.4 Ethidium Bromide

Ethidium bromide is a well-known DNA intercalator that is most commonly used to visualize DNA in gel electrophoresis. According to literature, EtBr binds to dsDNA by intercalating the phenanthridinium ring between adjacent base pairs while the amino substituents can hydrogen bond with O atoms of sugar phosphate backbone.[39] Additionally, EtBr may also bind to nucleic acids through electrostatic interaction with this anionic phosphate backbone due to cationic charge on the N atom. The EC-SERS in Figure 31 for ssDNA + EtBr and dsDNA + EtBr shows that EtBr interacts with both ssDNA and dsDNA. Unlike the EC-SERS of EtBr on a bare Au/Ag electrode, the SERS signal of ssDNA + EtBr changes on applying negative potential as shown in Figure 31a. The EC-SERS signal at OCP in this case is same as observed for EC-SERS of EtBr on a bare Au/Ag electrode, which could indicate that EtBr is perhaps bound non-specifically to the electrode surface. However, no SERS peak at 224 cm^{-1} due to (Ag-N) stretching vibration is observed that could indicate interaction with the electrode surface. The broadening and weakening of spectral feature could suggest that EtBr interacts with ssDNA through the non-intercalative mode since such change in peak intensity on applying potential is not observed during characterization. It is possible that as the potential is made more negative, the ssDNA on the electrode surface changes orientation in such a way that the distance between the electrode surface and the EtBr bound to ssDNA increases. Both increase in distance and change in orientation on varying potential may result in a relatively weaker spectrum. In case of dsDNA + EtBr, the EC-SERS signal is slightly broadened compared to that observed during EtBr characterization and a new peak at 735 cm^{-1} due to adenine is observed.

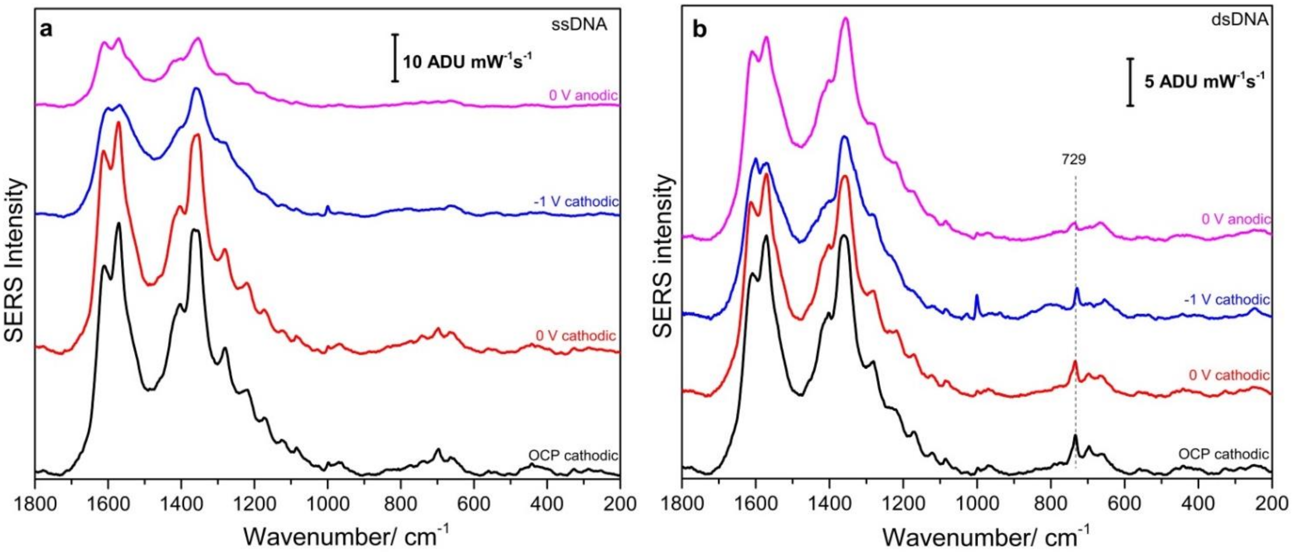

Figure 31: (a) Comparison of EC-SERS signal of P1+ 11-MUD + EtBr modified Au/Ag substrate, collected using 532 nm laser excitation at 3 mW for 30 s in 0.1M NaF supporting electrolyte at different potentials; **(b)** Comparison of EC-SERS signal of P1+ 11-MUD + T1+ EtBr modified Au/Ag substrate, collected using 532 nm laser excitation at 3 mW for 30 s in 0.1M NaF supporting electrolyte at different potentials.

A comparison between the ssDNA and dsDNA SERS signal in Figure 32a shows that EtBr + ssDNA has relatively stronger SERS signal than dsDNA + EtBr at OCP. On reversing the negative potential, the SERS signal intensity is almost identical for both ssDNA and dsDNA except the adenine peak at 735 cm^{-1} in Figure 32b. The composite values of reference spectra shown in Figure 33 further points that at any potential, EtBr peaks are more dominant in ssDNA spectra than dsDNA spectra. Therefore, hybridization between P1 and T1 cannot be detected indirectly using EC-SERS when EtBr is chosen a Raman reporter as EtBr could be bound to both ssDNA and dsDNA with similar affinity. Additionally, non-specific binding of EtBr to the electrode surface could also exist.

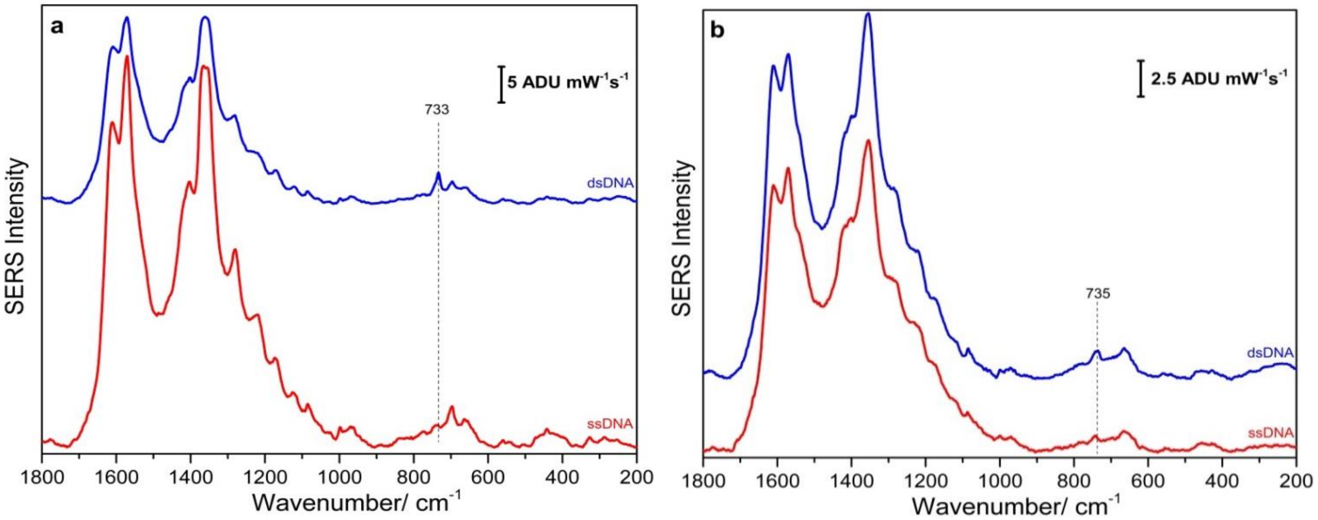

Figure 32: (a) Comparison of EC-SERS signal of EtBr from ssDNA vs dsDNA modified Au/Ag substrate collected using 532 nm laser excitation at 3 mW for 30 s, at OCP cathodic in 0.1M NaF supporting electrolyte; **(b)** Comparison of EC-SERS signal of EtBr from ssDNA vs dsDNA modified Au/Ag substrate collected using 532 nm laser excitation at 3 mW for 30 s, at OCP anodic in 0.1M NaF supporting electrolyte.

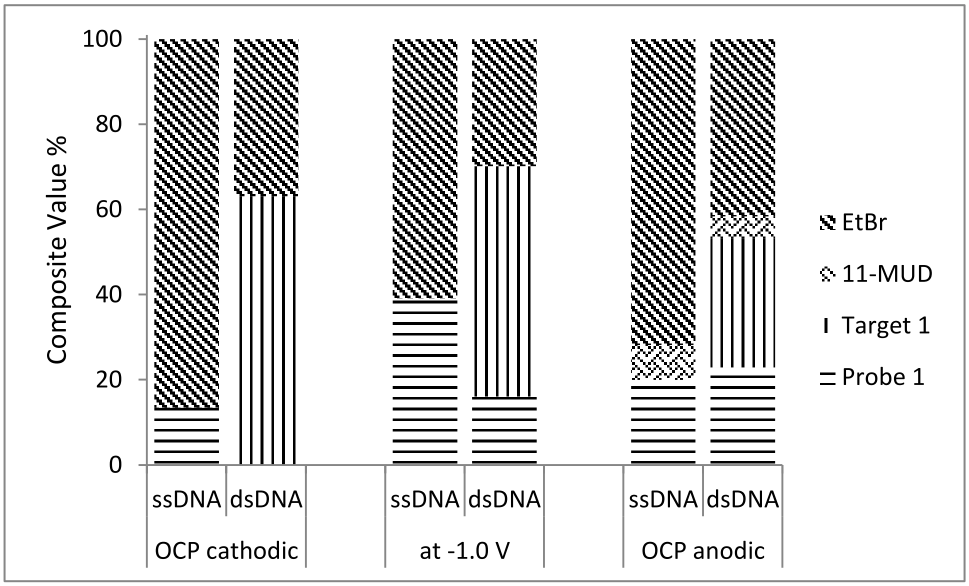

Figure 33: The composite value of each set of reference spectra of P1, T1, 11-MUD and EtBr at different potentials for ssDNA + EtBr and dsDNA + EtBr obtained using OMNIC Specta software.

Since hybridization could not be detected using EC-SERS, DPV was collected for ssDNA + EtBr and dsDNA + EtBr. The voltammogram in Figure 33 shows a E_{peak} at -0.278 V and -0.258 V for ssDNA and dsDNA respectively. This DPV raw data confirms that EtBr is present within the double layer of both the ssDNA and dsDNA modified electrodes as there is no significant difference in peak height (Δi). Therefore, DNA hybridization cannot be detected indirectly using DPV.

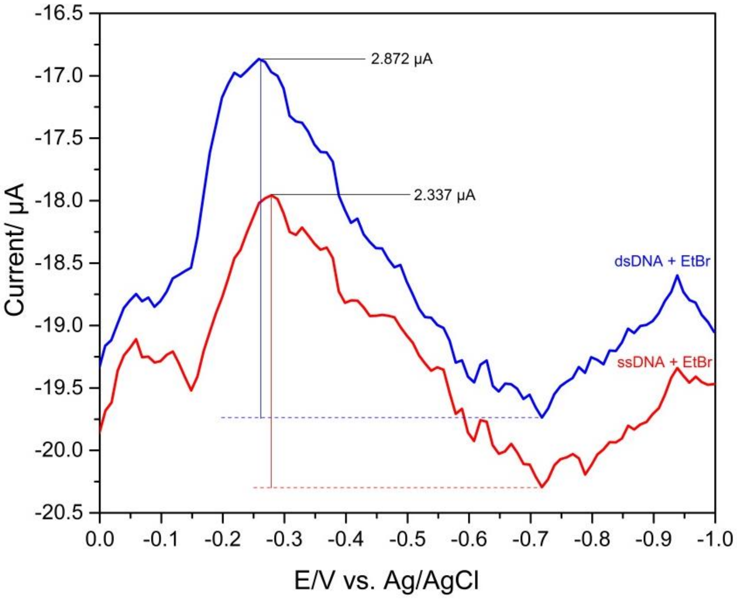

Figure 34: Comparison of DPV raw data of EtBr from ssDNA vs dsDNA modified Au/Ag substrate collected with amplitude of 25 mV at 10 mV increments in phosphate buffer (pH 7.4).

3.2.5 Bisbenzimide H 33258 (Hoechst 33258)

Hoechst 33258 has been known to selectively bind with dsDNA in the minor groove of DNA double helices, where it interacts with AT base pairs. In this study, adenines are only present in Target 1 sequence and therefore, the minor groove site would be formed for Hoechst 33258 only after hybridization takes place between Probe 1 and Target 1. The EC-SERS of ssDNA with Hoechst 33258 in Figure 35a shows weak SERS signal initially. On applying negative potential and reversing it in anodic direction, the SERS signal increases and remains strong. Similar trend of SERS signal intensity is observed in the case of EC-SERS of dsDNA with Hoechst 33258 in Figure 35b. This changing of SERS signal on varying potential was expected as observed during Hoechst 33258 characterization on a bare Au/Ag substrate. Interpretation of this data is therefore complicated in terms of the actual interaction of Hoechst 33258 with ssDNA and dsDNA. Like previous Raman reporters, it is possible that Hoechst 33258 is also binding to the substrate non-specifically. Nevertheless, the presence of adenine peak at 734 cm^{-1} confirms that hybridization has taken place between P1 and T1.

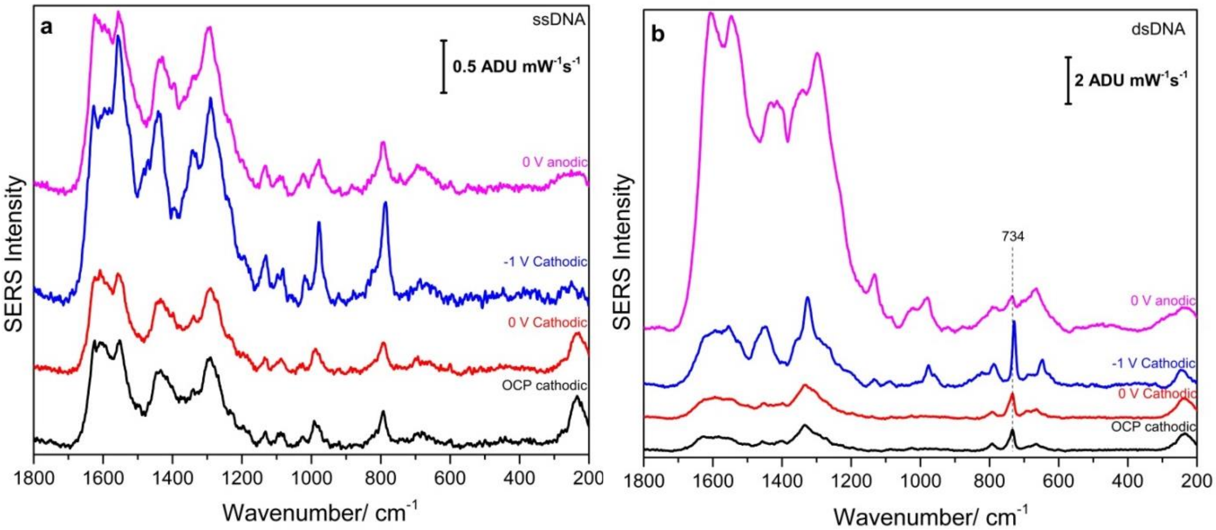

Figure 35: (a) Comparison of EC-SERS signal of P1+ 11-MUD + Hoechst 33258 modified Au/Ag substrate, collected using 532 nm laser excitation at 3 mW for 30 s in 0.1 M NaF supporting electrolyte at different potentials; **(b)** Comparison of EC-SERS signal of P1+ 11-MUD + T1+ Hoechst 33258 modified Au/Ag substrate, collected using 532 nm laser excitation at 3 mW for 30 s in 0.1 M NaF supporting electrolyte at different potentials.

To better interpret the interaction of Hoechst 33258, an overlay of ssDNA and dsDNA SERS spectra at OCP cathodic and anodic is plotted in Figure 36a and 36b. Peaks due to Hoechst 33258 are marked with an asterisk in the plots. However, these peaks of Hoechst 33258 were slightly shifted when compared with peaks in Table A-5. For example, a peak at 1443 cm^{-1}due to skeletal ring in-plane vibration of the benzimidazole moiety appears at 1457 cm^{-1} in Figure 36a. Such peak shifting makes it difficult to interpret the nature of Hoechst 33258 interaction. Since there are multiple overlaps in the peaks, a percentage contribution of P1, T1, 11-MUD and Hoechst 33258 towards a best match spectrum were calculated using OMNIC Specta software and is shown as a graph in Figure 37. Using both Figure 36a and Figure 37, it can be correlated that at OCP cathodic SERS signal is dominated by P1 for ssDNA and by T1 for dsDNA. On applying potential in the negative direction and reversing it, SERS peaks due to Hoechst 33258 increases while peaks due to P1 and T1 decreases. Although Figure 37 suggests that Hoechst 33258 signal is dominated for both ssDNA and dsDNA at OCP anodic, the SERS signal intensity is relatively higher for dsDNA than ssDNA in Figure 36a. This indicates that on applying potential, Hoechst 33258 reporters interact with dsDNA more than ssDNA and hence, could indicate that hybridization between P1 and T1 has taken place. Perhaps, it could also be due to electrochemical melting of dsDNA on applying negative potential, which in turn changes the orientation of the Hochest 33258. Additionally, DPV were also collected as can be seen in Figure 38, which shows there is no obvious peak in the DPV for both the ssDNA and dsDNA. Therefore, DPV also could not be used to indirectly detect DNA hybridization.

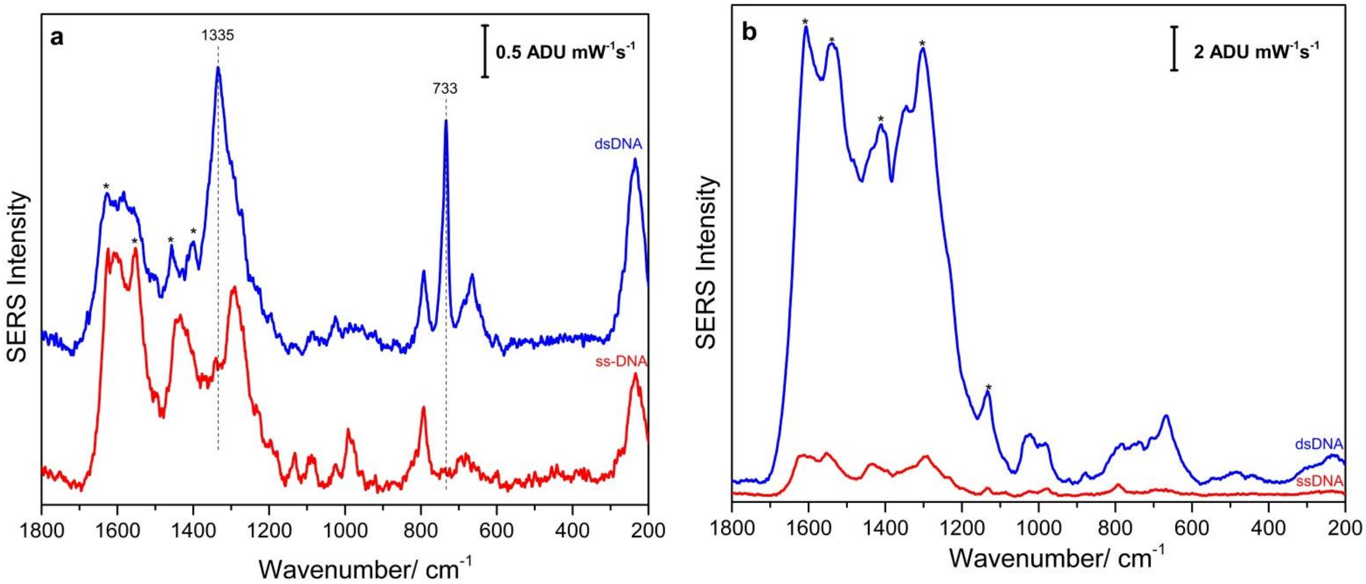

Figure 36: (a) Comparison of EC-SERS signal of Hoechst 33258 from ssDNA vs dsDNA modified Au/Ag substrate collected using 532 nm laser excitation at 3 mW for 30 s in 0.1 M NaF supporting electrolyte at OCP cathodic; **(b)** Comparison of EC-SERS signal of Hoechst 33258 from ssDNA vs dsDNA modified Au/Ag substrate collected using 532 nm laser excitation at 3 mW for 30 s in 0.1 M NaF supporting electrolyte at OCP anodic.

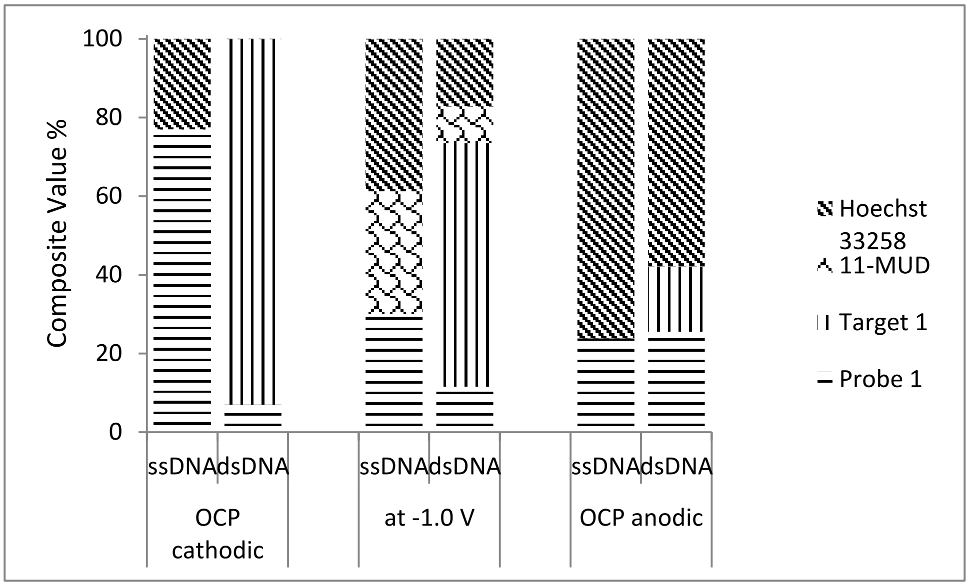

Figure 37: The composite value of each set of reference spectra of P1, T1, 11-MUD and Hoechst 33258 at different potentials for ssDNA + Hoechst 33258 and dsDNA + Hoechst 33258 obtained using OMNIC Specta software.

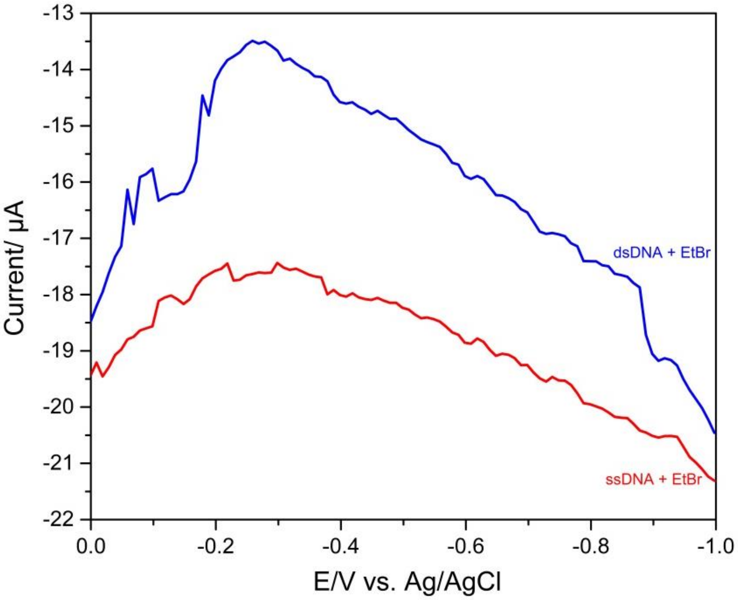

Figure 38: Comparison of DPV raw data of Hoechst 33258 from ssDNA vs dsDNA modified Au/Ag substrate collected with amplitude of 25 mV at 10 mV increments in phosphate buffer (pH 7.4).

3.2.6 Summary of DNA Hybridization studies by EC-SERS and DPV

All the chosen Raman reporters showed SERS signal for both ssDNA and dsDNA. There was insignificant amount of differences in SERS intensity for ssDNA and dsDNA and hence, could not be used to detect DNA hybridization indirectly. One possible reason for such observation could be non-selective interaction between the reporters and DNA, which is unlikely as the same trend is observed for all the reporters. While some obvious change in intensity was observed for DOX and Hoechst 33258 on applying negative potential and reversing it, such change could be due to the electrochemical melting of dsDNA, which in turn changes the orientation of the Raman reporters. Another more likely reason could be due to non-specific adsorption of the Raman reporters onto the SERS-active surface. In addition to EC-SERS, DPV was explored to detect DNA hybridization but proved unsuccessful for most cases. The issues with DPV were that it can only be used for Faradic process, which was not observed during characterization of the Raman reporters. The DPV obtained were noisy and therefore, for future studies the electrochemical system needs to be isolated from electrical noise using a Faraday cage.

3.3 Spacer studies

The five different Raman reporters studied so far did not provide a ‘signal on’ and ‘signal off’ response to DNA hybridization. As discussed earlier, it is possible that the Raman reporters are interacting with both ssDNA and dsDNA. However, there is also a possibility that the Raman reporters are binding non-specifically to the electrode surface. This can be possible only if there is a hole or defect present within the aptamer and spacer modified substrate. Therefore, a control study was performed to determine if the Raman reporter would bind to the electrode surface in the presence of the spacer monolayer alone. For this control study, a bare Au/Ag electrode was incubated in 1 mM 11-MUD for 2 h. Then, the spacer modified electrode was incubated in 20 μM DOX for 10 min while stirring as was done in previous studies. As can be seen in Figure 39, DOX can non-specifically interact with the surface of the electrode under the usual spacer incubation conditions (1 mM, 2 h). SERS peaks marked with an asterisk represent peaks due to DOX. The experiment was repeated with a longer incubation time of 6 h and 12 h, which yielded similar results. However, 11-MUD peaks at 705 and 1105 cm^{-1} due to –CH_2SH and C-C vibrations were present in all three cases with an increased intensity at longer incubation times.

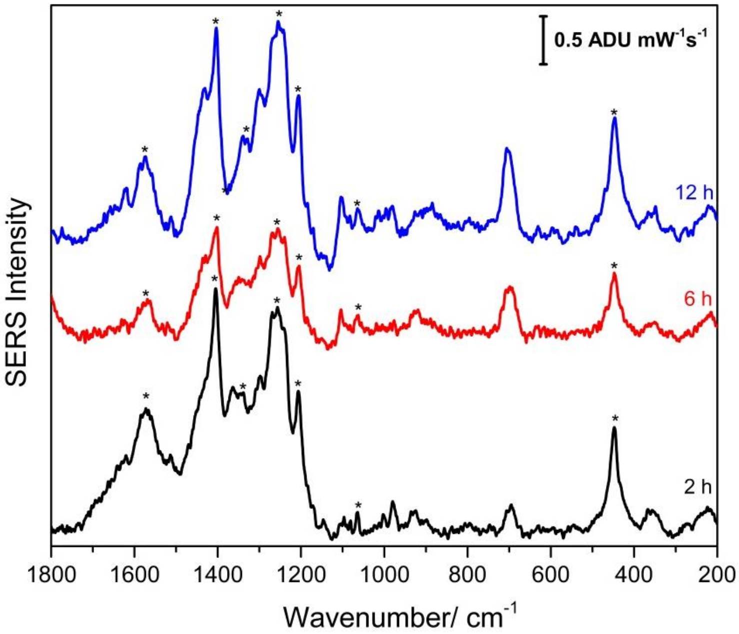

Figure 39: Au/Ag substrate incubated in 1 mM 11-MUD alkanethiol solution for 2 h, 6 h, and 12 h, followed by incubation in 20 μM DOX prepared in phosphate buffer while stirring for 10 min. Asterisks represent peaks due to the DOX molecule.

This control study could also suggest that DOX may interact with the hydroxyl terminal group of the 11-MUD spacer since the DOX structure contains a hydrophilic aminoglycosyl group. Therefore, the study was repeated with a more hydrophobic Raman reporter MB with 2 h and 4 h spacer incubation times as shown in Figure 40. Since MB is more hydrophobic in nature, it was expected that MB would not partition into the alkanethiol monolayer with the hydrophilic terminal group. Even in this case, a strong MB SERS signal was observed. This suggests that the presence of defects in the modified substrate is the likely the reason for non-specific adsorption of the Raman reporters.

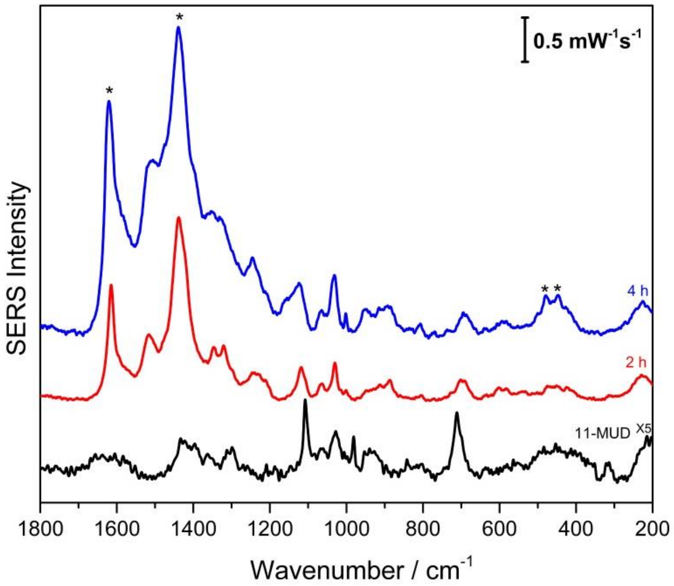

Figure 40: Au/Ag substrate incubated in 1 mM 11-MUD alkanethiol solution for 2 h and 4 h followed by incubation in 20 μM MB prepared in phosphate buffer while stirring for 10 min. Asterisks represent peaks due to MB molecule.

A different control study was performed in the presence of both the aptamer probe 1 and the 11-MUD alkanethiol. This was done in order to include any further defects introduced in the monolayer due to presence of the aptamer itself. Additionally, the complementary strand target 1 previously used for hybridization studies was replaced with scrambled target 1 (referred as s.T1). The DNA sequence of s.T1 has the same number of nucleotides including the same number of adenines as target 1, but the sequence is scrambled in such a way the nucleotides will not be able to base-pair with probe 1. The sequence for s.T1 is shown in the materials and method section. Since s.T1 does not base pair with probe 1, detecting its presence via the adenine peaks at 730 cm^{-1} and 1330 cm^{-1} in the EC-SERS signal would indicate the presence of monolayer defects. It is also well established in the literature that non-specific binding of DNA with spacer such as 6-MCH does not occur.[78] Since both 6-MCH and 11-MUD have the same hydroxyl terminal group, it is possible that non-specific binding of DNA does not occur with 11-MUD either.

The EC-SERS obtained for the control study is shown in Figure 41a, which shows the adenine peak around 730 cm^{-1} is present. Following this experiment, the SERS signal at 10 different spots was collected and averaged as shown in Figure 41b in order to better represent the uniformity of the SERS signal from the modified substrate. This data was later used to draw comparison between different spacer studies and to assess if a better monolayer could be formed under different conditions. For this purpose, the adenine peak intensity at around 730 cm^{-1} (I_{735}) was calculated as 0.05666 ADU mW^{-1}s^{-1} at OCP anodic.

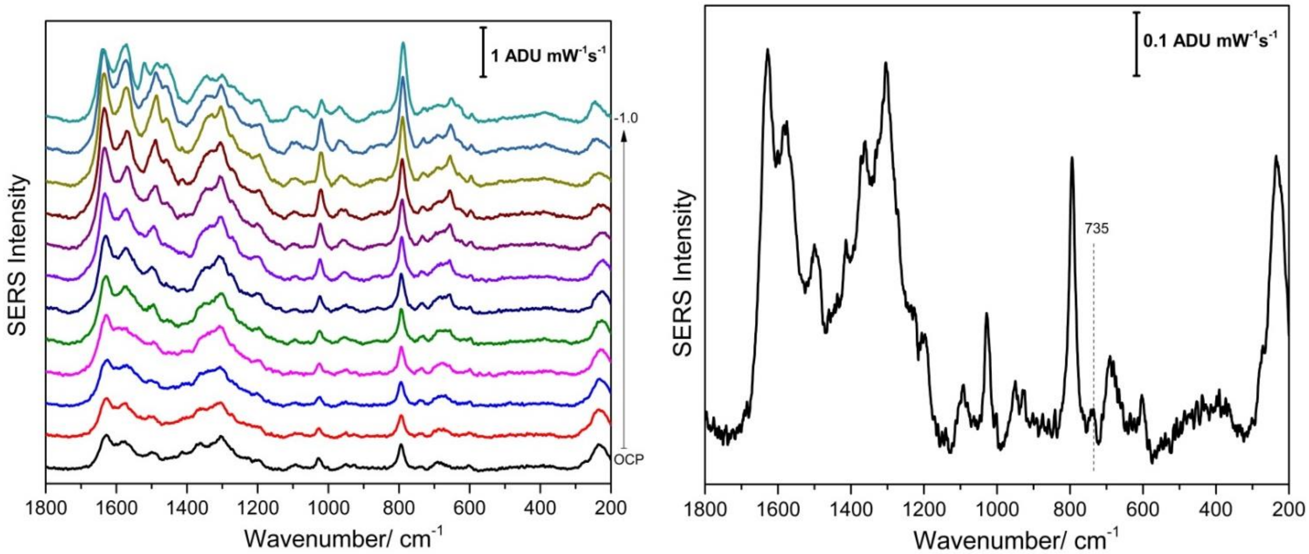

Figure 41: (a) EC-SERS of Au/Ag + P1 + 11-MUD (1 mM, 2 h) + s.T1 electrode collected using 532 nm laser excitation at 3 mW for 30 s in 0.1M NaF electrolyte solution; **(b)** Average of 10 different spots from the probe 1 + 11-MUD (1 mM, 2 h) + s.T1 modified electrode collected using 532 nm laser excitation at 3 mW and 30 s.

For the three different types of spacer studies, the incubation time of 2 h was kept constant. This is because of two main reasons; (i) Firstly, previous studies in our lab have shown that a compact monolayer can be formed within a 2 h incubation time, which is further supported by literature.[79] Secondly, a longer incubation time is undesirable for practical applications since the ultimate goal is to develop an aptasensor that could detect protein rapidly. The three different methods of monolayer fabrication are discussed in the following sections.

3.3.1 Electrochemically assisted fabrication

Two different types of electrochemically assisted monolayer fabrication were performed in an attempt to produce a self-assembled monolayer of alkanethiol without any defects. In the first study, EC-SERS was performed on a Au/Ag electrode prior to aptamer immobilization and monolayer assembly in order to remove surface adsorbed citrates. Citrate is used as a capping agent and reducing agent in the synthesis of colloidal silver nanoparticles and hence, the nanoparticles are covered in a layer of negatively charged citrate molecules. This adsorbed layer of citrate can block surface access during the formation of SAMs, and can cause surface adsorption of non-target analytes via electrostatic interaction. Therefore, electrochemical removal of citrate was attempted prior to monolayer fabrication. As can be seen in Figure 42, the peaks due to citrate are present at around 930 and 1390 cm^{-1}, which correspond to v($C\text{-}OOO^-$) and v(COO^-), respectively. On changing the applied potential in the cathodic direction, the intensity of the citrate peaks decreases, which is expected as the negative potential applied on the surface repels the negatively charged citrate.

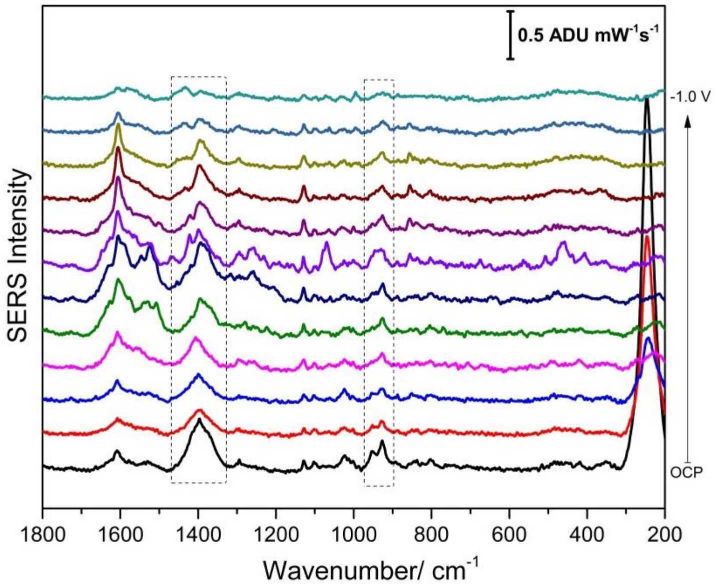

Figure 42: EC-SERS of Au/Ag electrode collected using 532 nm laser excitation at 3 mW for 30 s in 0.1M NaF electrolyte solution.

After collecting the EC-SERS, the electrode was gently washed, and the substrate was then modified with probe 1, 11-MUD followed by s.T1. After the modification, EC-SERS was collected again as shown in Figure 43. All the spectra collected were noisy, which remained consistent throughout the change in applied potential. Some of the prominent peaks observed were at 704 cm^{-1} and 1104 cm^{-1} due to the (C-S) bending and (C-C) vibration of the 11-MUD spacer. Additionally, a peak at 794 cm^{-1} due to –O-P-O phosphodiester group in DNA was also observed, which suggests that the probe 1 or s.T1 is present on the surface. This study suggests that performing EC-SERS on the Au/Ag prior to modification of the electrode results in deterioration of the SERS signal. This may be due to increased susceptibility of the silver surface to oxidation after removal of the adsorbed citrate layer.

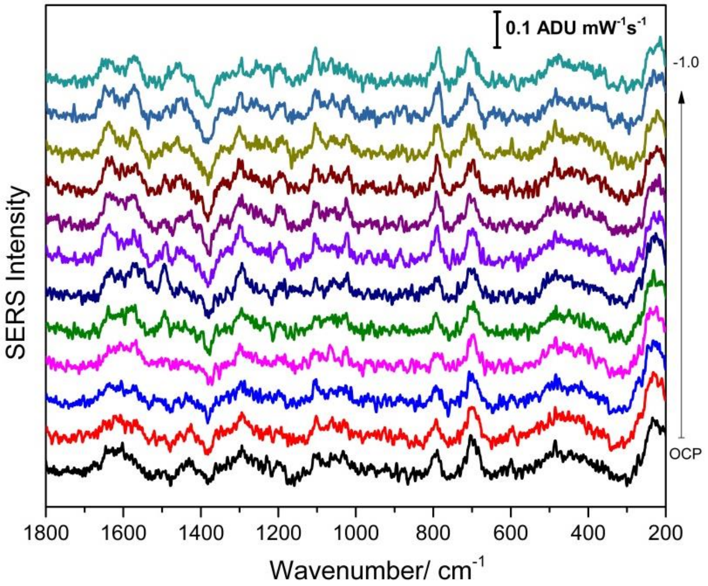

Figure 43: EC-SERS of P1 + 11-MUD (1 mM, 2 h) + s.T1 modified Au/Ag electrode, after the EC-SERS of bare electrode collected using 532 nm laser excitation at 3 mW for 30 s in 0.1M NaF electrolyte solution.

It is known from literature that when thiolated ssDNA immobilized on an electrode surface is exposed to an alkanethiol solution, any non-specifically adsorbed ssDNA are replaced by the alkanethiol.[78] Nevertheless, there is still a possibility that some of the non-specifically adsorbed ssDNA are not removed by the alkanethiol. For instance, ssDNA can be interacting with the electrode surface non-specifically through the nitrogen-containing nucleotide bases, which results in a defective SAM of alkanethiol. Therefore, EC-SERS was performed on the ssDNA modified substrate in order to electrochemically induce an upright orientation of the DNA. Once an upright configuration of the aptamer is achieved by applying a potential, it is thought that the thiol-backfilling with 11-MUD would be more efficient. After this, s.T1 was introduced followed by collection of the EC-SERS to detect the presence of adenine peaks. The experiment was initially done using the usual 2 mM concentration of the probe 1 (ssDNA), which unfortunately resulted in a degraded Au/Ag surface that could be visually observed. The experiment was repeated using a 100 times diluted concentration of probe 1 to reduce surface degradation. The collected spectra are as shown in Figure 44. As the negative potential is applied the peaks due to probe 1 increased in intensity. The Figure 44 shows several peaks of probe 1 present on the substrate such as peaks at 790, 1257 and 1577 cm^{-1} which are due to cytosine, thymine and guanine respectively.

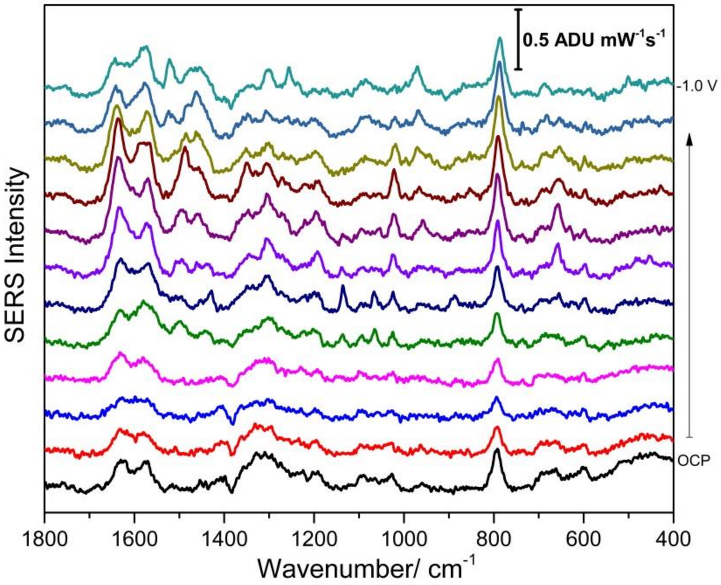

Figure 44: EC-SERS of P1 (X100 diluted) drop-coated on a Au/Ag electrode collected using 532 nm laser excitation at 3 mW for 30 s in 0.1M NaF electrolyte solution.

After collecting EC-SERS of the probe 1 modified Au/Ag substrate, it was incubated with the spacer, followed by s.T1. The EC-SERS collected after this modification can be seen in Figure 45. The EC-SERS signal is very noisy, similar to the results found in the previous experiment. This study further confirms that EC-SERS on either the bare Au/Ag or probe 1 modified Au/Ag followed by further modification of the electrode results in a deterioration of the SERS signal. One reason for such observation could be due to reversing the potential to anodic direction after applying a negative potential, which resulted in oxidation of the silver surface. Therefore, these experiments can be repeated in future where the potential is applied in negative direction only at the initial stage.

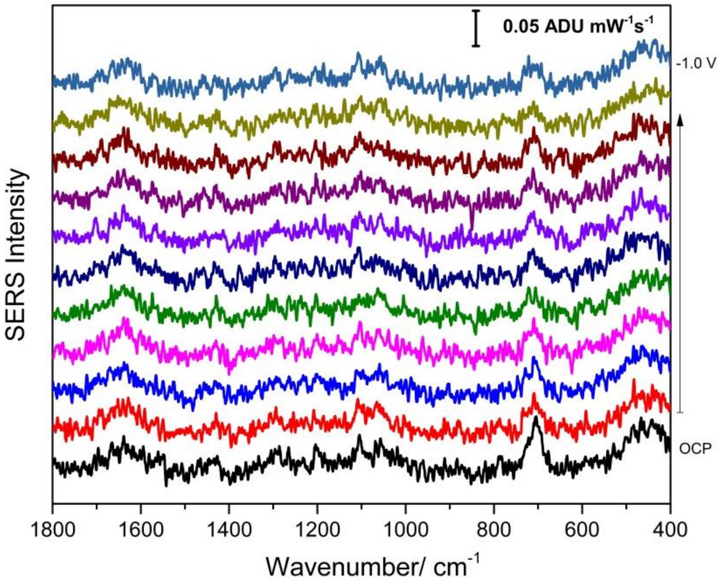

Figure 45: EC-SERS of P1 (X 100 diluted) + 11-MUD (1 mM, 2 h) + s.T1 modified Au/Ag electrode, after the EC-SERS of P1 modified electrode collected using 532 nm laser excitation at 3 mW for 30 s in 0.1M NaF electrolyte solution.

3.3.2 Mixed monolayer formation by coadsorption method

A mixed self-assembled monolayer was prepared by coadsorption of two alkanethiols that have same hydroxyl terminal groups but different chain lengths (C6 and C11). The mole percent of 6-MCH in the solution containing 6-MCH and 11-MUD alkanethiols was varied between 0 to 100%. An overlay of EC-SERS spectra of different electrodes fabricated by 20%, 40%, 60%, 80% and 100% mole percent of 6-MCH is shown in Figure 46. As can be seen, the intensity of the 735 adenine peak slightly increases at 20% mole percent of 6-MCH, but it weakens upon further increasing mole percent of 6-MCH. This could mean that increasing the mole percent of 6-MCH beyond 20% in the solution of alkanethiols results in a decrease in the presence of defects.

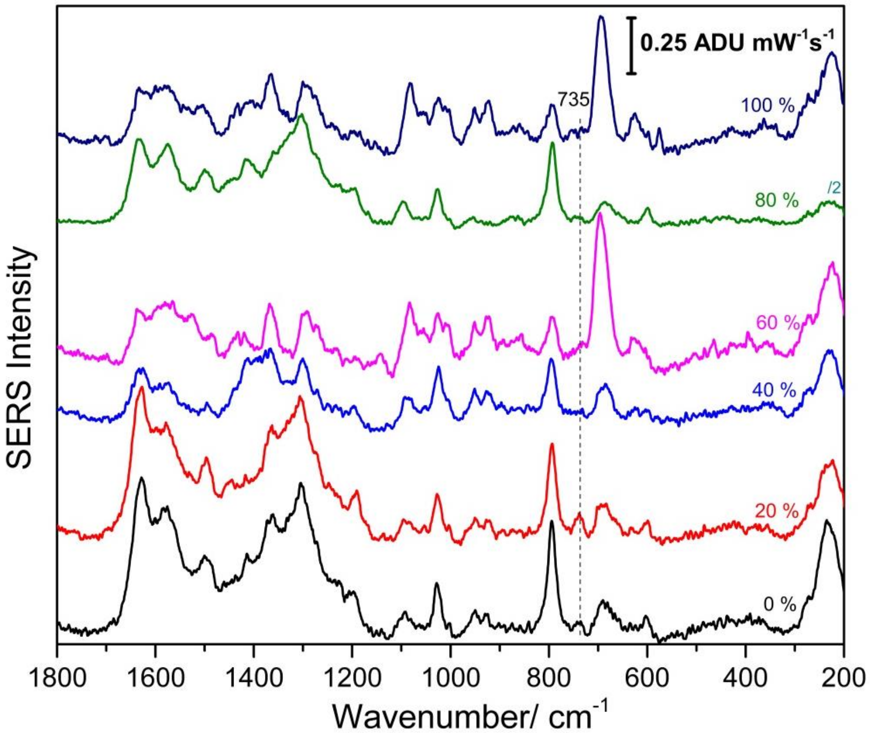

Figure 46: Overlay of EC-SERS spectra at OCP cathodic for 0%, 20%, 40%, 60%, 80%, and 100% mole percent of 6-MCH in the alkanethiol solution of 6-MCH and 11-MUD, collected using 532 nm laser excitation at 3 mW for 30 s in 0.1M NaF electrolyte solution.

An average of 10 spectra at different spots in each case was collected after performing EC-SERS to assess the quality of these mixed monolayers in a more qualitative fashion. These spectra are shown in Figures A–8 to A–12. The peak intensity (I_{738}) due to adenine was calculated from each of the averaged spectra and plotted as shown in Figure 47. The results reveal that a mixed monolayer or 6-MCH alone is relatively more stable, and defect free than 11-MUD alone. The average spectra shows that the lowest adenine signal was obtained when a mixed monolayer was formed at 20% and 80% mole percent of 6-MCH was present in the alkanethiol mixture. However, a definite conclusion cannot be drawn from these results since there is also a possibility that applying a negative potential and reversing it could introduce some disorder within the spacer monolayer. Therefore, the experiments need to be repeated with an average of 10 spectra at both OCP cathodic and anodic. An alternate approach to the coadsorption method is adopting a sequential immersion method as described in the next section.

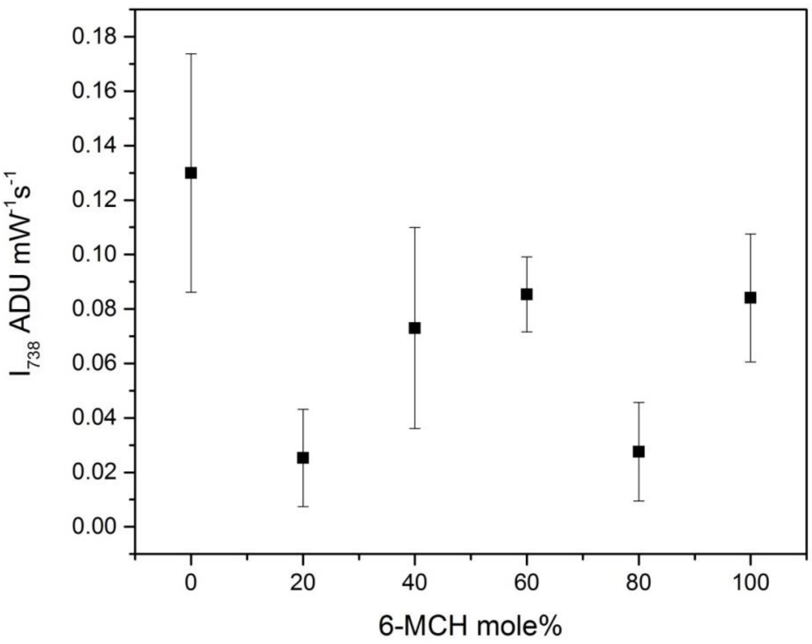

Figure 47: Adenine peak height at around 735 cm^{-1} measured from an average of 10 spectra collected at OCP anodic for different 6-MCH mole percent in the solution containing 6-MCH and 11-MUD alkanethiols.

3.3.3 Mixed monolayer formation by sequential immersion

A mixed monolayer of a shorter alkanethiol 6-mercaptohexanol along with 11-MUD was attempted by sequential immersion. In this method, the probe 1 modified Au/Ag electrode was first incubated in the shorter alkanethiol solution since it could more easily access any surface defects. The 6-carbon chain of MCH is the same length as the methylene group spacer in ssDNA, and is therefore not long enough to interfere with the hybridization of surface-bound DNA. The sensor platform was then sequentially incubated in the 11-MUD alkanethiol solution in order to fill in any larger unmodified areas. As can be seen in the EC-SERS in Figure 48a, a weak peak at 735 cm^{-1} due to adenine is present at OCP cathodic. On applying a negative potential, the peak at 730 cm^{-1} gets slightly stronger. The presence of this adenine peak indicates that there are still some defects present on the modified electrode. The peak intensity I_{735} at OCP cathodic was calculated as 0.11723 ADU mW^{-1}s^{-1}, which is almost double than the peak intensity observed for 11-MUD alone. A higher I_{735} value could suggest that a mixed monolayer of 6-MCH + 11-MUD introduces more defects within the monolayer. This is consistent with the literature whereby a lower surface coverage and presence of molecular defects were observed for ssDNA + 6-MCH + 11-MUD.[80] A lower surface coverage was obtained due to lower surface stability of the monolayer. FTIR spectrum indicated the CH_2 bending and hydrogen bonding between 6-MCH and 11-MUD is present. It was concluded that although 6-MCH and 11-MUD are hydrophobic in nature, their interactions are distinct because of differences in their chain lengths. It was also suggested that the mechanism of monolayer formation significantly affects the electrostatic blockade by monolayer.

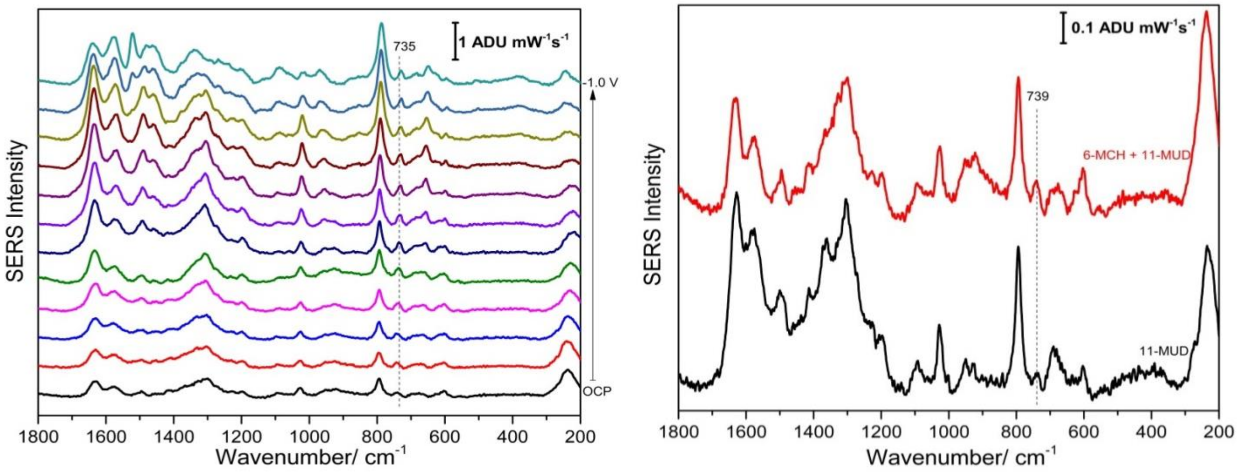

Figure 48: (a) EC-SERS of P1 + 6-MCH (1 mM, 1 h)+ 11-MUD (1 mM, 1h) + s.T1 modified electrode collected using 532 nm laser excitation at 3 mW for 30 s in 0.1M NaF electrolyte solution; **(b)** Overlay of average of 10 different spots from the P1 + 6-MCH (1 mM, 1 h) + 11-MUD (1 mM, 1h) + s.T1 modified electrode and P1 + 11-MUD (1 mM, 1h) + s.T1 modified electrode.

The study of mixed monolayer by sequential immersion method was repeated, but this time the ssDNA modified electrode was incubated in 11-MUD first, followed by 6-MCH. In this case, a shorter alkanethiol 6-MCH was introduced after 11-MUD to fill in any smaller unmodified areas. As can be seen from Figure 49a, the peak due to adenine at 730 cm^{-1} is absent or too weak to be observed, and remains absent as a negative potential is applied. This could mean that a compact monolayer is formed without any defects when 6-MCH is introduced after 11-MUD. Contrary to the previous result, Figure 49b suggests that the presence of 6-MCH in mixed monolayer does not necessarily increase defects as was observed previously. It is in fact the order in which 6-MCH is introduced in a mixed monolayer that makes a difference. This could be related to the length of the alkanethiol chain, which in turn affects the ease of accessibility towards any defects present.

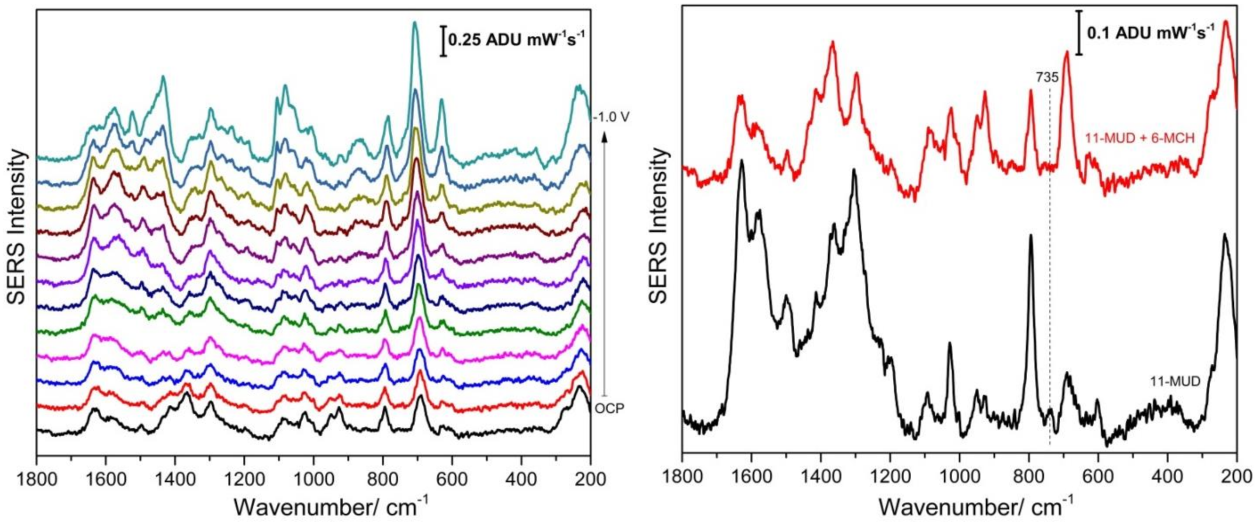

Figure 49: (a) EC-SERS of P1 + 11-MUD (1 mM, 1h) + 6-MCH (1 mM, 1 h) + s.T1 modified electrode by sequential incubation method; **(b)** Overlay of an average of 10 different spots in P1 + 11-MUD (1 mM, 1h) + 6-MCH (1 mM, 1 h) + s.T1 modified electrode and P1 + 11-MUD (1 mM, 1h) + s.T1 modified electrode.

Chapter 4: Conclusion

4.1 Conclusion:

Electrochemical surface enhanced Raman spectroscopy was explored as a method for the indirect detection of non-heme protein human IgE protein. SERS and EC-SERS were successfully used to characterize the five potential Raman reporters for this purpose. According to our knowledge, this is the first report of EC-SERS on PF, DOX, EtBr and Hoechst 33258 in literature. However, ssDNA and dsDNA cannot be easily distinguished based on the Raman reporter signal, as a 'signal off' and 'signal on' was not observed in EC-SERS. Additionally, since a significant redox signal was not observed in the CV within the specified potential window for several of the reporters chosen, DPV was not able to distinguish between the ssDNA and dsDNA. It was found that non-specific binding of the Raman reporters to the Au/Ag substrate was a key issue, and may be a reason for the poor selectivity in this case. Therefore, DNA hybridization could not be detected using Raman reporters. Despite previous studies in our research group as well as established literature data, it was realized that defects were present in the aptamer and thiol-backfilling modified substrate when 11-MUD was used as an alkanethiol spacer. Therefore, three different monolayer fabrication methods were chosen in an effort to reduce any defects present in the modified substrate. The first method of electrochemically assisted monolayer formation resulted in surface degradation and deterioration of SERS signal due to oxidation of the Ag surface. The second method of mixed monolayer formation by coadsorption did not eliminate the defects completely. The third method of mixed monolayer formation by sequential immersion resulted in a defect free monolayer formation when a shorter alkanethiol 6-MCH was introduced sequentially to the P1 + 11-MUD modified substrate. It was concluded that a shorter alkanethiol can better access any small defects present in the SAM. However, a control study needs to be performed with one of the Raman reporters to further confirm that a defect free monolayer is formed by this method. If successful, hybridization studies can be repeated with such a monolayer. On successful hybridization detection, non-heme protein IgE detection using anti-IgE aptamer can be explored.

The results presented in this thesis work show that an aptasensor for an indirect detection of IgE can be a promising method of detection due to the flexibility and availability of different potential Raman reporters. However, a more stable and defect free SAM of alkanethiol needs to be established, which would eliminate the non-specific adsorption of non-target analytes as otherwise it could lead to false positives in a clinical setting.

4.2 Future work:

For future work, a control study needs to performed with one of the Raman reporters to assess if a defect free SAM has indeed formed by the sequential immersion method. However, since multiple incubation steps can be a drawback for practical applications, a different alkanethiol can also be considered for use as a spacer. It was realized that multiple incubation and washing steps affect the quality and uniformity of the Au/Ag substrate, which can in turn affect the reproducibility of the SERS signal. Therefore, an ideal spacer would be polyethylene glycol (PEG). It has been well known in the literature for preventing non-specific adsorption of protein when immobilized on a surface due to its hydrophilicity, chain mobility, and lack of ionic charge.[81] Once a defect free monolayer is established and DNA hybridization can be indirectly detected, this proof of concept study can be extended to the indirect detection of IgE protein.

References:

1. Porter, M. D.; Lipert, R. J.; Siperko, L. M.; Wang, G.; Narayanan, R. SERS as a bioassay platform: fundamentals, design, and applications. *Chem. Soc. Rev.* **2008**, *37*, 1001-1011.
2. Zhou, W.; Huang, P.-J. J.; Ding, J.; Liu, J. Aptamer-based biosensors for biomedical diagnostics. *Analyst.*, **2014**, DOI: 10.1039/c4an00132j
3. Sur, U.K.; Chowdhury, J. Surface-enhanced Raman scattering: overview of a versatile technique used in electrochemistry and nanoscience. *Curr. Sci.* **2013**, *105*, 923-939.
4. Harroun, S.G. Development of a DNA aptamer biosensor for rapid detection and diagnosis of tuberculosis at the point of care. M.S. Thesis, Saint Mary's University, Halifax, NS, August 2014.
5. Wiegand, T. W.; Williams, P. B.; Dreskin,S. C.; Jouvin, M.-H.; Kinet, J.-P.; Tasset, D. High-affinity oligonucleotide ligands to human IgE inhibit binding to Fc epsilon receptor I. *J. Immunol.*, **1996**, *157*, 221-230.
6. Khezrian, S.; Salimi, A.; Teymourian, H.; Hallaj, R. Label-free electrochemical IgE aptasensor based on covalent attachment of aptamer onto multiwalled carbon nanotubes/ionic liquid/chitosan nanocomposite modified electrode. *Biosens. Bioelectron.* **2013**, *43*, 218-225.
7. Goda, T.; Miyahara, Y.; A hairpin DNA aptamer coupled with groove binders as a smart switch for a field-effect transistor biosensor. *Biosens. Bioelectron.* **2012**, *32*, 244-249.

8. Iliuk, A.B.; Hu, L.; Tao, W.A. Aptamer in Bioanalytical Applications. *Anal.Chem.* **2011**,83,4440-4452
9. O'Sullivan, C. K. Aptasensors – the future of biosensing?. *Anal. Bioanal. Chem.,* **2002,** *372*, 44-48.
10. Li, F.; Zhang, H.; Wang, Z.; Newbigging, A.M.; Reid, M.S.; Li, X.-F. Aptamers Facilitating Amplified Detection of Biomolecules. *Anal.Chem.* **2015**, *87*, 274-292.
11. Darmostuk, M.; Rimpelová, S.; Gbelcová, H.; Rumi T. Current approaches in SELEX: An update to aptamer selection technology. *Biotechnol. Adv.***2015,** DOI: 10.1016/j.biotechadv.2015.02.008
12. Liss, M.; Petersen, B.; Wolf, H.; Prohaska, E. An Aptamer-Based Quartz Crystal Protein Biosensor. *Anal. Chem.*, 2002, *74*, 4488-4495.
13. Katilius, E.; Flores, C.; Woodbury, N.W. Exploring the sequence space of a DNA aptamer using microarrays. *Nucleic Acids Res.*, 2007, *35*, 7626-7635.
14. Yu, J.; Jiang, Y.; Ma, X.; Lin, Y.; Fang, X. Energy Landscape of Aptamer/Protein Complexes Studied by Single-Molecule Force Spectroscopy. *Chem. Asian. J.*, 2007, *2*, 284-289.
15. Wu, Z.-S.; Zheng, F.; Shen, G.-L.; Yu, R.-Q. A hairpin aptamer-based electrochemical biosensing platform for the sensitive detection of proteins. *Biomaterials*. 2009, *30*, 2950–2955.
16. Gokulrangan, G.; Unruh, J.R.; Holub, D.F.; Ingram, B.; Jonhson, C.K.; Wilson, G.S. DNA Aptamer-Based Bioanalysis of IgE by Fluorescence Anisotropy. *Anal. Chem.* 2005, 77, 1963-1970.

17. Kim, Y. H.; Kim, J. P.; Han, S. J.; Sim, S. J. Aptamer biosensor for label-free detection of human immunoglobulin E based on surface plasmon resonance. *Sensor Actuat. B-Chem.*, **2009,** *139,* 471-475
18. Pollet, J.; Delport, F.; Janssen, K.P.F.; Maes, G.; Pfeiffer, H.; Wevers, M.; Lammertyn, J. Fiber optic SPR biosensing of DNA hybridization and DNA–protein interactions. *Biosens. Bioelectron.* **2009**, *25,* 864-869.
19. Jiang, Y.; Fang, X.; Bai, C. Signaling Aptamer/Protein Binding by a Molecular Light Switch Complex. *Anal.Chem.* **2004**,*76*, 5230-5235.
20. Feng, K.; Sun, C.; Jiang, J.; Yu, R. An aptamer-based competitive fluorescence quenching assay for IgE. *Anal. Lett.*, **2011,** *44*, 1301-1309.
21. Li, H.; Wang, C.; Wu, Z.; Lu, L.; Qiu, L.; Zhou, H.; Shen, G. An electronic channel switching-based aptasensor for ultrasensitive protein detection. *Anal. Chim. Acta.* **2013**, *758*, 130-137
22. Lee, C.-Y.; Wu, K.-Y.; Su, H.-L.; Hung, H.-Y.; Hsieh, Y.-Z. Sensitive label-free electrochemical analysis of human IgE using an aptasensor with cDNA amplification. *Biosens. Bioelectron.* **2013**, *39*, 133-138.
23. Wang, G.; Wang, Y.; Chen, L.; Choo, J. Nanomaterial-assisted aptamers for optical sensing. *Biosens. Bioelectron.* **2010**, *25*, 1859-1868.
24. Pozo, M.V.D.; Alonso, C.; Pariente, F.; Lorenzo, E. Electrochemical DNA sensing using osmium complexes as hybridization indicators. *Biosens. Bioelectron.* **2005**, *20*, 1549-1558.
25. Ozsoz, M. Electrochemical DNA Biosensors, 1st ed.; Pan Stanford Publishing: Singapore, 2012.

26. Karaballi, R. A.; Nel, A.; Krishnan, S.; Blackburn, J.; Brosseau, C.L. Development of an electrochemical surface-enhanced Raman spectroscopy (EC-SERS) aptasensor for direct detection of DNA hybridization. *Phys. Chem. Chem. Phys.,* **2015**, DOI: 10.1039/c4cp05077k.

27. Foister, S. Shape Selective Recognition of the DNA Minor Groove by Hairpin Polyamides. In *Thesis for the Degree of Doctor of Philosophy*; California Institute of Technology: Pasadena,CA, USA, 2003.
28. Tichoniuk, M.; Ligaj, M.; Filipiak, M. Application of DNA Hybridization Biosensor as a Screening Method for the Detection of Genetically Modified Food Components. *Sensors,* **2008**, *8*, 2118-2135.
29. Johnson, R.P.; Richardson, J.A.; Brown, T.; Bartlett, P.N. A Label-free, Electrochemical SERS-Based Assay for Detection of DNA Hybridization and Discrimination of Mutations. *J. Am. Chem. Soc*., **2012**, *134*, 14099-14107.
30. Tymoczko, J.; Schuhmann, W.; Gebala, M.Electrical Potential-Assisted DNA Hybridization. How to Mitigate Electrostatics for Surface DNA Hybridization. *ACS Appl. Mater. Interface*, **2014**, dx.doi.org/10.1021/am5027902.
31. Barhoumi, A.; Halas, N.J. Label-Free Detection of DNA hybridization Using Surface Enhanced Raman Spectroscopy. *J. Am. Chem. Soc*., **2010**, *132*, 12792-12793.
32. Rescifina, A.; Zagni, C.; Varrica, M.G.; Pistarà, V. Recent advances in small organic molecules as DNA intercalating agents: Synthesis, activity, and modeling. *Eur. J. Med. Chem.* **2014**, *74*, 95-115.
33. Girousi, S.Th.; Alexiadou, D.K.; Ioannou, A.K. An electroanalytical study of the drug proflavine. *Microchim. Acta.* **2008**, *160*, 435-439.

34. Erdem, A.; Kerman, K.; Meric, B.; Akarca, U.S.; Ozsoz, M. Novel hybridization indicator methylene blue for the electrochemical detection of short DNA sequences related to the hepatitis B virus. *Anal. Chim. Acta.* 2000, *462*, 139-149.

35. Kerman, K.; Ozkan, D.; Kara, P.; Meric, B.; Gooding, J.J.; Ozsoz, M. Voltammetric determination of DNA hybridization using methylene blue and self-assembled alkanethiol monolayer on gold electrodes. *Anal. Chim. Acta.* **2002**, *462*, 39-47.

36. Neto, B.A.D.; Lapis, A.A.M. Recent developments in the Chemistry of Deoxyribose Acid (DNA) Intercalators: Principles, Design, Synthesis, Applications and Trends. *Molecules.,* **2009**, *14*, 1725-1746

37. Bereznyak, E.G.; Gladkovskaya, N.A.; Khrebtova, A.S.; Dukhopelnikov, E.V.; Zinchenko, A.V. Peculiarities of DNA – Proflavine Binding under Different Concentration Ratios. *Mol. Biophys.***2009**, *54*, 805-812.

38. Grützke, S.; Abdali, S.; Schuhmann, W.; Gebala, M. Detection of DNA hybridization using electrochemical impedance spectroscopy and surface enhanced Raman scattering. *Electrochem. Commun.***2012**, *19*, 59-62.

39. Miljanic, S.; Dijanosic, A.; Matosevic, I.; Piantanida, I. Intercalator-DNA interactions revealed by NIR surface-enhanced Raman spectroscopy. *Vib. Spectrosc*., **2011**, *57*, 23-29.

40. Minasyan, S.H.; Tayadyan, L.A.; Antonyan, A.P.; Daytyan, H.G.; Parsadanyan, M.A.; Vardevanyan, P. O. Differential pulse voltammetric studies of ethidium bromide binding to DNA. *Bioelectrochem.***2006**, *68*, 48-55.

41. Perez-Arnaiz, C.; Busto, N.; Leal, J.M.; Garcia, B. New insights into the Mechanism of DNA/Doxorubicin interaction. *J. Phys. Chem. B.* **2014**, *118*, 1288-1295.

42. Zhang, X.; Zhang, S.C.; Sun, D.; Hu, J.; Wali, A.; Pass, H.; Fernandez-Madrid, F.; Harbut, M.R.; Tang, N. New Insight into the Molecular Mechanisms of the Biological Effects of DNA Minor Groove Binders. *Plos one*, **2011**.

43. Abu-Daya, A.; Brown, P.M.; Fox, K.R. DNA sequence preferences of several AT-selective minor groove binding ligands. *Nucleic Acids Research*, **1995**, *17*, 3385-3392.

44. Smith, E.; Dent, G. Modern Raman Spectroscopy A practical Approach, 1st ed.; Wiley: England, 2005.

45. Bantz, K.C.; Meyer, A.F.; Wittenberg, N.J.; Im, H.; Kurtulus, Ö.; Lee, S.H.; Lindquist, N.C.; Oh, S.-H.; Haynes, C.L. Recent progress in SERS biosensing. *Phys. Chem. Chem. Phys.* **2011**, *13*, 11551-11567

46. Aroca, R. Surface-Enhanced Vibrational Spectroscopy, 1st ed.; Wiley: England, 2006.

47. Cho, H.; Baker, B.R.; Wachsmann-Hogiu, S.; Pagba, C.V.; Laurence, T.A.; Lane, S.M.; Lee, L.P.; Tok, J. B.-H. Aptamer-Based SERRS Sensor for Thrombin Detection. *Nano Lett.* **2008**, *8*, 4386-4390.

48. Chen, J.; Jiang, J.; Gao, X.; Liu, G.; Shen, G.; Yu, R. A New Aptameric Biosensor for Cocaine Based on Surface-Enhanced Raman Scattering Spectroscopy. *Chem. Eur. J.* **2008**, *14*, 8374-8382.

49. Hu, J.; Zheng, P.-C.; Jiang, J.-H.; Shen, G.-L.; Yu, R.-Q.; Liu, G.-K. Electrostatic Interaction Based Approach to Thrombin Detection by Surface-Enhanced Raman Spectroscopy. *Anal. Chem.* **2009**, *81*, 87-93.

50. Han, X.X.; Zhao, B.; Ozaki, Y. Surface-enhanced Raman scattering for protein detection. *Anal. Bioanal. Chem*. **2009**, *394*, 1719-1727.
51. Robinson, A.M.; Harroun, S.G.; Bergman, J.; Brosseau C.L. Portable Electrochemical Surface-Enhanced Raman Spectroscopy System for Routine Spectroelectrochemical Analysis. *Anal.Chem*. **2012**, *84*, 1760-1764.
52. Skoog, D.A.; West, D.M.; Holler, F.J.; Crouch, S.R. Fundamentals of Analytical Chemistry, 8th ed.; Brooks/Cole: USA, 2004.
53. Compton, R.G.; Batchelor-M., C.; Dickinson, E.J.F. Understanding voltammetry: Problems and solutions, Imperial College press: London: UK, 2012
54. Bond, A.M. Broadening electrochemical horizons.1st ed.; Oxford university press: New York, USA, 2002.
55. Mahon, C.R.; Tice, D. Hypersensitivity. In Clinical Laboratory Immunology; Cohen, M., Eds.; Prentice Hall Clinical laboratory science series; Pearson Education Inc.: New Jersey, 2006; pp 89-92.
56. Huang, I.-Y.; Lee, M.-C. Development of a FPW allergy biosensor for human IgE detection by MEMS and Cystamine-based SAM technologies. *Sensor. Actuat. B-Chem*. **2008**, *132*, 340-348.
57. Kreuzer, M.P.; O'Sullivan, C.K.; Pravda, M.; Guilbault, G.G. Development of an immunosensor for the determination of allergy antibody (IgE) in blood samples. *Anal. Chim. Acta.* **2001**, *442*, 45-53.
58. Papamichael, K.I.; Kreuzer, M.P.; Guilbault, G.G. Viability of allergy (IgE) detection using an alternative aptamer receptor and electrochemical means. *Sensor. Actuat. B-Chem*. **2007**, *121*, 178-186

59. Su, X.; Zhang, J. Comparison of surface plasmon resonance spectroscopy and quartz crystal microbalance for human IgE quantification. *Sensor. Actuat. B-Chem*. **2004**, 100, 309-314.
60. Zhao, L.; Ding, K.; Ji, X.; Li, J.; Wang, H.; Yang, W.; Yang, W. Formation of hollow Ag/Au nanostructures in seeding approach: The competition of hydroxyl groups with chloride ions to Ag^+. *Colloids Surf. A Physicochem. Eng. Asp.* **2011**, *386*,172-178.
61. Baia, M.; Astilean, S.; Iliescu, T. Raman and SERS Investigations of Pharmaceuticals. Springer Science & Business Media. **2008**
62. Wu, D.-Y.; Li, J.-F.; Ren, B.; Tian, Z.-Q. Electrochemical surface-enhanced Raman spectroscopy of nanostructures. *Chem. Soc. Rev.,* **2008**, *37*, 1025–1041.
63. Wang, J. Analytical Electrochemistry, 2nd ed.; Wiley: USA,2000.
64. Nicolai, S.H.A; Rodrigues, P.R.P.; Agostinho, S.M.L; Rubim, J.C. Electrochemical and spectroelectrochemical (SERS) studies of the reduction of methylene blue on a silver electrode. *J. Electroanal. Chem.,* **2002**, *527*, 103-111.
65. Pfennig, B. W. Principles of Inorganic Chemistry, John Wiley & Sons: 2015
66. Bhattar, S.L.; Kolekar, G.B.; Patil, S.R. Fluorescence resonance energy transfer from proflavine hemisulphate to rose Bengal in aqueous micellar solution. *Indian J. Chem., Sect ,* **2010**, *49*, 896-900.
67. Sturgeon, R. J.; Schulman, S. G. Electronic Absorption Spectra and Protolytic Equilibria of Doxorubicin: Direct Spectrophotometric Determination of Microconstants. *J. Pharm. Sci.,* **1977,** *7,* 958-961.
68. Hahn, Y.; Lee, H. Y. Electrochemical Behavior and Square Wave Voltammetric Determination of Doxorubicin Hydrochloride. *Arch. Pharm. Res.,* **2004**, *1*, 31-34.

69. Raval, G. Thermodynamic and Spectroscopic Studies on the Molecular Interaction of Doxorubicin (DOX) with Negatively Charged Polymeric Nanoparticles. Master's Thesis, University of Toronto, Toronto, ON, 2012
70. Muniz-Mirandaa, M.; Neto, N.; Sbranab, G. Surface enhanced Raman scattering of pyrazole adsorbed on silver colloids. *Journal of Molecular Structure*, **1999,** *482–483,* 207–212.
71. Pubchem Open Chemistry Database http://pubchem.ncbi.nlm.nih.gov/compound/doxorubicin#section=3D-Conformer (accessed on April 2, 2015)
72. Luedtke, N.W.; Liu, Q.; Tor, Y. On the Electronic Structure of Ethidium. *Chem. Eur. J.*, **2005**, *11*, 495 – 508.
73. Hu, X.; Wang, Q.; He, P.; Fang, Y. Spectroelectrochemistry Study on the Electrochemical Reduction of Ethidium Bromide. *Anal Sci*.,**2002,** 18, 645-650.
74. Latt, S. A.; Stetten, G. Spectral studies on 33258 Hoechst and related bisbenzimidazole dyes useful for fluorescent detection of deoxyribonucleic acid synthesis. *J. Histochem. Cytochem.*, **1976**, *24*, 24-33.
75. Zimmermann, F.; Zimmermann, B.; Panitz, J.-C.; Wokaun, A. Surface-Enhanced Resonance Raman scattering study of the groove binding dye Hoechst 33258. *J. Raman Spectrosc.*, **1995**, *26*, 435-441.
76. Hashimoto, A.K.; Ito, K.; Ishlmori, Y. Sequence-Specific Gene Detection with a Gold Electrode Modified with DNA Probes and an Electrochemically Active Dye. *Anal. Chem.* **1994**, *66*, 3830-3833.

77. Johnson, R.P.; Gale, N.; Richardson, J.A.; Brown, T.; Bartlett, P.N. Denaturation of dsDNA immobilised at a negatively charged gold electrode is not caused by electrostatic repulsion. *Chem. Sci.*, 2013, 4, 1625–1632.
78. Herne, T.M.; Tarlov, M.J. Characterization of DNA probes immobilized on gold surfaces. *J. Am. Chem. Soc.* **1997**, *119*, 8916-8920.
79. Merchant, S.T. Electrochemical Surface-Enhanced Raman Spectroscopy used in the characterization of Langmuir Blodgett/Langmuir Schaefer Biomimetic Membranes. M.S. Thesis, Saint Mary's University, Halifax, NS, June 2014.
80. Dharuman, V.; Vijayaraj, K.; Radhakrishnan, S.; Dinakaran, T.; Narayanan, J.S.; Bhuvana, M.; Wilson, J. Sensitive label-free electrochemical DNA hybridization detection in the presence of 11-mercaptoundecanoic acid on the thiolated single strand DNA and mercaptohexanol binary mixed monolayer surface. *Electrochim. Acta*, **2011**, *56*, 8147– 8155.
81. Du. H.; Chandaroy, P.; Hui, S.W. Grafted poly-(ethylene glycol) on lipid surfaces inhibits protein adsorption and cell adhesion. *Biochim. Biophys. Acta*, **1997**, *1326*, 236-248.
82. Xiao, G.-N; Man, S.-Q. Surface-enhanced Raman scattering of methylene blue adsorbed on cap-shaped silver nanoparticles. *Chem. Phys. Lett.*, **2007**, *447*, 305-309.
83. Rivas, L.; Murza, A.; Cortes, S.S.; Ramos, J.V.G. Adsorption of acridine drugs on silver: surface-enhanced resonance Raman evidence of the existence of different adsorption sites. *Vib. Spectrosc.*, **2001**, *25*, 19-28.

84. Lee, C. J.; Kang, J. S.; Kim, M. S.; Lee, K. P.; Lee, M. S. The study of Doxorubicin and its complex with DNA by SERS and UV-resonance Raman Spectroscopy. *Bull. Korean Chem. Soc.*, **2004**, *25*, 1211-1216.
85. Gautier, J.; Munnier, E.; Douziech-Eyrolles, L.; Paillard, A.; Dubois, P.; Chourpa, I. SERS spectroscopic approach to study doxorubicin complexes with Fe^{2+} ions and drug release from SPION-based nanocarriers. *Analyst*, **2013**, *138*, 7354-7361.

Appendix

Table A-1: Band assignment for the SERS spectrum of Methylene blue.

SERS Peak (cm^{-1})	Band Assignment[82]
1625	(C-C) ring stretching
1430	(C-N) ring stretching
1393	(C-H) deformation in plane (α)
1152	(C-N) stretching
1072	(C-H) Out-of-plane bending
1036	(C-H) in plane bending
670	(C-H) Out-of-plane bending
594	(C-S-C) skeletal deformation
499	(C-N-C) skeletal deformation
446	(C-N-C) skeletal deformation; Thiazine ring in plane bending

Table A-2: Band assignment for the SERS spectrum of Proflavine.

SERS Peak (cm^{-1})	Band Assignment[83]
1569	(N-H) bending; ring deformation
1480	(N-H) deformation
1359	(C-N) stretching
1166	(C-H) in plane bending
853	(C-H) out-of-plane bending
752	(C-H) out-of-plane bending
645	Skeletal vibration
590	Skeletal vibration
430	(C-N-C) skeletal deformation
345	(C-N-C) skeletal deformation

Table A-3: Band assignment for the SERS spectrum of Doxorubicin.

SERS Peak (cm^{-1})	Band Assignment[84, 85]
344	δ Ring, w C-O-H, wC-H_2
451	δ Ring (Phe), w C-H, δ C=O
855	ou Ring
981	C-H_2 (ali), δ C=O, δ C-OH, δC-C-C
1014	δ C-C=O, δ C-H (ali), C-H_2
1065	δ C-C=O, δ C – OH, δ C-H, δ C-C
1096	v Ring, w C-H_2, v C-OH, C-H_3, v C-N, δ C-C, δ C-O-C
1206	Ring external, C-NH^+, HC-CN, CH_3, δ O-H---O, δ C-OH, N-H_2
1267	C-H_2, C-H, O-H, C-O-C
1336	δ O-H---O, Ring, C-H_2, C-OH, C-H
1405	v Ring(Phe), O-H, C-H_2, δ C-H, ou-NH_2
1503	Ring, δ C-H_3
1574	Ring, Ring (Phe)
1641	v Ring, δ CO-H

Table A-4: Band assignment for the SERS spectrum of Ethidium bromide.

SERS Peak (cm^{-1})	Band Assignment[39]
224	v (Ag-N)
254	γ (phenanthridinium)
288	γ (phenanthridinium)
327	γ (phenanthridinium)
401	γ (phenanthridinium)
440	γ (phenanthridinium)
502	-
559	δ (phenanthridinium)
607	δ (phenanthridinium)
652	-
695	δ (phenanthridinium)
720	-
771	-
839	δ (phenanthridinium)
961	δ (C-C) phenyl
998	δ (C-C) phenyl
1027	v (C-C) phenanthridinium
1085	v (C-C) phenanthridinium
1125	δ in-plane (C-H)
1176	δ in-plane (C-H)
1216	-
1278	δ wg (CH_2)
1369	v (C-C) phenanthridinium, δ (CH_3)
1403	v (C-C) phenanthridinium
1567	v (C-C)/(C-N) phenanthridinium
1600	v (C-C) phenyl
1615	v (C-C) phenanthridinium

v – stretching; γ – torsion (out-of-plane); δ – bending; wg – wagging

Table A-5: Band assignment for the SERS spectrum of Hoechst 33258.

SERS Peak (cm^{-1})	Band Assignment[75]
247	(Ag-O), (Ag-N)
647	Ring deformation, (C-H) deformation
693	(C-H) deformation/out-of-plane bending
733	Heterocyclic ring breathing (benzimidazole)
829	(C-H) deformation/out-of-plane (benzimidazole)
917	Out-of-plane ring deformation
956	Ring breathing benzenoid
978	Ring breathing benzenoid
1139	-
1174	(C-H) deformation, ring deformation (in-plane benzimidazole)
1265	(C-H) deformation, ring deformation (in-plane benzimidazole)
1361	Skeletal ring (in-plane benzimidazole)
1443	Skeletal ring (in-plane benzimidazole)
1553	(C=C), (C=N) stretching
1625	(C=C), (C=N) stretching

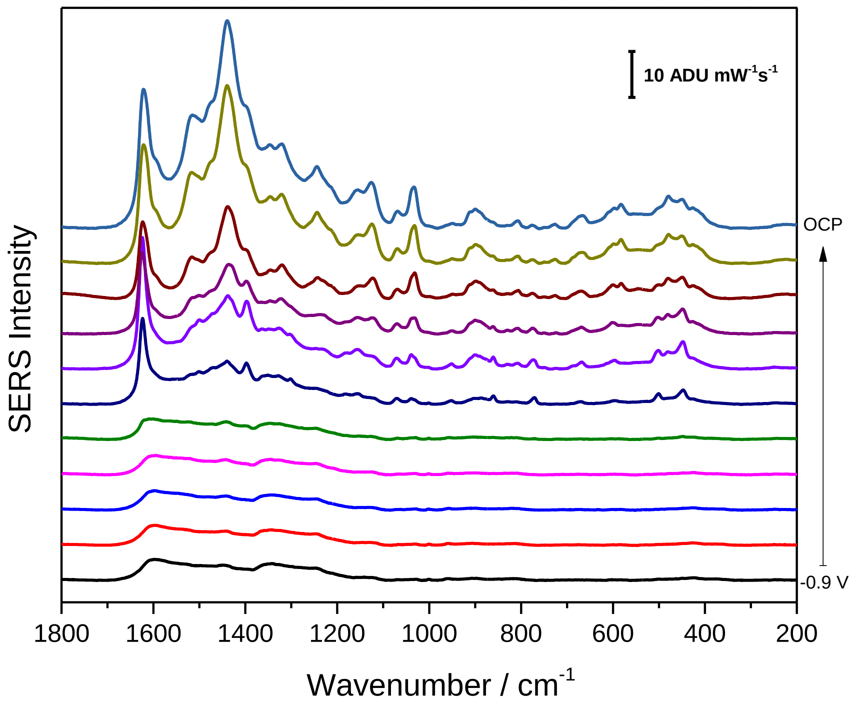

Figure A – 1: EC-SERS signal of MB (1 mM) drop-coated on a Au/Ag modified SERS substrate, collected using 532 nm laser excitation at 3 mW for 30 s, at the anodic direction in 0.1M NaF supporting electrolyte.

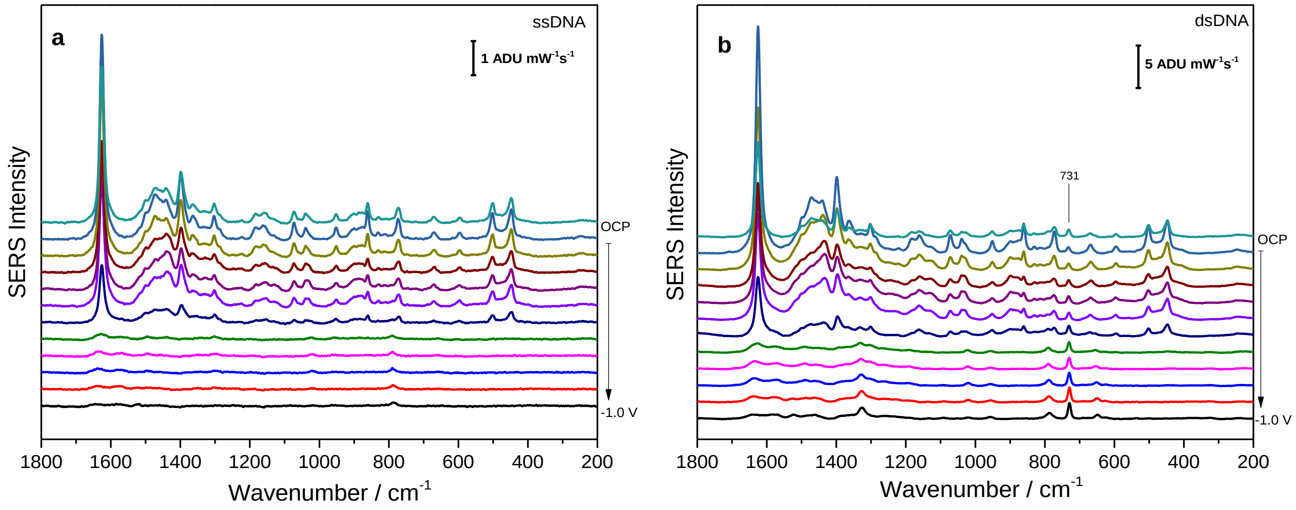

Figure A – 2: EC-SERS signal of **(a)** ssDNA + MB and **(b)** dsDNA + MB modified Au/Ag SERS substrate without spacer, collected using 532 nm laser excitation at 3 mW for 30 s, at cathodic direction in 0.1M NaF supporting electrolyte.

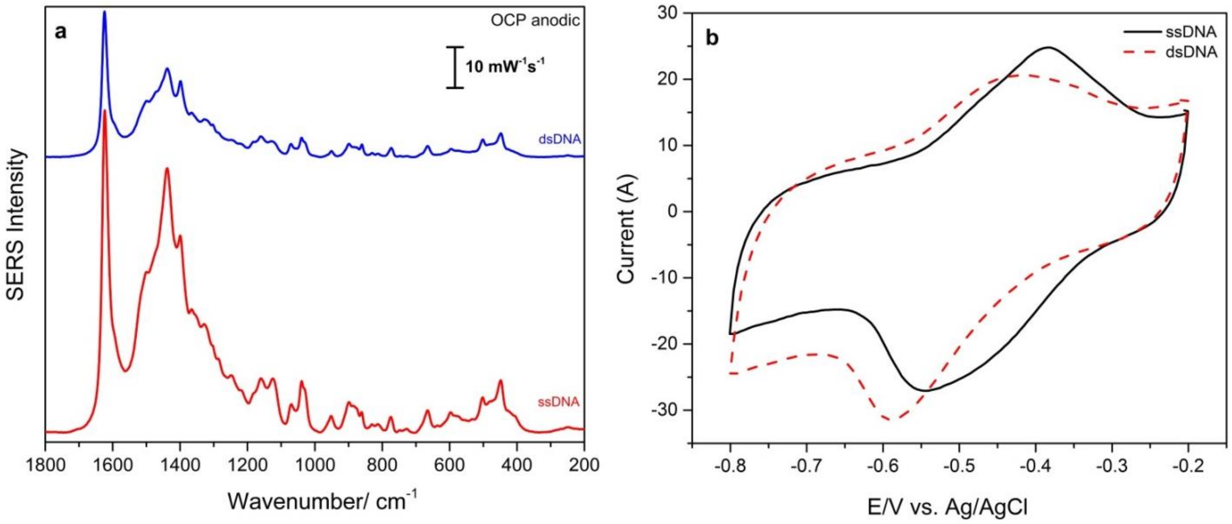

Figure A – 3: (a) EC-SERS signal of ssDNA + MB and dsDNA + MB modified Au/Ag SERS substrate, collected using 532 nm laser excitation at 3 mW for 30 s at OCP anodic in 0.1M NaF supporting electrolyte; **(b)** Cyclic voltammogram of ssDNA + MB and dsDNA + MB modified Au/Ag electrode in 0.1 M NaF supporting electrolyte.

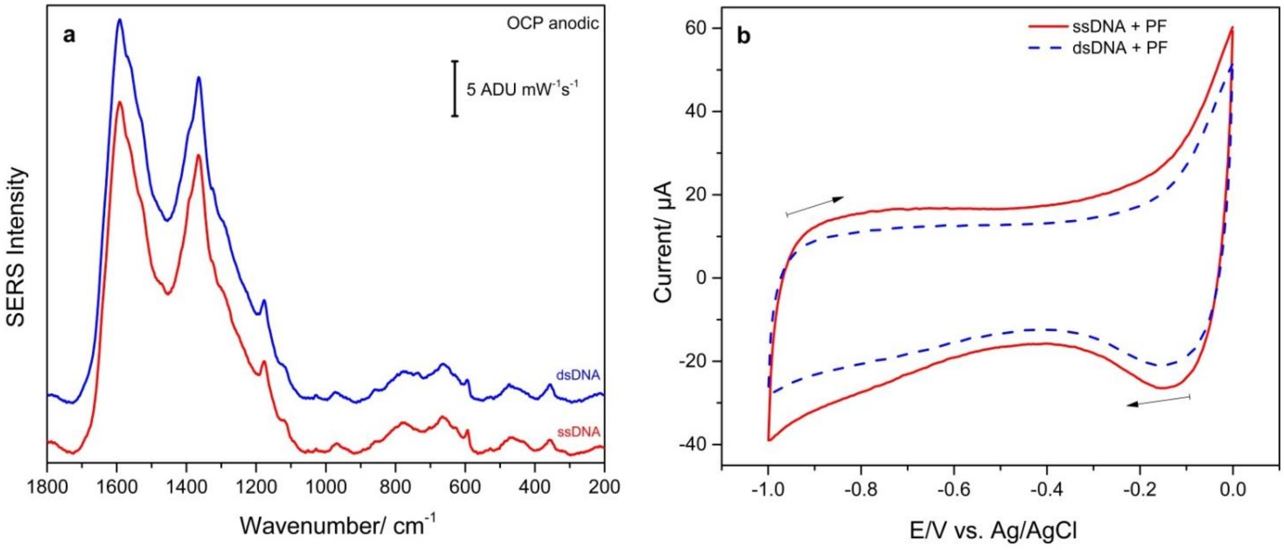

Figure A – 4: (a) EC-SERS signal of ssDNA + PF and dsDNA + PF modified Au/Ag SERS substrate, collected using 532 nm laser excitation at 3 mW for 30 s at OCP anodic in 0.1M NaF supporting electrolyte; **(b)** Cyclic voltammogram of ssDNA + PF and dsDNA + PF modified Au/Ag electrode in 0.1 M NaF supporting electrolyte.

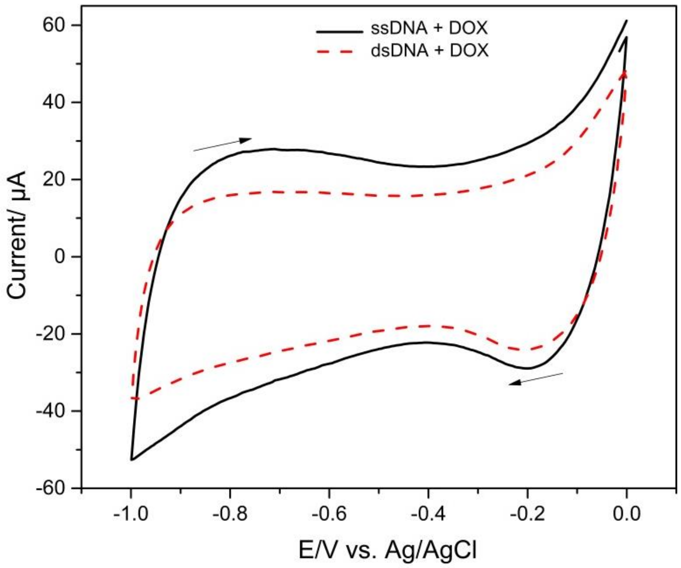

Figure A – 5: Cyclic voltammogram of ssDNA + DOX and dsDNA + DOX modified Au/Ag electrode in 0.1 M NaF supporting electrolyte.

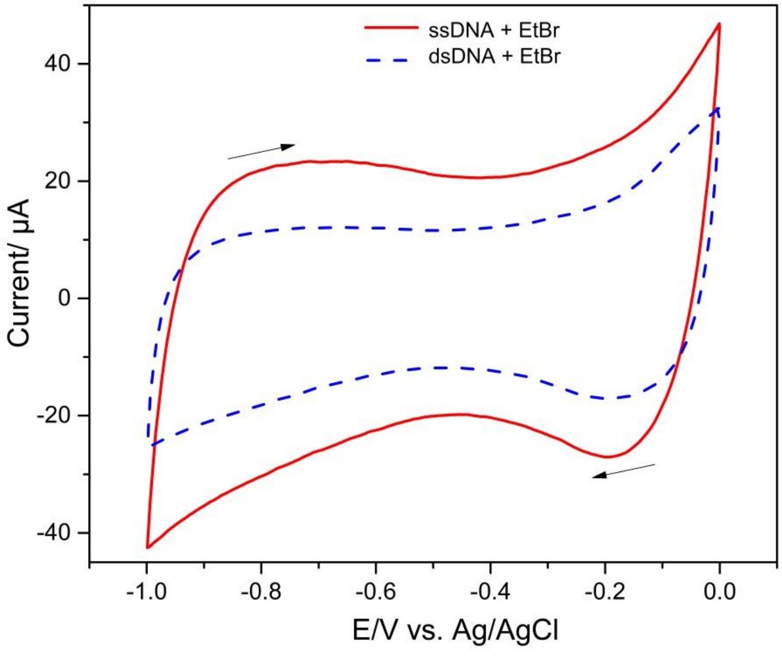

Figure A – 6: Cyclic voltammogram of ssDNA + EtBr and dsDNA + EtBr modified Au/Ag electrode in 0.1 M NaF supporting electrolyte.

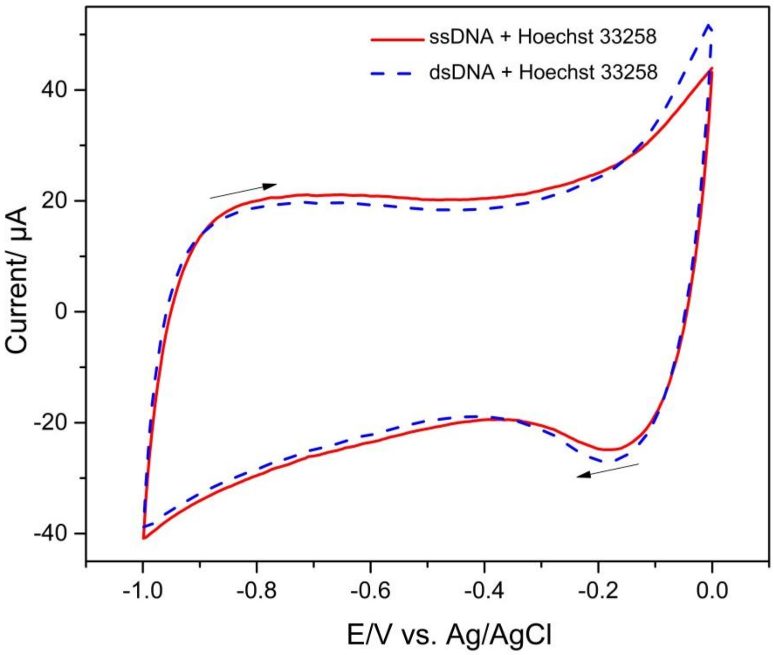

Figure A – 7: Cyclic voltammogram of ssDNA + Hoechst 33258 and dsDNA + Hoechst 33258 modified Au/Ag electrode in 0.1 M NaF supporting electrolyte.

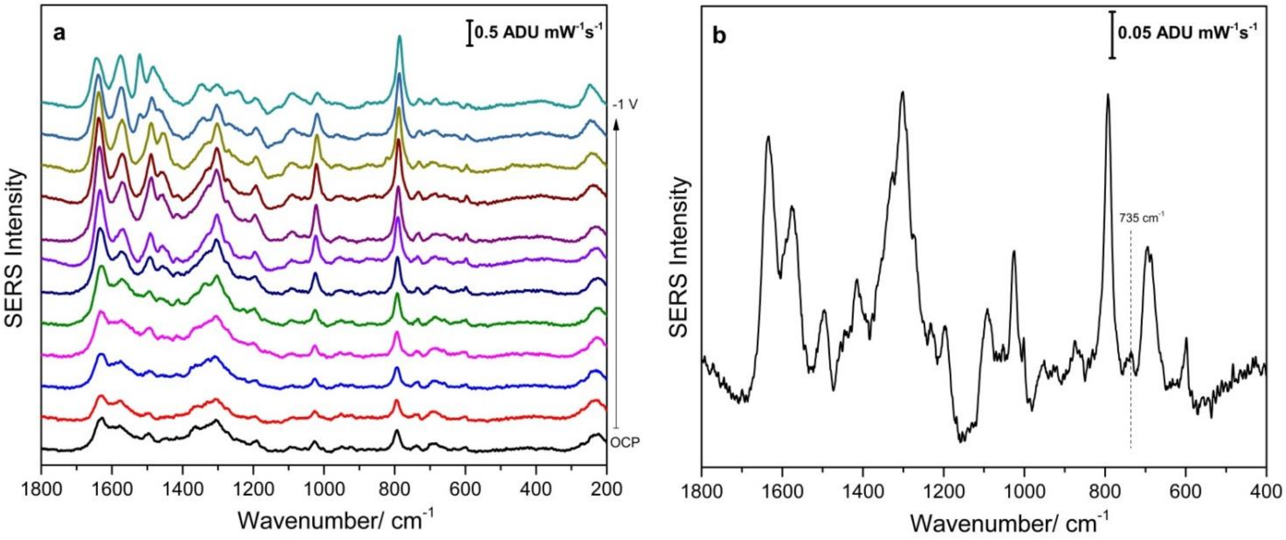

Figure A – 8: (a) EC-SERS of Au/Ag + P1 + 20% mole percent of 6-MCH + s.T1 electrode collected using 532 nm laser excitation at 3 mW for 30 s in 0.1M NaF electrolyte solution; **(b)** Average of 10 different spots from the Au/Ag + P1 + 20% mole percent of 6-MCH + s.T1 modified electrode collected using 532 nm laser excitation at 3 mW and 30 s in 0.1 M NaF electrolyte solution at OCP anodic.

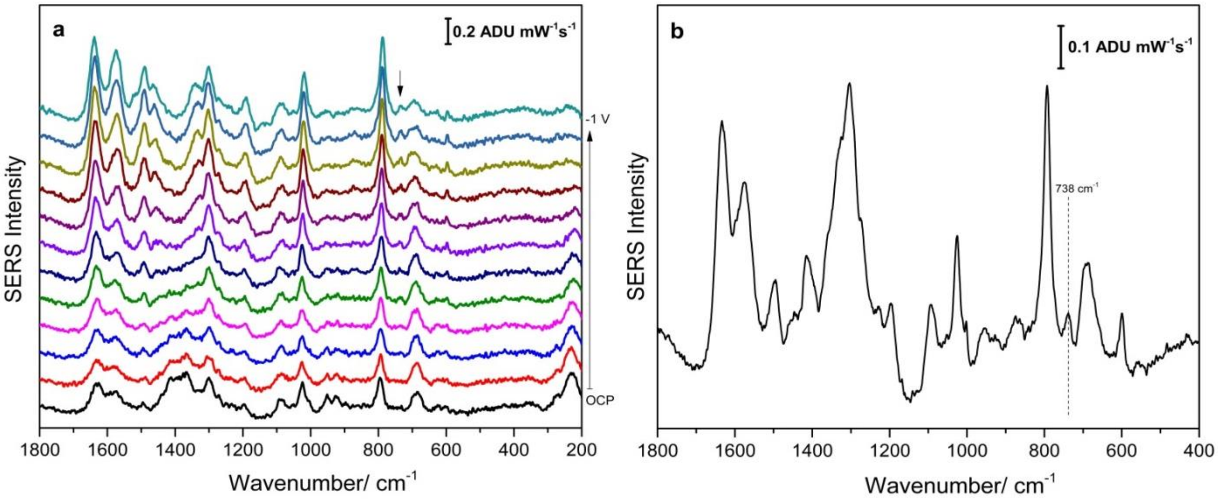

Figure A – 9: (a) EC-SERS of Au/Ag + P1 + 40% mole percent of 6-MCH + s.T1 electrode collected using 532 nm laser excitation at 3 mW for 30 s in 0.1M NaF electrolyte solution; **(b)** Average of 10 different spots from the Au/Ag + P1 + 40% mole percent of 6-MCH in 11-MUD solution + s.T1 modified electrode collected using 532 nm laser excitation at 3 mW and 30 s in 0.1 M NaF electrolyte solution at OCP anodic.

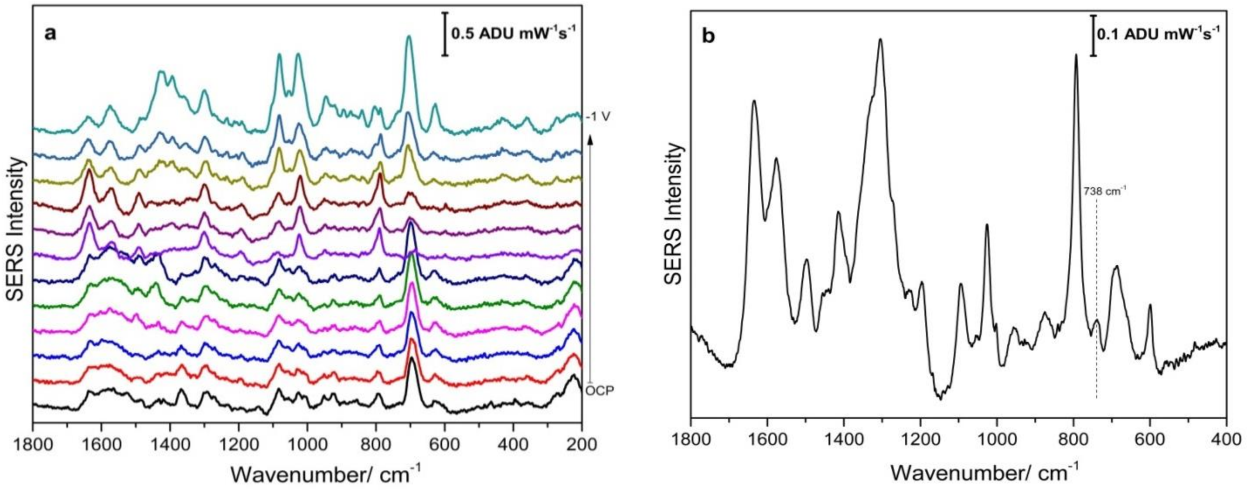

Figure A – 10: (a) EC-SERS of Au/Ag + P1 + 60% mole percent of 6-MCH + s.T1 electrode collected using 532 nm laser excitation at 3 mW for 30 s in 0.1M NaF electrolyte solution; **(b)** Average of 10 different spots from the Au/Ag + P1 + 60% mole percent of 6-MCH + s.T1 modified electrode collected using 532 nm laser excitation at 3 mW and 30 s in 0.1 M NaF electrolyte solution at OCP anodic.

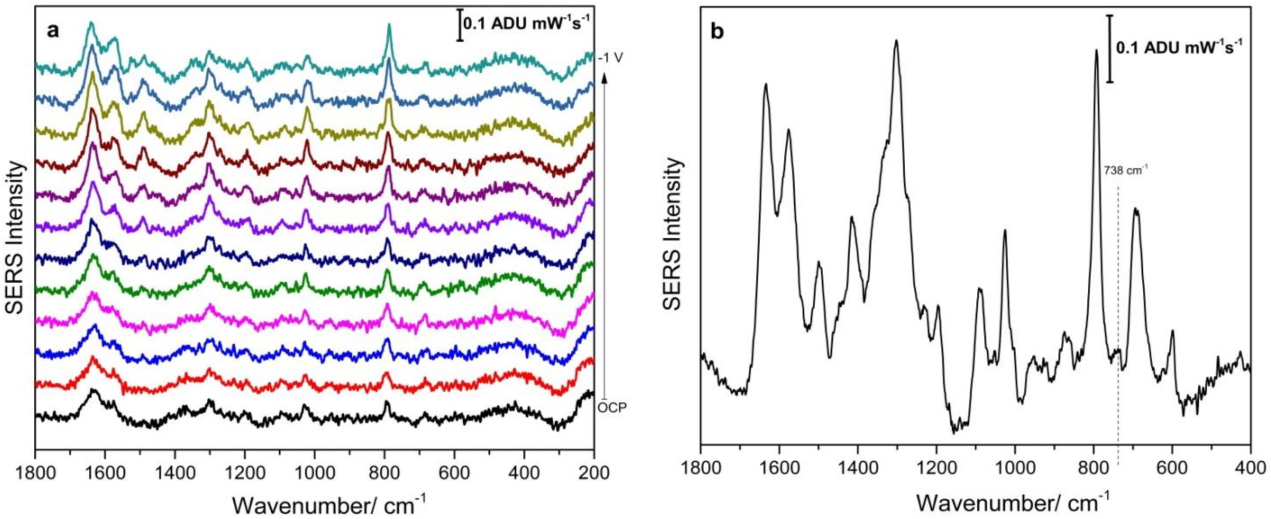

Figure A – 11: (a) EC-SERS of Au/Ag + P1 + 80% mole percent of 6-MCH + s.T1 electrode collected using 532 nm laser excitation at 3 mW for 30 s in 0.1M NaF electrolyte solution; **(b)** Average of 10 different spots from the Au/Ag + P1 + 80% mole percent of 6-MCH + s.T1 modified electrode collected using 532 nm laser excitation at 3 mW and 30 s in 0.1 M NaF electrolyte solution at OCP anodic.

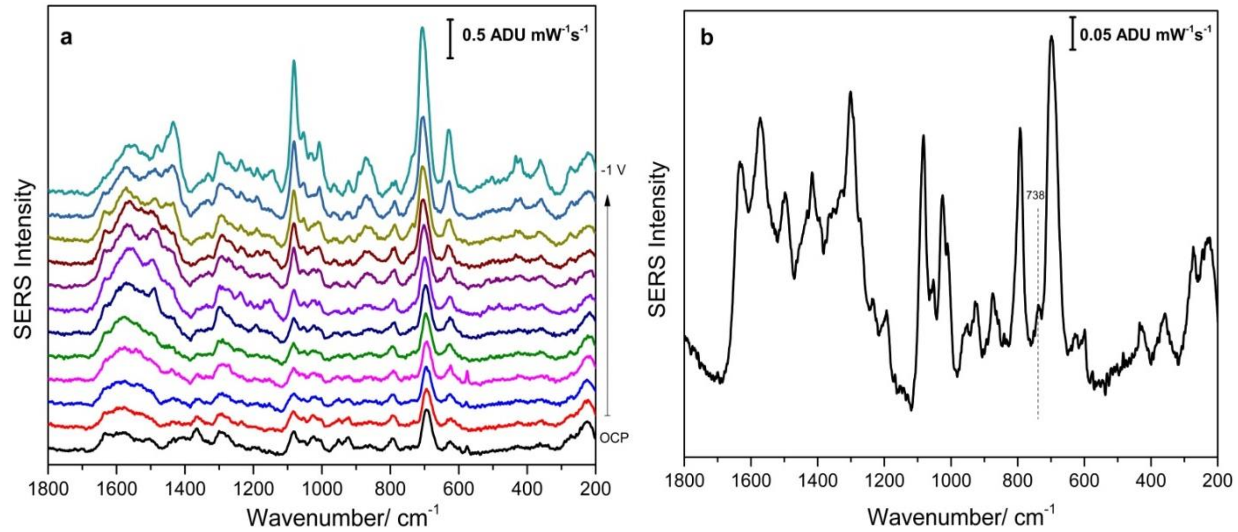

Figure A – 12: (a) EC-SERS of Au/Ag + P1 + 6-MCH + s.T1 electrode collected using 532 nm laser excitation at 3 mW for 30 s in 0.1M NaF electrolyte solution; **(b)** Average of 10 different spots from the Au/Ag + P1 + 6-MCH + s.T1 modified electrode collected using 532 nm laser excitation at 3 mW and 30 s in 0.1 M NaF electrolyte solution at OCP anodic.